MONTE CARLO SIMULATION OF DRIFTING CHARGE CARRIERS IN PHOTOCONDUCTIVE INTEGRATING DETECTORS

A Thesis
Submitted to the College of Graduate and Postdoctoral Studies
in Partial Fulfillment of the Requirements
for the degree of
Master of Science
in the Department of Electrical and Computer Engineering
University of Saskatchewan
Saskatoon

by

KIERAN OLIVER RAMASWAMI
Saskatoon, Saskatchewan

Permission To Use

In presenting this thesis/dissertation in partial fulfillment of the requirements for a Postgraduate degree from the University of Saskatchewan, I agree that the Libraries of this University may make it freely available for inspection. I further agree that permission for copying of this thesis/dissertation in any manner, in whole or in part, for scholarly purposes may be granted by the professor or professors who supervised my thesis/dissertation work or, in their absence, by the Head of the Department or the Dean of the College in which my thesis work was done. It is understood that any copying or publication or use of this thesis/dissertation or parts thereof for financial gain shall not be allowed without my written permission. It is also understood that due recognition shall be given to me and to the University of Saskatchewan in any scholarly use which may be made of any material in my thesis/dissertation.

Disclaimer

Reference in this thesis/dissertation to any specific commercial products, process, or service by trade name, trademark, manufacturer, or otherwise, does not constitute or imply its endorsement, recommendation, or favoring by the University of Saskatchewan. The views and opinions of the author expressed herein do not state or reflect those of the University of Saskatchewan, and shall not be used for advertising or product endorsement purposes.

Requests for permission to copy or to make other uses of materials in this thesis/dissertation in whole or part should be addressed to:

Head of Electrical and Computer Engineering
57 Campus Drive
University of Saskatchewan
Saskatoon, Saskatchewan S7N 5A9 Canada

OR

Dean, CGPS
College of Graduate and Postdoctoral Studies
University of Saskatchewan
116 Thorvaldson Building, 110 Science Place
Saskatoon, Saskatchewan S7N 5C9 Canada

Abstract

Semiconductors behaviour is often assumed and modeled under small signal conditions. One of the most common properties used to describe semiconductors is their collection efficiency (CE) the most common model being the Hecht collection efficiency model (HCE) η_0 . HCE and its modified expressions for exponential absorption have been widely used in time-of-flight type transient photoconductivity experiments as well as in the assessment of the sensitivity of integrating-type radiation detectors. However, the equations apply under small signals in which the internal field remains uniform (unperturbed) while electron hole pairs (EHPs) move in the semiconductor. In this thesis I have used Monte Carlo simulation of the continuity, trapping rate and Poisson equations to calculate the collection efficiency η_r (CCE). Each injected carrier is tracked as it moves in the semiconductor until it is either trapped or reaches the collection electrode. Trapped carriers do not contribute to the photocurrent but continue to contribute to the field through the Poisson equation. The instantaneous photocurrent $i_{ph}(t)$ is calculated from the drift of the free carriers through the Shockley-Ramo theorem. $i_{ph}(t)$ is integrated over the duration of the photocurrent to calculate the total collected charge and hence the collection efficiency η_r. η_r has been calculated as a function of the charge injection ratio r, the electron and hole ranges (drift mobility and lifetime products, $\mu\tau$), mean photoinjection depth δ and drift mobility ratio b. The deviation of the collection efficiency η_r from the uniform field case η_0, in the worst case, can be as much as 30% smaller than the small signal model prediction. However, for a wide range of electron and hole schubwegs and photoinjection ratios, the typical error remained less than 10% at full injection, the worst case. The present study provides partial justification for the wide-spread use of the uniform field collection efficiency η_0 formula in various applications, even under high injection conditions.

Acknowledgements

I would like to thank my supervisor Prof. Safa Kasap for his guidance along with my co-supervisor Prof. Robert Johanson and Dr. Cyril Koughia. I would also like to thank Prof. M. Zahangir Kabir at Concordia University for working with our group. I would also like to express my gratitude to my lab-colleagues who are always willing to lend an ear and provide fresh perspectives.

Finally, I would like to thank my parents, Dr. Ruth E. Hoffmeyer and Dr. Ramaswami Sammynaiken and my siblings Bdhanya and Devin Ramaswami for their continued support, encouragement and advice in my academic and non-academic life.

Table of Contents

List of Figures

List of Tables

List of Terms

- PDF Probability density function
- CDF Cumulative distribution function
- DOS Density of states
- E_A Deep Trapping upper energy limit
- E_B Deep Trapping lower energy limit
- EHP Electron hole pair
- TOF Time of Flight
- CCE Charge collection efficiency
- HCE Hecht collection efficiency
- NCE Normalized collection efficiency
- UFCE Uniform field collection efficiency
- t_0 Electron transit time
- MC Monte Carlo

1 Introduction

Photoconductive detector research is one of the most innovative fields in modern solid-state material science. Various classes of semiconductors have been used in photodetectors such as x-ray detectors and *pn* junction photodiodes. Characterization of the properties and performance of photodetectors is an important aspect of photodetector research. One of the most common ways to assess the detector performance is by measuring the photocurrent and charge collection efficiency (CCE) of the detector. These aspects have been predicted with a multitude of condition-specific models and simulation methods, that align well with experimental data under the same conditions. This work presents the development of a Monte Carlo (MC) simulation program that enables the performance of a photodetector to be evaluated under pulsed light excitation and under small and large signals. This program uses Monte Carlo methods and the Poisson equation to generate the electric field in the detector and the photocurrent due to the drifting carriers. The MC program can simulate the transient photocurrent and CCE outside of the usual limited conditions used in other published works e.g. those in which the field is assumed to be constant. The MC program can simulate the performance of the detector under a variety of new conditions, such as any combination of charge trapping, photogenerated charges, perturbed electric field, thermal diffusion, electron-hole recombination, CCE variance and any photogeneration function. In this thesis, Chapter 2 presents features implemented in the software. Chapters 3 and 4 present the published papers that show the results and implications of some of these new findings.

1.1 A simplified photoconductive semiconductor model

A simple photoconductive detector is shown in Figure 1.1. This detector works by measuring the photocurrent due to the drift of the charge carriers within the semiconductor. These charge carriers (electrons and holes) are generated in the semiconductor, when it is exposed to a light source of appropriate energy. A battery connected to the left transparent electrode and to the right electrode establishes an electric field in the semiconductor. As shown, the light passes though a transparent electrode and those photons that are absorbed photogenerate electron and hole pairs (EHPs) in the semiconductor. Consequently, the bulk of the semiconductor contains space charges that modify the electric field. The voltage V_0 between the electrodes is kept constant by the battery. Thus, $V = V_0$ is a boundary condition that requires the integration of the electric field across the detector to be V_0 under all circumstances. When charges are photogenerated in the semiconductor, they move, due to the electric field, and produce a photocurrent in the external circuit.

The integration of the photocurrent represents the collected charge i.e. charge drawn from the battery. The maximum collected charge is when EHPs are produced at the transparent electrode. In Fig 1.1, this would mean the holes are neutralized immediately and the photoinjected electrons have to travel the whole length L of the photoconductor under the influence of the electric field. This condition is called single carrier (election) type near-surface or surface photogeneration. In detector technology, CCE is defined as the ratio of charges (Q_c) drawn from the battery to single

type near-surface photogeneration (Q_i). This is also equivalent to the ratio of Q_c to the charge generated as an electron and hole pair at any location in the semiconductor, assuming that both are collected (no trapping). As such, the CCE can also be defined as the normalized integral of the photocurrent [1].

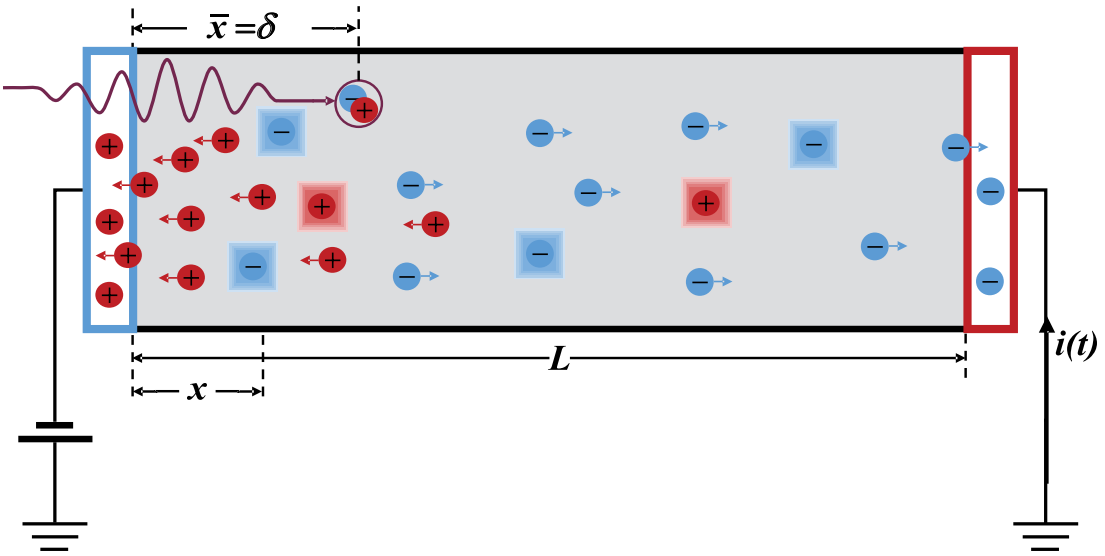

Figure 1.1:1-D representation of semiconductor detector with trappable photogenerated electron hole pairs under an external voltage.

In Figure 1.1, a schematic of a semiconductor photodetector is shown. Holes are attracted to the electrode exposed to light and electrons are attracted to the other electrode. The choice of the polarity of the battery and hence the direction of drift of carriers are arbitrary with different authors using positive or negative bias on the radiation receiving electrode.

1.2 Monte Carlo

Monte Carlo simulation (MC) is a mathematical technique to simulate physical problems in which one or more processes are stochastic. The MC technique relies on random number generation following a specific probability density function to represent the stochastic process and normalization. The Monte Carlo method is particularly useful in evaluating problems with a well-defined probability distribution such as those that occur in the motion of carriers in semiconductors. For example, an electron drifting in the conduction band has an exponential probability distribution in the time domain for being captured by a deep trap. The principal method to simulate statistical phenomena with Mont Carlo is by using cumulative density functions (CDF).[2, 3] The CDF is defined as the valid space bounded integral of the associated probability density function (PDF). The probability density function is a function that represents the relative likelihood of its variables being in specific ranges or equal to specific values. The CDF is the net probability of an event happening over a range of the variable. This range starts from the lower

bound of the variable, which is the lowest value at which the PDF is non-zero.[4] A simple example of this is a PDF with a uniform distribution over a range of values *a* to *b* in its variable *x*

$$\mathrm{PDF}(x) = \begin{cases} \dfrac{1}{b-a} & , \ a \le x \le b \\ 0 & , \ \text{else} \end{cases} \tag{1.1}$$

The CDF of the PDF is calculated from the integral over *x*:

$$\mathrm{CDF}(x) = \int_{-\infty}^{x} \mathrm{PDF}(y)dy \tag{1.2}$$

$$\mathrm{CDF}(x) = \begin{cases} 0 & , x < a \\ \displaystyle\int_{a}^{x} \frac{1}{b-a} dy & , \mathrm{a} \le x < b \\ 1 & , b \le x \end{cases} \tag{1.3}$$

$$\mathrm{CDF}(x) = \begin{cases} 0 & , x < a \\ \dfrac{x-a}{b-a} & , a \le x < b \\ 1 & , b \le x \end{cases} \tag{1.4}$$

The CDF is always equal to a number between zero and one as shown in Equation (1.4). In the range zero to one, a randomly selected CDF value (*X*) with an even distribution is generated. From *X*, the corresponding variable *x* can be generated. The selected value of *x* will follow the PDF distribution.

$$X = \mathrm{CDF}(x) = \begin{cases} 0 & , x < a \\ \dfrac{x-a}{b-a} & , a \le x < b \\ 1 & , b \le x \end{cases} \tag{1.5}$$

$$x_X = X(b-a)+a \tag{1.6}$$

Figure 1.2 shows a distribution of *x* where *a* is 3 and *b* is 7. This distribution also matches the theoretical distribution described in Equation (1.1).

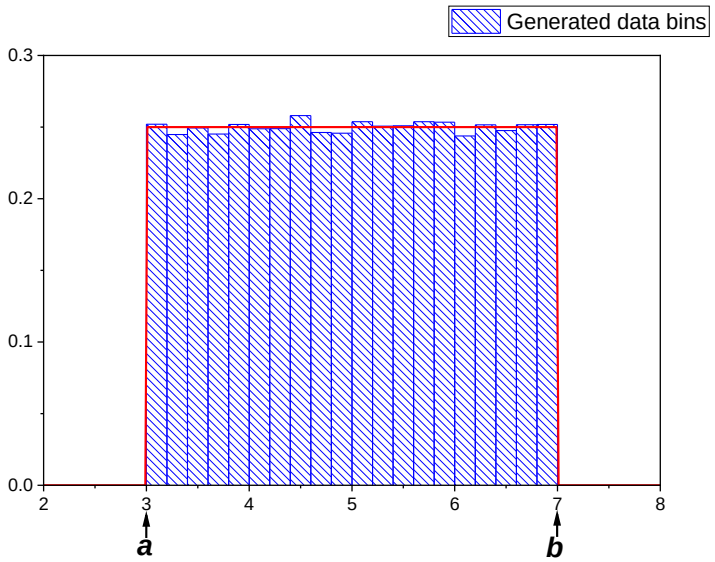

Figure 1.2: Histogram plot of random values generated using CDF method of uniform distribution over with a = 3, and b = 7.

A more complicated example can be shown by using a Gaussian function, with a PDF given as:

$$\mathrm{PDF}(x) = \frac{e^{\frac{-(x-\mu)^2}{2\sigma^2}}}{\sigma\sqrt{2\pi}} \tag{1.7}$$

where σ is the standard deviation (σ^2 is the variance) and μ is the mean of the Gaussian. The CDF of the distribution is determined by the integral of the PDF:

$$\mathrm{CDF}(x) = \int_{-\infty}^{x} \mathrm{PDF}(y)dy \tag{1.8}$$

$$\mathrm{CDF}(x) = \frac{1}{2}\left[1 + \mathrm{erf}\left(\frac{x-\mu}{\sigma\sqrt{2}}\right)\right] = X \tag{1.9}$$

where erf is the error function. Equation (1.9) is then rearranged to return the x value (x_X) based on the randomly chosen CDF value X

$$x_X = \sigma\sqrt{2}\,\mathrm{erf}^{-1}(2X - 1) + \mu \tag{1.10}$$

Using Equation (1.10), N random X values between are used to generate N (= 10000) values of x_X with a σ value of 2 and μ of 3. The distribution of these values is plotted, in bins with a width of

0.2, in Figure 1.33 and roughly approximates a Gaussian of the same parameters. The distribution approaches the Gaussian as *N* is increased and the bin size is made smaller.

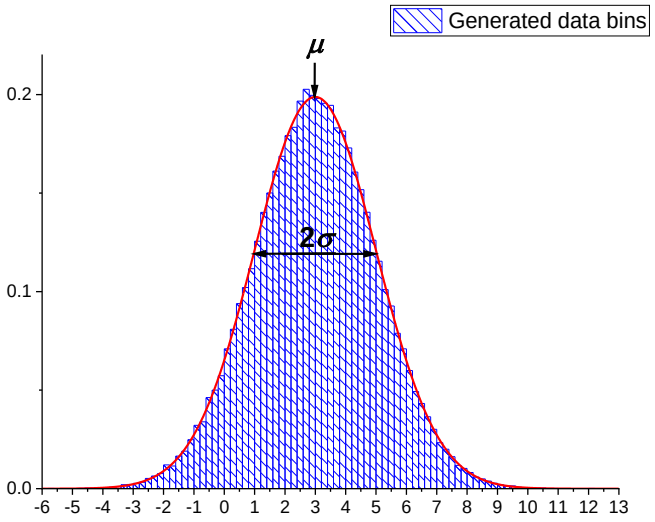

Figure 1.3: Histogram plot of random values generated using CDF method of gaussian with σ = 2, and μ = 3.

1.2.1 Monte Carlo vs. Analytical or Numerical Technique

Unlike other methods, Monte Carlo has an error associated with its results, however running the Monte Carlo method multiple times and averaging its results can produce a net result that should be sufficiently accurate. In cases where the problem can be completely solved analytically, Monte Carlo is not useful although the analytical solution can verify the MC simulation or vice versa. In some situations, analytical solutions may be prohibitively complex or outright unsolvable without approximations or numerical evaluations [5]. A common occurrence is when the problem is defined by a set of partial differential equations. In this case, the Monte Carlo simulation may be a better approach, provided the correct PDFs and physical laws (e.g. the Poisson equation) are used. Sometimes statistics and probability are an inherent part of the problem to solve; a typical case is whenever quantum properties are involved, such as for photons or electrons. The random error produced by Monte Carlo also contains information, such as variance (see Chapter 2.5), and can be used as well, unlike with analytical methods, which must set up and derive new equations for the variance [2]

1.3 References

[1] Kasap S 2012 *Optoelectronics and photonics : principles and practices* (Upper Saddle River, N.J.: Upper Saddle River, N.J. : Pearson)

[2] Sabel′fel′d K K 1991 *Monte Carlo methods in boundary value problems* (Berlin ; New York: Springer-Verlag)

[3] Kroese D P and Rubinstein R Y 2012 Monte Carlo methods *Wiley Interdisciplinary Reviews: Computational Statistics* **4** 48-58

[4] Papoulis A 1984 *Probability, random variables, and stochastic processes* (New York: New York : McGraw-Hill)

[5] Kasap S, Ramaswami K O, Kabir M Z and Johanson R 2019 Corrections to the Hecht collection efficiency in photoconductive detectors under large signals: non-uniform electric field due to drifting and trapped unipolar carriers *Journal of Physics D: Applied Physics* **52** 135104

2 Monte Carlo Simulation Methods

2.1 Introduction

In this work, several effects were modeled: (a) Electron-hole pair (EHP) photogeneration occurs near the surface [1], as a rectangular distribution with a well-defined width [2, 3], and exponential distribution. (b) Discrete-energy level deep and shallow trapping. These photogeneration events can also have time delay modifications in the form of Gaussian pulses. (c) Thermal diffusion, (d)recombination were simulated. From the photocurrent, the charge collection efficiency (CCE) and the variance of collection efficiency were also calculated. The code flow diagram used to simulate the photocurrent and CCE is given in Appendix A.

2.2 EHP Generation

The photogeneration of electron hole pairs is simulated in many ways. These models give different initial distributions of the electrons and holes. The models currently used are, near-surface distribution, rectangular distribution and exponential distribution. Additionally, multiple photogeneration events have been added to the software assuming a Gaussian probability distribution in time for each EHP generation event. Initial photogeneration of charges plays a very important role in the shape of the photocurrent and the CCE value.

2.2.1 Near-Surface Photogeneration

In many photocurrent and CCE models, the EHP are assumed to be photogenerated at only one of the electrodes (the so-called radiation receiving electrode), meaning that only one charge carrier (electrons in this work as in Fig. 1.1) travels and produces a current in the external circuit. The holes are immediately collected by the negative electrode and produce no current. Near-surface generation is easy to implement as it simply requires the electron and hole positions to start at zero. This type of generation is useful if a dispersive element is added, like trapping. Otherwise, the charge carriers will travel together with the same relative position, which is equivalent to a single charge carrier.

2.2.2 Rectangular Photogeneration

Rectangular photogeneration of EHP was used for two reasons. The first is to allow the simulations to represent the same problem that has been analytically considered in the literature. The second is that the near-surface distribution model implies a sheet of charge with no width, which make the space charge density infinite and complicates solving the Poisson equation. Using rectangular generation, the EHPs are generated by the photons as they permeate the semiconductor to a depth w_0. The initial distribution of the EHP is statistically even in position from zero to w_0. It should be noted that holes are usually assumed to be immediately collected, as the rectangular model was developed to approximate near-surface EHP generation. Put differently, holes move infinitely quickly and become neutralized at the radiation receiving electrode (negative)

2.2.3 Exponential generation

Exponential generation is the most realistic model of EHP generation. In this instance, the photons enter the semiconductor and generate EHPs in an exponentially decaying distribution. The decay rate of this photogeneration is the same as the attenuation coefficient (α) and is a well discussed and measured phenomenon. The inverse of the attenuation coefficient is known as the mean injection or photogeneration depth δ. Such a process also has statistical properties associated with it, so Monte Carlo is appropriate to simulate the photogeneration process. In this code, the EHPs initial positions are randomly assigned with a truncated exponential distribution defined as:

$$\mathrm{PDF}(x) = \frac{\delta e^{-x/\delta}}{1-e^{-L/\delta}} \tag{2.1}$$

where L is the length of the semiconductor and δ is the mean injection depth or the inverse of the attenuation coefficient α. The exact position of the EHP can be derived and generated from the CDF and a random number X from 0 to 1.

$$\begin{aligned} &\mathrm{CDF}(x) = \int_0^x \mathrm{PDF}(y)dy = \int_0^x \frac{e^{-y/\delta}}{\delta(1-e^{-L/\delta})}dy = \frac{1-e^{-x/\delta}}{1-e^{-L/\delta}} \\ &X = \mathrm{CDF}(x) = \frac{1-e^{-x/\delta}}{1-e^{-L/\delta}} \\ &-X(1-e^{-L/\delta})+1 = e^{-x/\delta} \\ &x = -\delta \ln[1-X(1-e^{-L/\delta})] \end{aligned} \tag{2.2}$$

A truncated exponential is used instead of a true exponential to prevent the generation of charge carriers beyond the semiconductor. With an exponential distribution, some carriers would be generated past the semiconductor and would not produce a current, especially if the mean injection depth is greater than the length of the semiconductor. These charges in the simulation would cause an unrealistic situation and give no information on how trapping and other interactions affect the photocurrent and CCE. Using a truncated exponential that is truncated to the length of the semiconductor, ensures that all the charge carriers used in the simulations are utilized. This assumption has been used in analytical derivations of the photocurrent and CCE [4-7]. However, a truncated exponential does deviate slightly from a true exponential when the same injection depth parameters are used. This means that if this code were to be used to simulate a real semiconductor with a known injection depth (attenuation coefficient) there may be a slight deviation in the simulation results from the experiment. However, these differences should be negligible.

2.2.3.1 Pulse Photoexcitation

Near-surface, rectangular and exponential photogeneration are all standard models used in photocurrent and CCCE models. However, most reports ignore the time delay, inherent in the light sources, that causes EHP generation. Instead, the photogeneration event is assumed to occur instantaneously [2, 8]. In reality, the light source that emits photons to photogenerate EHP is not a time delta pulse. The intensity of light generated from the source is best modelled as a narrow

Gaussian pulse in time. In fact, since the Gaussian has no cut-off in time, it should be a truncated Gaussian. This effect has been added to the code used in this thesis by assigning each EHP a random photogeneration time derived from a Gaussian distribution, as described in Equation (1.10).

$$t_n = \sigma\sqrt{2}\,\mathrm{erf}^{-1}\left(2X_n - 1\right) \tag{2.3}$$

where σ is the standard deviation of the Gaussian pulse and X_n is a randomly generated number from 0 to 1 with even distribution. The distribution of EHP generation times is offset by the earliest release of EHPs. Offsetting the time distribution ensures that the first photogeneration event coincides with the start of the simulation. Once a generation time is reached within a specific time step (Δt), all EHPs, released in that time step, are given an initial position based on near-surface, rectangular or exponential generation models.

2.2.3.2 Multiple Photoexcitation Sources

Multiple pulsed signals are an important issue to address. In all devices that use semiconductor photodetectors, multiple signals cause multiple EHP generation events. Most models assume that the spacing between each pulse is large enough that any previous charge carriers have left the system (assuming no deep trapping). In the code written for this thesis, repeated EHP generation events with a Gaussian time distribution was implemented as a feature. This feature is used to determine a realistic minimum separation time between sets of photoexcitation events where trapping, coulombic field interaction or diffusion have an impact.

The set of generation times is a combined set of n_T Gaussian distributions as described in Equation (2.3), each separated by a pulse period T_p, and given as

$$\{t\} = \frac{1}{n_T}\bigcup_{i=0}^{n_T}\left\{\sigma\sqrt{2}\,\mathrm{erf}^{-1}\left(2\{X\} - 1\right) - i\cdot T_p\right\} \tag{2.4}$$

As with a single pulse, the distribution of EHP photogeneration times is offset so the earliest release of EHPs coincides with the start of the simulation. Once a generation time is reached within a specific Δt step, all EHPs released in that time step are given an initial position, which is generated using near-surface, rectangular or exponential photogeneration distribution.

2.3 Deep Trapping

Charge carrier trapping is an effect where a charge carrier becomes captured by a localized state in the bandgap i.e. at a lower energy than the transport band. The captured carrier obviously does not produce a photocurrent. Uncontrolled imperfections or purposeful doping of the semiconductor create these localized energy levels (traps). Deep traps are those traps from which there is no release of carriers over the time scale of the experiment. There is no requirement that the deep trap must be at a well-defined discrete energy level. All traps with energies such that there is no detrapping from that particular level would act as deep traps and those captured carriers would not

be released over the time scale of the experiment. Consider electron traps that are below the conduction band and are distributed in energy from E_A (from E_c) to E_B (from E_c). The mean release times t_A and t_B from the traps at E_A and E_B respectively are

$$t_A = \nu^{-1} \exp\left(\frac{E_A}{kT}\right) \tag{2.5}$$

and

$$t_B = \nu^{-1} \exp\left(\frac{E_B}{kT}\right) \tag{2.6}$$

where ν is the attempt escape frequency, k is the Boltzmann constant and T is the absolute temperature. Since E_A is smaller than E_B, $t_A < t_B$. As long as the present time $t << t_A$, there will be no detrapping from the localized states between E_A and E_B. The release of carriers occurs at time $t = t_A$ from the level E_A first.

The rate of trapping per electron into a single energy level with a total concentration of traps N_t is

$$\frac{1}{\tau} = SuN_t \tag{2.7}$$

where S is the capture cross section, u is the mean speed of the carrier and N_t is the concentration of traps at the discrete energy level. In the case where the traps are distributed in energy as $N_t(E)$ (concentration of localized states per unit energy), we need to use

$$\frac{1}{\tau} = Su\int_{E_A}^{E_B} N_t(E)dE \tag{2.8}$$

where it is assumed that all traps from E_A to E_B have the same capture cross section. It should be clear that N_t in (a) is equivalent to the integration of $N(E)$ from E_A to E_B.

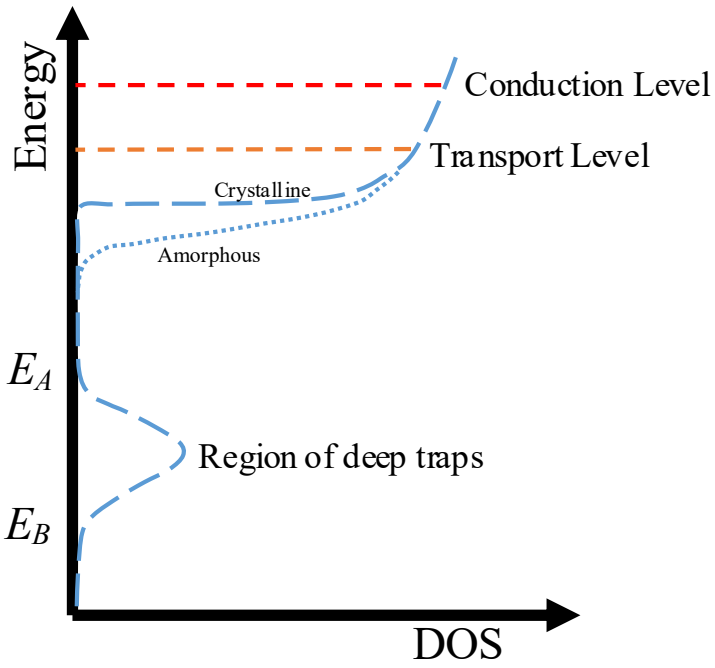

Figure 2.1: Density of States diagram of a material (either amorphous or crystalline) , as seen by charges, with conduction and transit energy levels and trapping states in energy region from E_A to E_B.

Two ways that the charge-trapping time can deviate from the mean trapping time are in the averaging approximation and quantum statistics. The first effect is classical in nature since it is based on the average energy in a range. The actual trapping time is determined by a trap at any energy value in the range. This energy selection in the range would make the selection of a specific energy trapping have a variance from the mean value. The second effect is due to the quantum properties of the traps themselves. A single dopant trap has a non-zero and non-unity chance to trap a carrier at any distance. The statistics of this trapping probability vs. distance is represented by a Gaussian. This Gaussian approximation describes an ideal scenario where there is only one trap and one charge carrier in an infinitely long semiconductor. In this thesis, the semiconductor is of a finite length, L. Ignoring any interactions with electrodes and anything outside the semiconductor; a Gaussian model can still be used. The Gaussian model is still valid as the statistical trapping probability spread is typically much narrower than L. In this thesis, an evenly distributed, infinite number of available charge carrier traps are assumed. This even, infinite distribution means the trapping probability of a single charge carrier at any position is the same and does not change during the simulation, as the sum of the Gaussians converges to a even distribution over L[9]. It is possible to simulate a finite number of traps, but that was not undertaken in this thesis [10].

Deep trapping generally occurs as the result of intrinsic traps (such thermodynamically derived defects) or imperfections and impurities introduced during the preparation of the semiconductor. Deep traps can also be induced by external means such as absorbed radiation. As trapped carriers cannot be collected, the collection efficiency becomes less than 1. Since deep trapping is a stochastic process, it has a variance. This variance means noise in the collected charge. Secondly, if trap filling is significant, repetitive trapping would fill traps and hence increase the trapping time, leading to changes in the collected charge with repetitive excitation. Furthermore, trapped carriers modify the electric field and hence change the photocurrent and the CCE.

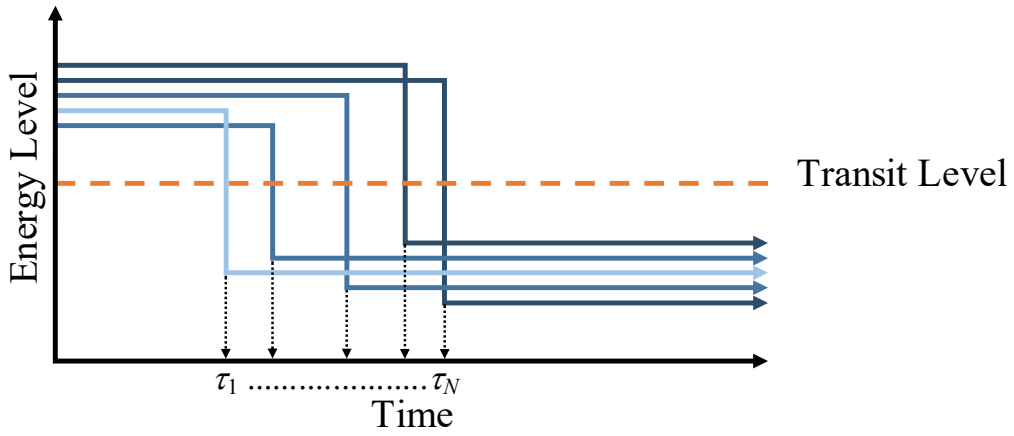

Figure 2.2: Plot of *N* charge carriers energy state, which drops when trapped at time τ_n where a smaller τ_n corresponds to a more probable trap energy level.

The simulation of charge trapping using Monte Carlo has been done before. The main drawback of previous MC simulations is how trapping and free time are generated and recorded. In some publications, each free carrier is tested as to whether it will be trapped at each time step [10]. The probability of not trapping in a time step is given by the partial probability density function:

$$\mathrm{PDF}(\Delta t) = t_0 \tau^{-1} e^{-\Delta t/\tau} \tag{2.9}$$

where τ is the mean deep trapping time (i.e. mean lifetime) and t_0 is the untrapped transit time. A random number between 0 and 1 is generated and compared against this value. If the number is less than the PDF then the carrier is trapped, if not, then the carrier is still free and progresses to the next time-step in which the whole process is repeated. The problem with this method is that its accuracy strongly depends on the ratio of Δt to τ. If the ratio is too large or small, computational errors can occur due to the accuracy limits of the computer or software.

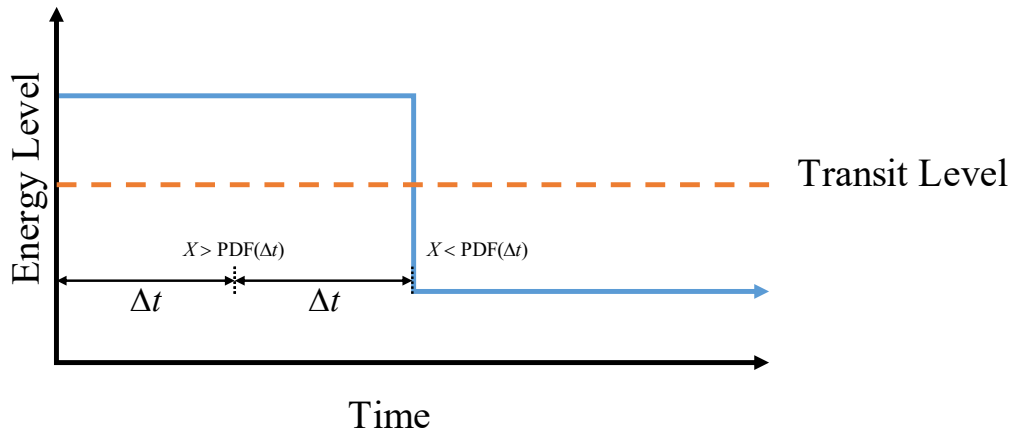

Figure 2.3: Plot of a charge carrier *n*'s energy state, which drops when trapped at a specific time step Δt, when a randomly generated number between 0 on 1 , X, is less than the probability of a charge carrier being trapped in that time step, PDF(Δt).

Another method, which is similar to the work in this thesis, is to generate the trapping time for each carrier right from the beginning. The trapping time, for each carrier, is generated based on the probability of a charge not being trapped up to a time t [11]. The cumulative density function of this PDF is given as:

$$\mathrm{CDF} = \int_0^t \mathrm{PDF}(t')dt' = \int_0^t \tau^{-1} e^{-t'/\tau} dt' = 1 - e^{-t/\tau} \tag{2.10}$$

If for electron labeled n, the time until trapping is τ_n, the CDF where $t = \tau_n$ has to be equal to a number between 0 and 1 with an even distribution, called X.

$$\begin{aligned} \mathrm{CDF} = X &= 1 - e^{-\tau_n/\tau} \\ 1 - X &= e^{-\tau_n/\tau} \\ \ln(1-X) &= -\tau_n / \tau \\ \tau_n &= -\tau \ln(1-X) \end{aligned} \tag{2.11}$$

The term $1 - X$ is equivalent to the probability space of X and can be rewritten as:

$$\tau_n = -\tau \ln(X) \tag{2.12}$$

This trapping time is then approximated into $m\Delta t$ steps where

$$m = \lfloor \tau_n / \Delta t \rfloor \tag{2.13}$$

Unfortunately, this process truncates the actual trapping time and decreases the simulated photocurrent. A smaller Δt reduces this effect, but the accuracy of the simulation is still tied directly to the relationship between the mean trapping time and time step size.

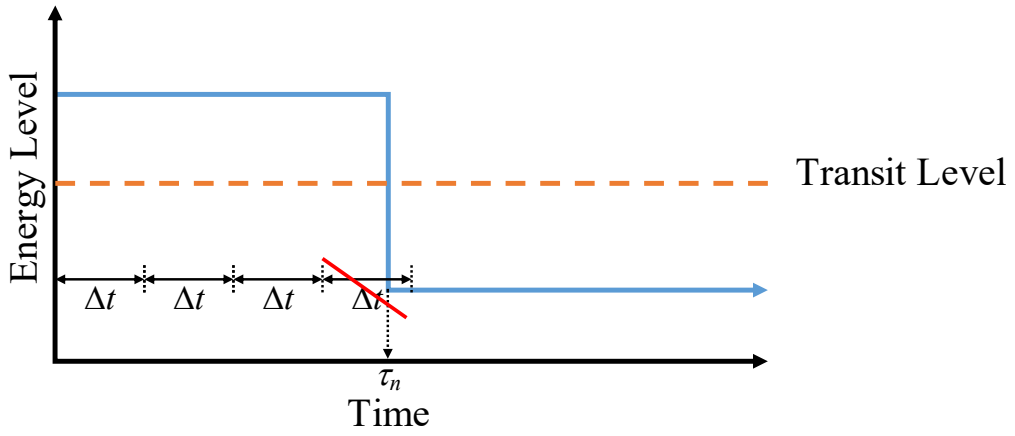

Figure 2.4: Plot of a charge carrier *n*'s energy state, which drops when trapped at a generated time τ_n, where τ_n is subdivided to the maximum number of Δt steps that fit in τ_n.

This thesis implements a more accurate method using a new variable, free time t_f. Free time is the amount of time a carrier is untrapped during a specific Δt step. The free time is evaluated at each time step for every charge carrier. Typically, this value is equal to Δt, but when the carrier is trapped, the free time is equal to $m\Delta t - \tau$, which is less than Δt.

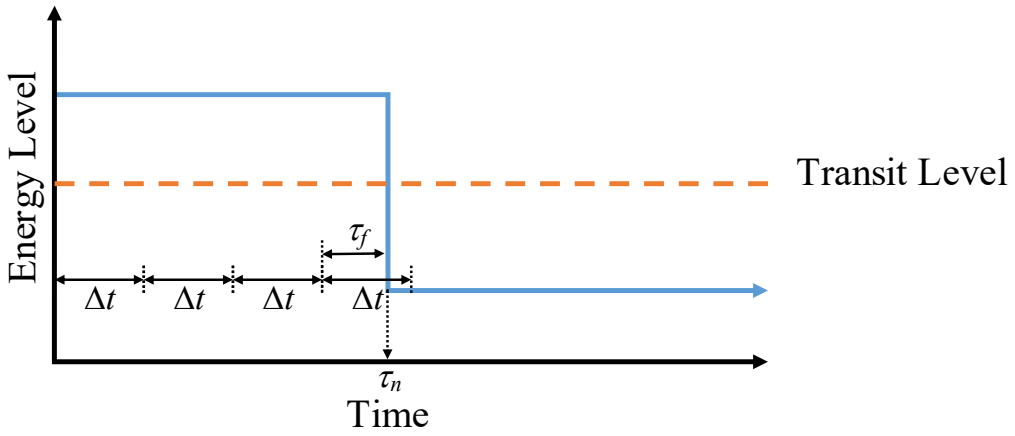

Figure 2.5: Plot of a charge carrier *n*'s energy state, which drops when trapped at a generated time τ_n, where τ_n is subdivided using free time variable τ_f.

The free time is used to calculate the photocurrent in the Shockley-Ramo theorem [12, 13]. Using this method eliminates the dependence of photocurrent accuracy on the $\Delta t/\tau$ ratio. The current generated by moving charges is given by the Shockley-Ramo Theorem as:

$$i(t) = \frac{e}{L} \sum_{\text{All untrapped } n} v_n(t) \tag{2.14}$$

,where $v_n(t)$ is the instantaneous velocity of charge carrier n at time t. According to the Shockley-Ramo theorem, the instantaneous velocity $v(t)$ is:

$$v_n(t) = \mu E_n \tag{2.15}$$

where μ is the drift mobility of the charge carrier and E_n is the electric field driving the carrier labeled n. However, this method ignores all other effects that could change the perceived instantaneous velocity during a time step. The best way to calculate the instantaneous velocity is to calculate it for every time step based on the free time. In this thesis, the velocity is calculated by dividing the displacement of each charge carrier per time step by the time step itself. This displacement Δx_f is found from the free time τ_f and instantaneous velocity from Equation (2.15).

$$\Delta x_f = \tau_f \mu E_n \tag{2.16}$$

which leads to the new photocurrent:

$$i(t) = \frac{e}{L}\sum_{\text{All}\,n} v_n^{\text{new}}(t) = \frac{e}{L}\sum_{\text{All}\,n}\frac{\Delta x_f^n}{\Delta t} = \frac{e}{L}\sum_{\text{All}\,n}\frac{\tau_f^n \mu E_n}{\Delta t} \tag{2.17}$$

The calculation of the photocurrent by this method avoids any rounding errors and removes the effects due to the accuracy of the Δt to τ ratio. If Δt were taken to be very large, then the photocurrent measured for that particular time step would equal the average of a set of photocurrent values generated with a smaller Δt ($\Delta(\Delta t)$) over the same region of time.

In deep trapping only conditions, analytical derivations of the photocurrent and CCE have been done with exponential and near-surface generation in small signal cases. Assuming near-surface generation and only deep trapping, the normalized photocurrent density (normalized to the current that would flow under a uniform field in a trap-free solid) is [14]:

$$J(t) = \begin{cases} e^{-\frac{t}{\tau}} & ,0 \le t \le t_0 \\ 0 & ,t_0 \le t \le \infty \end{cases} \tag{2.18}$$

This current has an associated CCE called the Hecht collection efficiency [14]:

$$\eta_0 = \frac{Q_c}{Q_i} = \frac{s}{L}\left[1 - \exp\left(-\frac{L}{s}\right)\right] \tag{2.19}$$

where Q_i is the injected charge and Q_c is the collected charge, L is the length of the semiconductor and s the mean travel distance of a charge carrier until it is trapped, also called the charge carrier schubweg. The schubweg is defined as $\mu_e \tau_e E_0$ where μ_e is the mobility of the charges (electrons), E_0 is applied electric field due to the battery and τ_e is the mean trapping time. The expression for the HCE assumes that the field is uniform; that the space charge of the injected and trapped carriers is negligible. Nonetheless, it is a very common model used to analyze experimental data [15-29]. A modified CCE equation by Ruzin and Nemirovsky [5] expanded the HCE by considering the EHP photogeneration process where the charge distribution decays exponentially from the radiation receiving electrode and independent trapping times and mobilities, written as:

$$\eta_0 = \eta_0^h + \eta_0^e \tag{2.20}$$

where CCE is the sum of independent individual VVEs, η_0^e and η_0^h . The electron CCE is given by

$$\eta_0^e = \frac{Q_c^e}{Q_i^e} = \frac{s_e}{L}\left(1 - \frac{\left[\exp\left(-\frac{L}{s_e}\right) - \exp\left(-L/\delta\right)\right]}{\left[1-\exp\left(-L/\delta\right)\right]\left[\frac{\delta}{s_e} - 1\right]}\right) \tag{2.21}$$

where $s_e = \mu_e \tau_e E_0$ is the electron schubweg and δ is the exponential mean injection depth over a finite L. When $s_e = \delta$ the limit is:

$$\lim_{\delta \to s_e} \eta_0^e = \frac{\delta}{L} + \frac{1}{1 - e^{\frac{L}{\delta}}} \tag{2.22}$$

The hole CCE is given by

$$\eta_0^h = \frac{Q_c^h}{Q_i^h} = \frac{s_h}{L}\left(1 - \frac{\left[1 - \exp\left(-\frac{L}{s_h} - L/\delta\right)\right]}{\left[1-\exp\left(-L/\delta\right)\right]\left[\frac{\delta}{s_h} + 1\right]}\right) \tag{2.23}$$

where $s_h = \mu_h \tau_h E_0$ is the hole schubweg with hole drift mobility μ_h and mean hole trapping time τ_h. The fitting of experiential data using this model is also very common [16, 30].

2.4 Perturbed Electric Field

The electric field at the location of the charge carrier is the main force responsible for moving the carrier between the electrodes. This movement is responsible for generating the current that is measured as the signal. Typically, this electric field is assumed to be constant, and solely due to the applied field generated by the battery voltage applied across the semiconductor. However, the charge carriers inside the semiconductor, both trapped and untrapped, produce their own electric fields that can perturb the field applied and hence change the current they produce. The field inside the semiconductor that is due to the applied bias, the space charge of the drifting and trapped carriers is called the perturbed field, i.e. the applied field becomes perturbed by the photoinjected carriers.

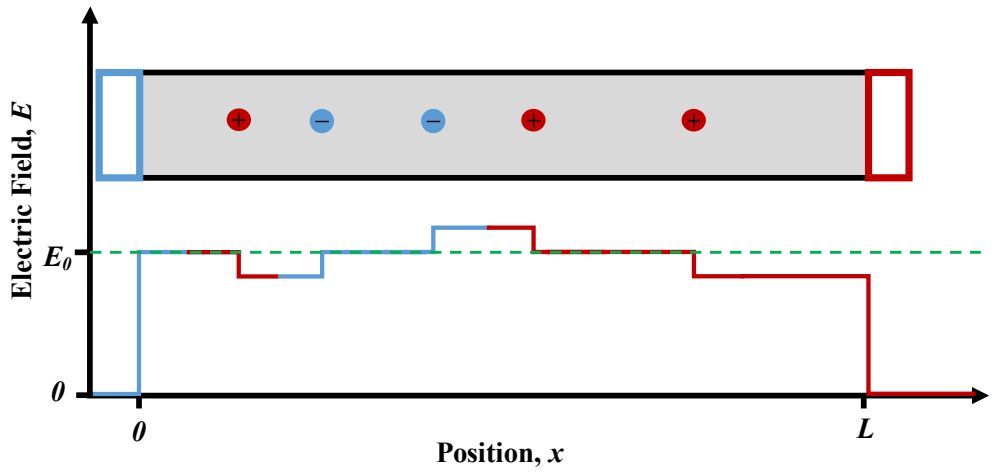

Figure 2.6: The electric field across the detector perturbed by charge carriers (the charge carriers' effect have been enhanced for clarity).

An analytical solution to perturbed electric fields was reported assuming a rectangular distribution of EHP generation of a single charge type. This assumption of an initial uniform distribution of charges over a small width w_0 simplifies the field perturbation problem as described in references. [2, 3] The normalized photocurrent is of the form:

$$J(t) = \left(1 - \frac{r}{2}\right) e^{rt/t_0} \tag{2.24}$$

where r ($1/\beta$ in the original paper) is the ratio of number of charges photoinjected to the charges on the electrodes, the so-called the injection ratio. Other analytical investigations into perturbed electric field systems have been reported, but these methods and equations derived require assumptions that may or may not be realistic [31, 32].

A numerical method has been employed, in the past, to solve for the photocurrent from rectangular generated charge carriers, with deep trapping [33]. This method is based on the continuity, trapping rate, and Poisson equations.

$$\frac{\partial \rho_f}{\partial t} = -\mu \frac{\partial (\rho_f E)}{\partial x} - \frac{\rho_f t_0}{\tau} \tag{2.25}$$

$$\frac{\partial \rho_t}{\partial t} = \frac{\rho_f t_0}{\tau'} \tag{2.26}$$

$$\frac{\partial E}{\partial x} = \frac{e\left(\rho_f + \rho_t\right)}{\varepsilon} \tag{2.27}$$

where, ρ_f, is the normalized space density of free charge carriers, ρ_t is the normalized space density of deep trapped carriers, τ is the mean trapping time, t_0 is the free transit time, μ is the charge

mobility, ε is the charge permeability and E is the electric field defined over the x-axis. The initial and boundary conditions of these sets of partial differential equations are:

$$\left\{ \begin{array}{c} \rho_f(0,t) = 0, \text{ if } t > 0 \\ \rho_f(x,0) = \dfrac{rQ_o}{ew_0}, \text{ if } x \le w_0 \text{ else } 0 \\ \int_0^L E(x,t)dx = V_o \end{array} \right\} \tag{2.28}$$

Where w_0 is the width of the rectangular initial distribution of charges, r is the ratio of photogenerated charges to the charges on the electrodes, L is the length of the detector and V_0 is the voltage across the detector. Using Equations (2.25) to (2.28) and numerical solution techniques for solving partial differential equations, the photocurrent can be calculated at each time step using the E and ρ_f values at each time step with the Shockley-Ramo theorem.

$$J(t) = \mu \sum_{n=0}^{n=L/\Delta x} E(n \cdot \Delta x, t)\rho_f(n \cdot \Delta x, t) \tag{2.29}$$

The obvious limitation of the numerical method is that its accuracy depends on the size of Δx and Δt. A more in-depth comparison is seen in chapter 3 section 5.2 and Figure 3.4.

In Monte Carlo simulation, the perturbation can be added by calculating the individual coloumbic electric field attractions or repulsions between each hole and electron carrier such that the field at a particular location, P, is

$$\mathbf{E}(P) = \mathbf{E}_0 + \sum_n \frac{\mathbf{r}_{+n}(P)e^-}{4\pi\varepsilon_0\varepsilon_r r_{+n}(P)^3} + \sum_n \frac{\mathbf{r}_{-n}(P)e^+}{4\pi\varepsilon_0\varepsilon_r r_{-n}(P)^3} \tag{2.30}$$

where $\mathbf{E}_0$ is the electric field created by the battery (along the x-direction), $\mathbf{r}_{-n}$ is the distance vector from an electron labeled n to the point P and r_{+n} is the distance vector from a hole labeled n to P. Computationally this method is intensive and inefficient due to including the addition of vectors. Attempts have been made to optimize this process by limiting the range of particle interactions [34]. This method requires evaluation of the distance between the carriers. The distance is evaluated with a mesh simplification, where the carriers are placed on a 2D grid with spacing Δx. The effects of charges within a sub-grid of area $4r^2$, where r an arbitrarily chosen radius (sufficiently small to speed the calculations and sufficiently large to approximate the electric field) centered on point P, are used to calculate the electric field. The compromises of using a Δx step on top of a Δt step are an increase in resolution error and memory usage. Also, using only nearby charges may introduce an error in the simulation.

This thesis uses, a more practical solution by applying the Poisson equation in one dimension and the MC method for trapping. The one-dimensional Poisson equation is:

$$\nabla E(x,t) = -\frac{\rho(x,t)}{\varepsilon} \tag{2.31}$$

or

$$\frac{\partial}{\partial x} E(x,t) = -\frac{\rho(x,t)}{\varepsilon} \tag{2.32}$$

where $\rho(x,t)$ is the net space charge density and ε is the permittivity of the medium. Using the fundamental calculus theorem of differentiating integrals, Equation (2.32) leads to

$$\int_0^x \frac{d}{dy} E(y,t)dy = -\int_0^x \frac{\rho(y,t)}{\varepsilon} dy \tag{2.33}$$

i.e.

$$E(x,t) = \int_0^x -\frac{\rho(y,t)}{\varepsilon} dy - C_E(t) \tag{2.34}$$

where $CCE(t)$ is an integration constant. One important constraint of the system is the battery voltage. Due to the battery, the voltage drop across the semiconductor will remain constant regardless of charge carrier movement. This constraint imposes a boundary condition

$$\int_0^L E(x,t)dx = V_0 \tag{2.35}$$

Given that V_0 is always the voltage across the semiconductor, Equation (2.35) can be rewritten in terms of the electric field in the semiconductor without any charge carriers, E_0.

$$V_0 = \int_0^L E(x, 0-\Delta t)dx = \int_0^L E_0 dx = LE_0 \tag{2.36}$$

i.e.

$$E_0 = \int_0^L E(x,t)dx / L = \left\langle E(x,t) \right\rangle \Big|_t \tag{2.37}$$

Assuming the simulation uses a small enough Δt step, then $E(t + \Delta t)$ can be found from equation (2.34)

$$E(x, t+\Delta t) = \int_0^x -\frac{\rho(y,t)}{\varepsilon} dy - C_E(t) \tag{2.38}$$

Using the boundary equation, $CCE(t)$ can now be found

$$E_0 = (1/L)\int_0^L \left[\int_0^x -\frac{\rho(y,t)}{\varepsilon} dy - C_E(t) \right] dx \tag{2.39}$$

$\therefore$

$$E_0 = (1/L)\int_0^L \int_0^x -\frac{\rho(y,t)}{\varepsilon} dydx + (1/L)\int_0^L C_E(t)dx \tag{2.40}$$

$\therefore$

$$E_0 = \frac{\int_0^L \int_0^x -\frac{\rho(y,t)}{\varepsilon} dydx}{L} + C_E(t) \tag{2.41}$$

Assuming Δt is small

$$E_0 = \frac{\int_0^L \int_0^x -\frac{\rho(y,t-\Delta t)}{\varepsilon}\,dydx}{L} + C_E(t) \tag{2.42}$$

$\therefore$

$$C_E(t) = \frac{\int_0^L \int_0^x \frac{\rho(y,t-\Delta t)}{\varepsilon}\,dydx}{L} + E_0 \tag{2.43}$$

$\therefore$

$$C_E(t) = \frac{\int_0^L E(x,t-\Delta t) - C_E(t-\Delta t)dx}{L} + E_0 \tag{2.44}$$

$$C_E(t) = \left\langle E(x,t)\right\rangle\Big|_t - C_E(t-\Delta t) + E_0 \tag{2.45}$$

From equations (2.38) and (2.45), there is sufficient information to find the position(density) of charge carriers and the electric field change over time:

$$C_E(t) = \left\langle E(x,t)\right\rangle\Big|_t - C_E(t-\Delta t) + E_0 \tag{2.46}$$

$\therefore$

$$E(x,t+\Delta t) = \int_0^x -\frac{\rho(y,t)}{\varepsilon}\,dy - C_E(t) \tag{2.47}$$

Equation (2.46) was used to find CCE at time *t* in the Monte Carlo simulations because the average field over the sample length can be readily evaluated and CCE($t - \Delta t$) is known from the previous time step.

In the thesis, using Equations 2.44 and 2.45, ρ corresponds to a discrete number of charge carriers. These carriers can be represented in ρ by a sum of Kronecker delta functions.

$$\rho(x,t)/e = \sum_{\text{All } e^- < L} \delta_k(x_e - x) - \sum_{\text{All } e^+ > 0} \delta_k(x_h - x) \tag{2.48}$$

i.e.

$$\int_0^x \rho(y,t)dy = \int_0^x \sum_{\text{All elelctrons}} e\,\delta_k\left(x_e(t) - y(t)\right) - \sum_{\text{All holes}} e\delta_k\left(x_h(t) - y(t)\right)dy \tag{2.49}$$

This expression can be restated as the size of sets that satisfy the conditions

$$\int_0^x \rho(y,t)dy = e\left|\{x_h; x_h \le x\} \cap \{x_h; x_h > 0\}\right| - e\left|\{x_e; x_e \le x\} \cap \{x_e; x_e < L\}\right| \tag{2.50}$$

where $\{x_h; x_h \le x\}$ is the set of hole positions in which each hole position is less than *x*, $\{x_h; x_h > 0\}$ is the set of hole positions in which each hole position is more than zero (holes are not collected), $\{x_e; x_e \le x\}$ is the set of electron positions in which each electron position is less than *x*, and $\{x_e; x_e < L\}$ is the set of electron positions in which each electron position is less than *L* (electrons are not collected),

By using this method to calculate the net space charge density, the electric field experienced by each charge carrier can be evaluated. The order of complexity of this method is O(N^2). A new optimization routine was implemented to calculate the electric field. This routine sorts the sets of charge carrier positions using a quick-sort method. This quick-sort reduces the complexity of Equation (2.51) giving a new evaluation method:

$$\int_0^{x_n} \rho(y,t)dy = e\sum_{i=1}^{i=N}\left(\left[i-1;0<x_i<L\right]-\left[N-m+n;x_i>0\right]\right) \tag{2.51}$$

where x_n is the position specific charge carrier, n is the index of the sorted charges carriers of one type, m is the index of the sorted set of all charge carriers that corresponds to charge carrier n. The use of a quick-sort method reduces the order of complexity from O(N^2) to O(Nln$N$) [35]. This electric field in combination with the free time for each carrier can evaluate the position step each charge carrier takes and its photocurrent.

$$x_h(t+\Delta t) = x_h(t) + E\left(x_h(t), t+\Delta t\right)\tau_f\left(x_h(t)\right)\mu_h \tag{2.52}$$

and

$$x_e(t+\Delta t) = x_e(t) + E\left(x_e(t), t+\Delta t\right)\tau_f\left(x_e(t)\right)\mu_e \tag{2.53}$$

Subsequent *CCE* and ρ are computed until a designated maximum time or until all carriers are in a deep trap or collected by their appropriate electrodes.

This process, while accurate, is still computationally expensive as the quick sort is of order O(Nln$N$). This makes the computation time of the simulation of order O($N_T N$ln$N$), where N_T is the number of time steps used. A linear interpolation reduces the operational complexity to O(NN_TN_x). This is done by evaluating the electric field at N_x positions with an even Δx spacing, making an array of positions, P_x. Electric field values are then evaluated at the values of P_x into an array E_x. The electric field at each charge carrier is found by interpolation based on the electric field values in E_x that correspond to the positions in P_x excluding the specific charge carrier position. These positions are found by calculating the indices of P_x by rounding up and down the carrier position divided by Δx.

2.5 Diffusion

One-dimensional thermal diffusion has also been implemented in this thesis. In this model, thermal diffusion is considered small relative to other effects so independence can be assumed, where the diffusion of a single charge carrier is unconstrained by length and independent of other charge carriers. In this thesis the effect of diffusion is modeled using the one-dimensional diffusion displacement function which is a Gaussian function [36]:

$$\text{PDF} = \frac{e^{\frac{\Delta x_{\text{diff}}{}^2}{2\sigma_{\text{diff}}{}^2}}}{\sigma_{\text{diff}}\sqrt{2\pi}} \tag{2.54}$$

where σ_{diff} is the diffusion variance defined as $\sigma_{\text{diff}} = \sqrt{2D_{\text{diff}}\Delta t}$ where D_{diff} is the diffusion coefficient. The set of displacements of the charge carriers is found using the CDF and a random number X from 0 to 1:

$$\text{CDF}(\Delta x_{\text{diff}}) = \frac{1}{2}\left(1 + \text{erf}\left(\frac{\Delta x_{\text{diff}}}{\sigma_{\text{diff}}}\right)\right) \tag{2.55}$$

$$X = \text{CDF}(\Delta x_{\text{diff}}) = \frac{1}{2}\left(1 + \text{erf}\left(\frac{\Delta x_{\text{diff}}}{\sigma_{\text{diff}}}\right)\right) \tag{2.56}$$

$$\Delta x_{\text{diff}} = \sigma_{\text{diff}}\,\text{erf}^{-1}(2X - 1) \tag{2.57}$$

2.6 References

[1] Rudenko A I and Arkhipov V I 1978 Trap-Controlled Transient Current Injection in Amorphous Materials *J Non-Cryst Solids* **30** 163-89

[2] Schwartz L M and Hornig J F 1965 Photocurrents generated by intense flash illumination *J Phys Chem Solids* **26** 1821-4

[3] Papadakis A C 1967 Theory of Transient Space-Charge Perturbed Currents in Insulators *J Phys Chem Solids* **28** 641-7

[4] Kasap S O 2000 X-ray sensitivity of photoconductors: application to stabilized a-Se *J Phys D Appl Phys* **33** 2853-65

[5] Nemirovsky Y 1999 Statistical modeling of charge collection in semiconductor gamma-ray spectrometers *J Appl Phys* **85** 8-15

[6] Kabir M Z and Kasap S O 2002 DQE of photoconductive x-ray image detectors: application to a-Se *J Phys D Appl Phys* **35** 2735-43

[7] Vanheyningen R S and Brown F C 1958 Transient Photoconductivity in Silver Chloride at Low Temperatures *Phys Rev* **111** 462-71

[8] Many A, Simhony M, Weisz S Z and Levinson J 1961 Studies of photoconductivity in iodine single crystals *J Phys Chem Solids* **22** 285-92

[9] Kasap S 2006 *Principles of electronic materials and devices* (Boston: Boston : McGraw-Hill)

[10] Yunus M, Kabir M Z and Kasap S O 2004 Sensitivity reduction mechanisms in amorphous selenium photoconductive x-ray image detectors *Appl Phys Lett* **85** 6430-2

[11] Ballendine J 2011 Monte Carlo Simulation of Time of Flight Transient Photocurrents in High Resistivity Semiconductors with Shallow and Deep Traps: Effects of Photoinjection Strength, Duration and Absorption Depth. In: *Electrical and Computer Engineering,* (University of Saskatchewan: University of Saskatchewan) p 118

[12] Shockley W 1938 Currents to conductors induced by a moving point charge *J Appl Phys* **9** 635-6

[13] Ramo S 1939 Currents Induced by Electron Motion *Proceedings of the IRE* **27** 584-5

[14] Hecht K 1932 For the mechanism of the photoelectric primary current in insulating crystals. *Z Phys* **77** 235-45

[15] Boothman V, Alruhaili A, Perumal V, Sellin P, Lohstroh A, Sawhney K and Kachanov S 2015 Charge transport optimization in CZT ring-drift detectors *J Phys D Appl Phys* **48**

[16] Auden E C, Vizkelethy G, Serkland D K, Bossert D J and Doyle B L 2017 Modeling charge collection efficiency degradation in partially depleted GaAs photodiodes using the 1-and 2-carrier Hecht equations *Nucl Instrum Meth B* **399** 12-9

[17] Zanichelli M, Santi A, Pavesi M and Zappettini A 2013 Charge collection in semi-insulator radiation detectors in the presence of a linear decreasing electric field *J Phys D Appl Phys* **46**

[18] Street R A, Wong W S and Lujan R 2009 Low-temperature amorphous silicon p-i-n photodiodes *Phys Status Solidi B* **246** 1854-7

[19] Shrestha S, Fischer R, Matt G J, Feldner P, Michel T, Osvet A, Levchuk I, Merle B, Golkar S, Chen H W, Tedde S F, Schmidt O, Hock R, Ruhrig M, Goken M, Heiss W, Anton G and Brabec C J 2017 High-performance direct conversion X-ray detectors based on sintered hybrid lead triiodide perovskite wafers *Nat Photonics* **11** 436-40

[20] Qureshi S, Perezmendez V, Kaplan S N, Fujieda I, Cho G and Street R A 1989 Material Parameters in a Thick Hydrogenated Amorphous-Silicon Detector and Their Effect on Signal Collection *Mat Res S C* **149** 649-54

[21] Maynard B, Long Q, Schiff E A, Yang M J, Zhu K, Kottokkaran R, Abbas H and Dalal V L 2016 Electron and hole drift mobility measurements on methylammonium lead iodide perovskite solar cells *Appl Phys Lett* **108**

[22] Ling Y P, Min J H, Liang X Y, Zhang J J, Yang L Q, Zhang Y, Li M, Liu Z X and Wang L J 2017 Carrier transport performance of Cd0.9Zn0.1Te detector by direct current photoconductive technology *J Appl Phys* **121**

[23] Hossain A, Cui Y, Bolotnikov A E, Camarda G S, Yang G, Kochanowska D, Witkowska-Baran M, Mycielski A and James R B 2009 Vanadium-Doped Cadmium Manganese Telluride (Cd1-x Mn (x) Te) Crystals as X- and Gamma-Ray Detectors *J Electron Mater* **38** 1593-9

[24] Guo R R, Jie W Q, Wang N, Zha G Q, Xu Y D, Wang T and Fu X 2015 Influence of deep level defects on carrier lifetime in CdZnTe:In *J Appl Phys* **117**

[25] Fang Y J, Dong Q F, Shao Y C, Yuan Y B and Huang J S 2015 Highly narrowband perovskite single-crystal photodetectors enabled by surface-charge recombination *Nat Photonics* **9** 679-89

[26] Dirin D N, Cherniukh I, Yakunin S, Shynkarenko Y and Kovalenko M V 2016 Solution-Grown CsPbBr3 Perovskite Single Crystals for Photon Detection *Chem Mater* **28** 8470-4

[27] Yu P F, Xu Y D, Chen Y R, Song J, Zhu Y, Zhang M J, Zhang B G, Wanga Y, Li W, Luan L J, Du Y Y, Ma J, Zheng J H, Li Z, Bai M, Li H and Jie W Q 2018 Investigation of effective annealing on CdMnTe:In crystals with different thickness for gamma-ray detectors *J Cryst Growth* **483** 94-101

[28] Williams M L and Donnelly I J 1996 An investigation of electric field behaviour in semi-insulating GaAs using current pulses *J Phys D Appl Phys* **29** 1997-2003

[29] Street R A, Ready S E, Van Schuylenbergh K, Ho J, Boyce J B, Nylen P, Shah K, Melekhov L and Hermon H 2002 Comparison of PbI2 and HgI2 for direct detection active matrix x-ray image sensors *J Appl Phys* **91** 3345-55

[30] Kabir M Z and Kasap S O 2002 Charge collection and absorption-limited sensitivity of x-ray photoconductors: Applications to a-Se and HgI2 *Appl Phys Lett* **80** 1664-6

[31] Many A and Rakavy G 1962 Theory of Transient Space-Charge-Limited Currents in Solids in Presence of Trapping *Phys Rev* **126** 1980-8

[32] Uxa S, Grill R and Belas E 2013 Evaluation of the mobility-lifetime product in CdTe and CdZnTe detectors by the transient-current technique *J Appl Phys* **114**

[33] Kasap S, Ramaswami K O, Kabir M Z and Johanson R 2019 Corrections to the Hecht collection efficiency in photoconductive detectors under large signals: non-uniform electric field due to drifting and trapped unipolar carriers *Journal of Physics D: Applied Physics* **52** 135104
[34] van der Kaap N J and Koster L J A 2016 Massively parallel kinetic Monte Carlo simulations of charge carrier transport in organic semiconductors *J Comput Phys* **307** 321-32
[35] Hoare C A R 1961 Algorithm 64: Quicksort *Commun. ACM* **4** 321
[36] Ianik Plante F A 2013 *Theory and Applications of Monte Carlo Simulations,* ed V W K Chan: InTech)

3 Corrections to the Hecht Collection Efficiency in Photoconductive Detectors under Large Signals: Non-Uniform Electric Field due to Drifting and Trapped Unipolar Carriers

Published as: Safa Kasap, Kieran Ramaswami, Kabir M.Z. and Robert Johanson, "*Corrections to the Hecht Collection Efficiency in Photoconductive Detectors under Large Signals: Non-Uniform Electric Field due to Drifting and Trapped Unipolar Carriers*", Journal of Physics D: Applied Physics, 2019.

Author contributions: In this work, the Safa Kasap contributed to the preparation of the manuscript, specifically in the writing of the introduction, experiment, problem definition and conclusion sections. Kabir Zahangir wrote the first half of the numerical section. Kieran Ramaswami wrote the Monte Carlo section and the analysis of the numerical method to Monte Carlo. Kabir Zahangir developed the numerical evaluation code. Kieran Ramaswami developed and ran the Monte Carlo simulations, ran the numerical evaluation, identified the resolution requirements of the numerical evaluation compared to the Monte Carlo method, fitted all data and created Figure 3.3 to Figure 3.10.

3.1 Abstract

The Hecht collection efficiency η_0 and its modified expressions for exponential absorption have been widely used in time-of-flight type transient photoconductivity experiments as well as in the assessment of the sensitivity of integrating-type radiation detectors. However, the equations apply under small signals in which the internal field remains uniform (unperturbed). We have used Monte Carlo simulation and the numerical solution of the continuity, trapping rate and Poisson equations to calculate the collection efficiency η_r (CCE) for various levels of charge injection and deep trapping. The carriers are injected instantaneously very near the radiation receiving electrode and then drift under space charge perturbed conditions. The CCE deviation from the ideal Hecht value has been quantified in terms of the injection ratio r and the normalized trapping time τ with respect to the transit time under small signals. The results can be represented by scaled, stretched exponential with coefficients that depend on τ. A plot is provided for these coefficients. The CCE drops significantly below the Hecht value as r increases and the deviation is more pronounced for smaller τ values. The errors in extracting τ from the application of the Hecht equation has been also calculated and mapped as a function of different r and τ values.

3.2 Introduction and the Problem

The Hecht collection efficiency (HCE) equation [1] has been widely used by researchers for two primary reasons. First is the extraction of the drift mobility μ and charge carrier lifetime (or the deep trap capture time) τ' product, known as the carrier range, from time-of-flight (TOF) transient photoconductivity (TP) experiments; there are several well-known papers dating back to the fifties in which the carrier trapping time was extracted from TOF measurements. The second reason is the evaluation of the sensitivity of a radiation detector operating in the integration mode, *i.e.* the

transient photocurrent $i(t)$ induced by an absorbed dose of radiation is integrated to find the collected charge Q_c. The sensitivity is then Q_c per unit incident radiation dose and per unit area of the detector. If some of the charge carriers become trapped during their drift, then the HCE plays an important role in controlling the sensitivity [2-4]. In the latter case, the HCE has been modified to account for the exponential photogeneration of both electrons and holes and their subsequent drift, which includes trapping, and collection. If carrier ranges can be measured independently, as in the case of a-Se based photoconductors, the x-ray sensitivity can be readily predicted [2]. There are several important very recent examples in which the HCE has been used, one way or another, to relate the collected charge to the carrier $\mu\tau'$ products or vice versa [5-17]. It should be emphasized that in all cases there is a tacit assumption that small signal conditions are maintained *i.e.* the space charge of the photogenerated carriers can be neglected. The collection efficiency (CCE) calculations in the presence of bulk space charges, including ionized dopants and trapped carriers, involves the numerical or simulated solution of the continuity, semiconductor rate and Poisson equations; we need to find the spatial distribution of the field and carrier distribution from which the transient current and hence Q_c and CCE can be calculated. Some examples that consider a nonuniform field and use numerical computations or approximations, can be found in references [16, 18-25]. A semi-analytical treatise and full numerical solutions for the x-ray sensitivity of a-Se under large signals were given in reference [20].

The objective of this work is to provide a quantitative assessment of the accurateness of, and hence the errors in, the HCE equation as small signal conditions are violated and the injected charge Q_i becomes comparable or equal to the charge Q_0 on the electrodes. We assume that the bulk is initially space charge free but once carriers are injected, the bulk has space charge due to the drifting injected carriers and due to trapped carriers left behind as the packet drifts. We use both Monte Carlo (MC) simulation (as described in [19, 26] but for a single level of trapping) and numerical solutions of the continuity and Poisson equations as a comparison (as described in [20, 21] but without the electrons and trap filling effects)

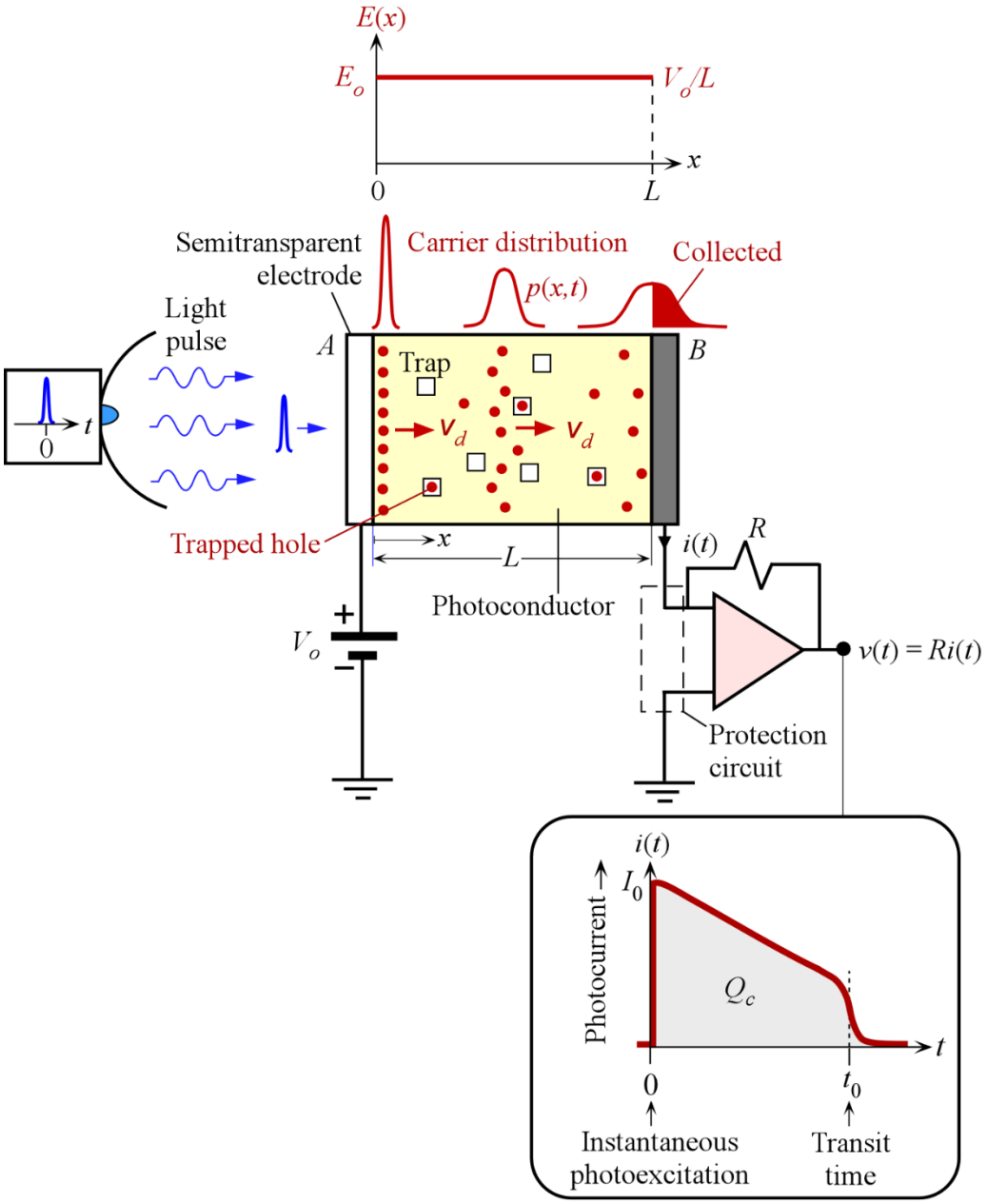

Figure 3.1: A TOF type TP experiment for unipolar charge carrier drift. The photoexcitation is near the surface and is assumed to be within an infinitesimally thin depth. The drifting holes experience diffusion as well as deep trapping. The op amp configured as a current-to-voltage transconductor detects the induced external photocurrent and has a negligible input impedance. The field in the sample is assumed to be uniform.

3.3 The Experiment

Consider the TOF experiment shown in Figure 3.1 where a photoconductor of thickness L is sandwiched between two electrodes, A and B, where A is semitransparent. An infinitesimally short light pulse is absorbed inside a photoconductor just under the positive electrode (A) so that the

electrons are immediately collected and the holes drift towards the negative electrode (*B*). The ratio of the photoinjected charge (holes) Q_i to the charge Q_0 on the electrode (prior to injection and given by CV_0, where *C* is the sample capacitance) is defined as the *injection ratio r*. If $r << 1$, the field in the photoconductor remains practically unperturbed and equal to $E_0 = V_0/L$, which defines the *small signal* case. (In reality, the field can never be unperturbed. Indeed, it is the rate of change of perturbation in field at the electrodes that causes an external transient current.) The photoinjected carrier packet is drifted by the field and generates an external current $i(t)$, which can be measured. As the photoinjected carrier packet distribution $\rho(x,t)$ drifts towards *B*, it also experiences trapping and diffusion as shown in Figure 3.1. We neglect diffusion. The time it takes for the mean of $\rho(x,t)$ to reach *B* is called the *transit time* t_0, and, for $r << 1$, $t_0 = \mu E_0/L$. If Q_c is the collected charge (integration of the observed photocurrent), the HCE is [1]

$$\eta_0 = \frac{Q_c}{Q_i} = \frac{\mu\tau' E_0}{L}\left[1-\exp\left(-\frac{L}{\mu\tau' E_0}\right)\right] = \tau\left[1-\exp\left(-\frac{1}{\tau}\right)\right] \qquad (3.1)$$

where $\tau = \tau'/t_0 = L/\mu\tau' E_0$ and $\mu\tau' E_0$ is the carrier schubweg, the mean travel distance of a charge carrier until trapping. The experimental examination of η_0 vs E_0 using (3.1) would then yield the $\mu\tau'$ product; again, assuming small signals. The greatest advantage of (3.1) is that η_0 does not depend on Q_i/Q_0 or *r*. Consequently, we can represent any complicated photoexcitation process in time as a summation of delayed delta excitations with appropriate magnitudes and for each delta-excitation we can use (3.1) and thereby construct the collected charge – the basic virtue of linear systems (Q_c depends linearly on Q_i). Once the small signal condition is lost, (3.1) develops a dependence on *r*, and we lose the greatest advantage of linear systems.

3.4 The Problem

The problem loses its analytical tractability once the internal field is perturbed, that is, the injected charge becomes comparable with Q_0. Consider an injected carrier distribution that is rectangular with a width w_o as in Figure 3.2. The field at the front (x_1) and rear (x_2) ends of the carrier packet experience E_1 and E_2, where $E_1 > E_2$. The photocurrent $i(t)$ that flows is driven by a combination of the applied field E_0 and the perturbing field E_i and hence is often called *space charge perturbed* (SCP) photocurrent; and have been analyzed by Papadakis [27] and Mirchina and Peled [28]. The case that corresponds to full injection in which the photoinjected charge Q_i is the same as the charge Q_0 on the electrode represents the space charge limited case; in a different form in which suddenly a step-bias is applied, has been treated as a space charge limited transient current by Many and Rakavy [29]. As distribution $\rho(x,t)$ drifts, the fields E_2 and E_1 change, and these changes lead to the observed external current. Since x_2 drifts more slowly than x_1, the packet widens; it become dispersed. The dispersion can be very significant at high injection, which means that some carriers spend more time in the detector and hence are more likely to be trapped. The CCE then becomes smaller than the small-signal case in (3.1). The SCP photocurrent $i(t)$ in a trap-free solid rises and reaches a peak at time t_1 after which extraction begins. From t_1 onwards, $i(t)$ falls rapidly

and at a time t_2 (the transit time of the rear-edge of the packet) it reaches zero where $t_2 > t_0$ as shown in Figure 3.2 for r =0.5, $t_2/t_0 \approx 1.76$.

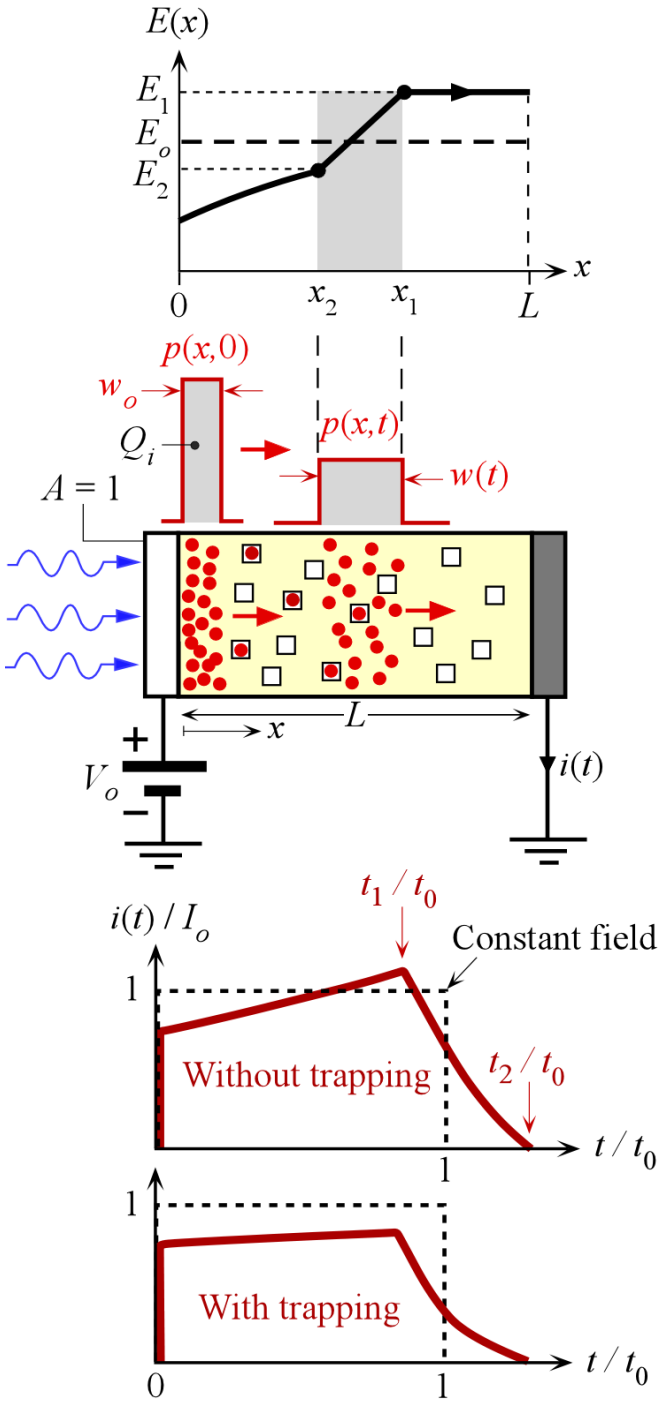

Figure 3.2: Unipolar photo injection at time $t = 0$ with a rectangular hole concentration distribution $\rho(x,0)$ with initial width w_o. The holes drift and the distribution become broader. The fields in front and behind the distribution are E_1 and E_2 respectively. The photocurrents with and without trapping are also shown

3.5 Computational Techniques

3.5.1 Monte Carlo Simulation

Monte Carlo (MC) simulations were carried out by generating particles (holes) distributed uniformly in $0 < x < w_o$ using a random number generator and setting $w_o = 0.0001L$. The total number of particles is N (50,000 used). Each particle, labelled by a unique n from 1 to N, is tagged and followed as it drifts. We know the carrier's position x'_n, where x' is the set of N carriers, along the x axis and its state, whether it is free or captured. The time domain of interest, $2t_0$, is divided into small steps of Δt (2,000 used). For each carrier n, we generate a capture time τ_n from $\tau_n = -\tau' \ln(X)$ where X is a random number between 0 and 1. The mean capture time, τ', was evaluated from 0.001 to 10 in 20 equal logspace intervals. If for a particle n, $\tau_n < t$, particle n is captured and is removed from drift but kept in the Poisson equation.

The MC cannot realistically use rQ_o/e number of particles but instead uses N. We therefore use a scaling factor $S = rQ_o/eN$ and assign a charge rQ_o/N to each MC particle. At each Δt step, we calculate the field $E(x,t)$ by integrating the Poisson equation, *i.e.*

$$E(x,t) = \left(\frac{Se}{\varepsilon}\right)\sum_{n=1}^{N}\begin{Bmatrix} 1 & \text{if } (x'_n \le x) \cap (x'_n < L) \\ 0 & \text{else} \end{Bmatrix} + C(t) \tag{3.2}$$

where ε is permittivity of the medium, $C(t)$ is an integration constant at time t that is found from the boundary condition over L,

$$\int_0^L E(x, t-\Delta t)dx = V_o \tag{3.3}$$

$$C(t) = E_0 - \overline{E(t-\Delta t)} + C(t-\Delta t) \tag{3.4}$$

where $\overline{E(t-\Delta t)}$ is the field averaged over x. The sampling of E is done at each particle position. Each particle n at the location x'_n drifts with a velocity

$$v_n(x'_n) = \mu E(x'_n) \tag{3.5}$$

The current $i(t)$ is calculated from the Shockley-Ramo theorem

$$i(t) = \frac{eS}{L}\sum_{\text{All}\,n} v_n = \frac{eS}{L}\sum_{\text{All}\,n} \mu E_n \tag{3.6}$$

The collected charge is then the integration of (6), $Q_c = \int i(t)dx$, up to a convenient end, *e.g.* $2t_0$.

3.5.2 Numerical Solution of Differential Equations

For a numerical solution, the physical modeling of the problem involves the continuity equation, rate equation (where ρ_t is the trapped carrier concentration) and the Poisson equation

$$\frac{\partial \rho}{\partial t} = -\mu \frac{\partial(\rho E)}{\partial x} - \frac{\rho}{\tau'} \tag{3.7}$$

$$\frac{\partial \rho_t}{\partial t} = \frac{\rho}{\tau'} \tag{3.8}$$

$$\frac{\partial E}{\partial x} = \frac{e(\rho + \rho_t)}{\varepsilon} \tag{3.9}$$

In the latter equations, ρ, ρ_t and E are space and time dependent. Trap filling effects and saturation are neglected. The initial and boundary conditions are:

$$\left\{ \begin{array}{c} \rho(0,t) = 0, \text{ if } t > 0 \\ \rho(x,0) = \dfrac{rQ_o}{ew_0}, \text{ if } x \le w_0 \text{ else } 0 \\ \int_0^L E(x,t)dx = V_o \end{array} \right\} \tag{3.10}$$

The partial differential equations above were solved by using the backward Euler technique in which the space-time (x,t) domain is divided into a sufficiently fine mesh until the results converged and produced reasonably accurate $\rho(x,t)$, $E(x,t)$ and $\rho_t(x,t)$. Numerical solutions were done to verify MC simulations and the agreement was excellent; in all cases, the results were within 0.5% for the resulting currents (Figure 3.3 (a)) for no trapping and $\tau = 0.5$ with $r = 0.5$, but only when 200,000 time-steps (N_t) where used per transit time and 5,000,000 position steps (N_x) over L as shown in Figure 3.4, independent of τ and r. Figure 3.3 (b) and (c) show SCP photocurrents under large injection (r = 0.5, 1.0), without and with trapping, corresponding to τ = 1. The large number of steps significantly increased the computation time compared to the MC method resulting in the primary use of MC in this work.

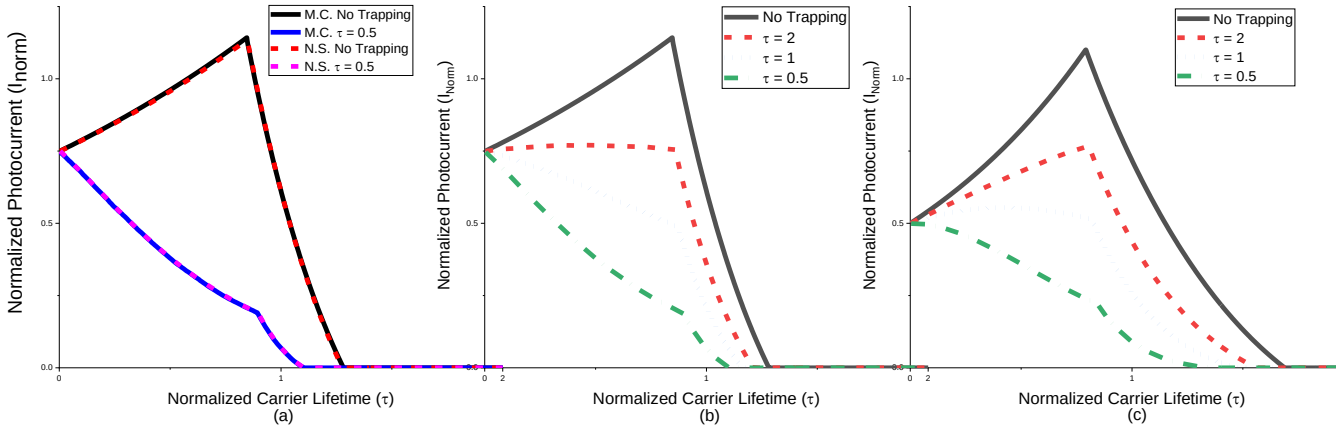

Figure 3.3: (a) Typical SCP TOF photocurrents with Numerical Simulation (N.S.) and Monte Carlo (M.C.) without and with ($\tau = 0.5$) at r = 0.5, (b) M.C. without and with (τ = 0.5, 1, and 2) trapping and injection r = 0.5. (c) M.C. without and with (τ = 0.5, 1, and 2) trapping and injection r = 1.0

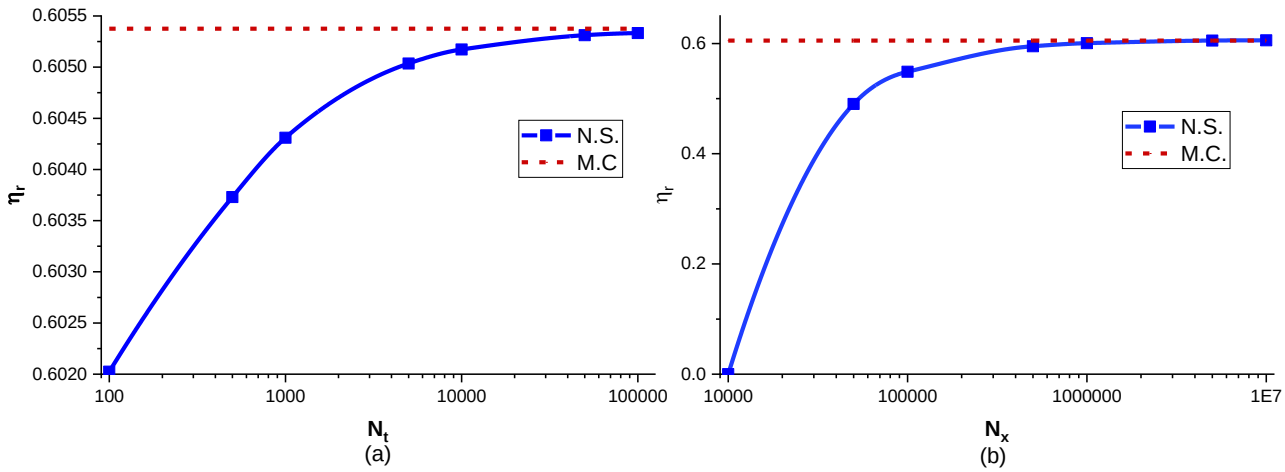

Figure 3.4: Comparison of Numerical Simulation (N.S.) accuracy to Monte Carlo vs. simulation mesh size at $\tau = 1$, $r = 0.5$ (Akima spline used). N_t is the number of time steps and N_x is the number of position steps. (a) 5 million position steps used. (b) 200,000 time steps used.

3.6 Results and Discussion

Figure 3.3 (b) and (c) show SCP photocurrents under large injection (r = 0.5, 1.0), without and with trapping, corresponding to $\tau = 1$. The trap-free solid SCP photocurrent is typical and has been already derived [27]. With sufficient trapping, the photocurrent rise is lost, and the photocurrent decays as in Figure 3.3; but the shape cannot be used to extract τ as in the small signal case. The trapping of carriers reduces the photocurrent rise before transit. The carrier distribution $\rho(x,t)$ without and with trapping remains rectangular (not shown) and the trapped carrier distribution profiles for r = 0.5 and $\tau = 1$ at various times are shown in Figure 3.5. As expected $\rho_t(x,\infty)$ decays with distance into the photoconductor, seemingly exponentially.

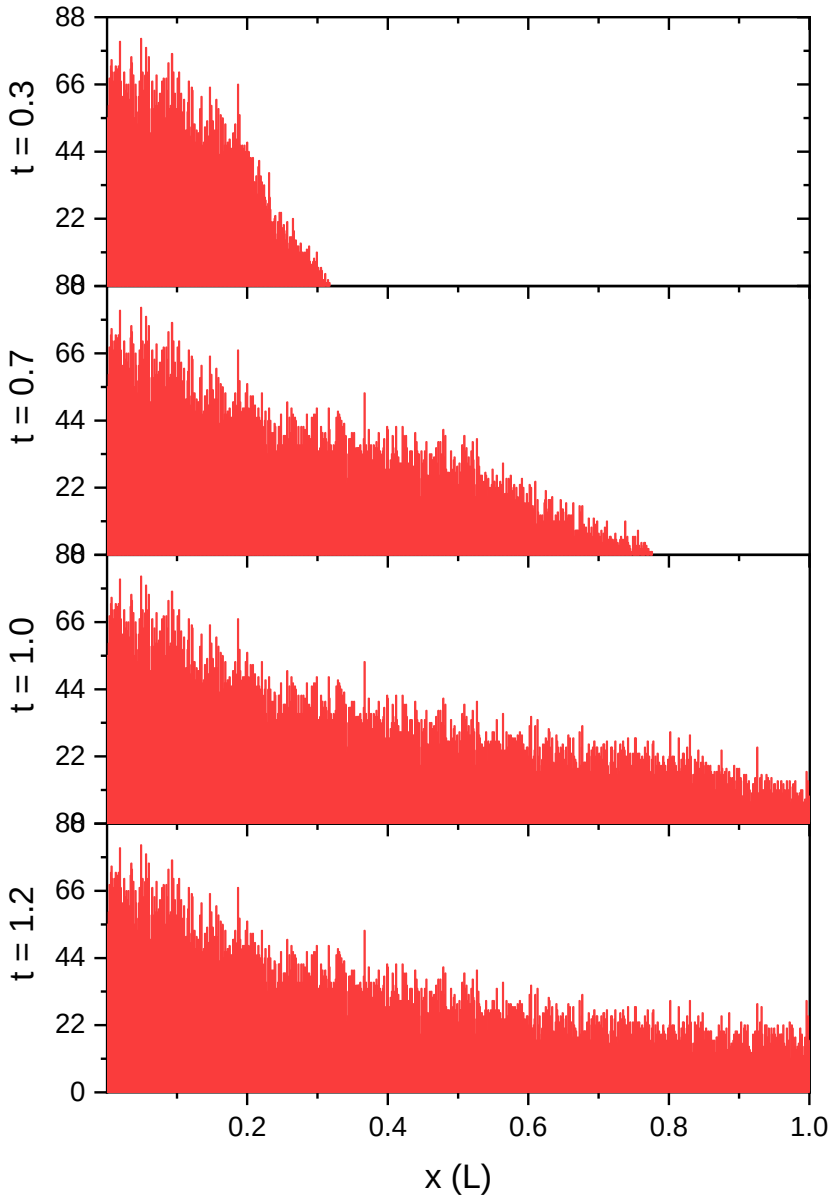

Figure 3.5: Trapped carrier distribution along the photoconductor at various times (normalized to weak-injection transit time) from MC simulations at $r = 0.5$ and $\tau = 1$.

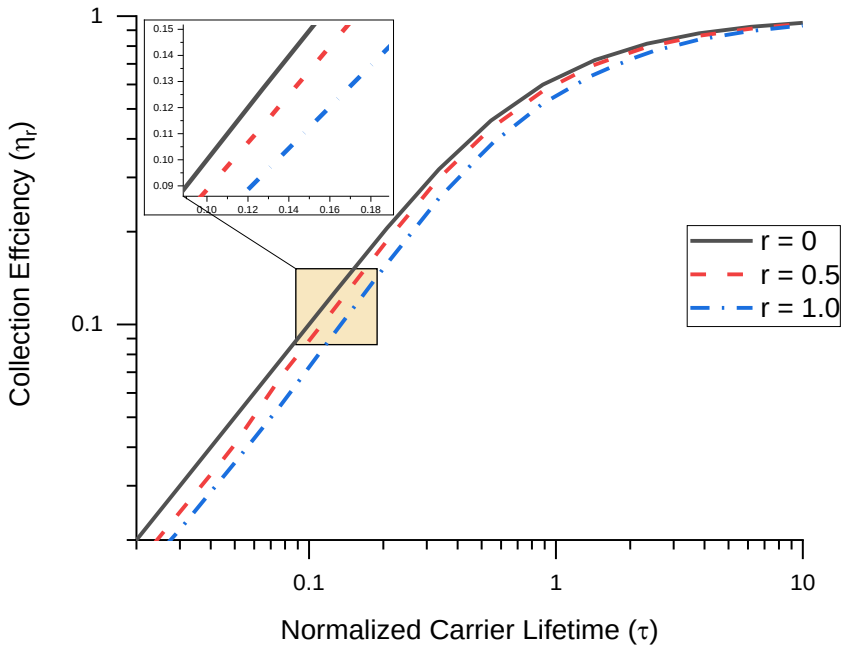

Figure 3.6: CCE η_r vs normalized lifetime τ under small signals and r = 0.5 and r = 1.0

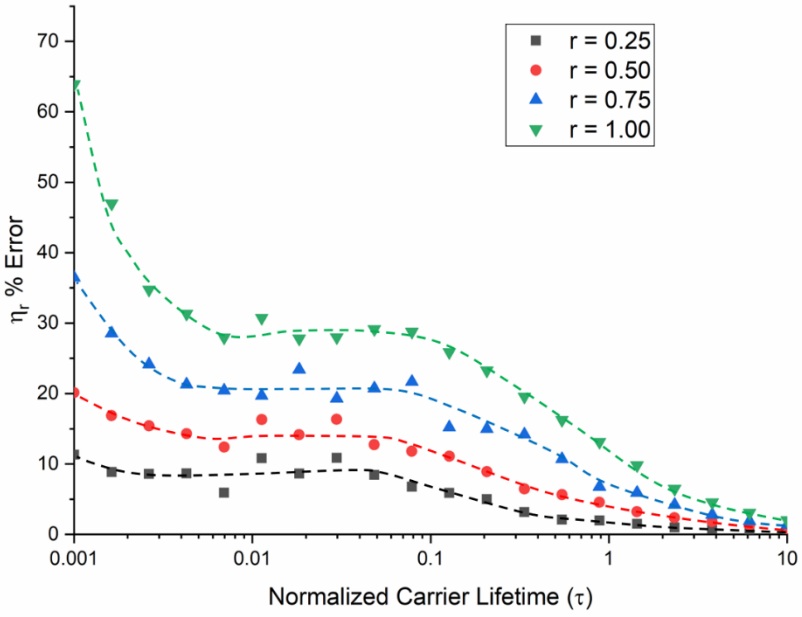

Figure 3.7: η_r % Error vs normalized lifetime τ for different injection levels. (Dashed curves are guides to the eye and not any particular function)

The calculation of collected charge is straightforward because we can integrate the SCP photocurrents in Figure 3.3 for various values of τ and r. Figure 3.6 shows the plot of the collection efficiency η_r vs. normalized trapping time τ for various values of r. This type of plot is typically used to extract $\mu\tau'$ in experimental work assuming small signals. The experimenter increases the

field, which decreases t_0 so that τ becomes longer, and the CCE increases. Notice the significant effect of r on the value and shape of the CCE. We can assess the deviation from the small signal case in (3.1) by plotting the % change in the collection efficiency (η_r % Error) $100(\eta_0-\eta_r)/\eta_0$ vs τ for various injection ratios r as in Figure 3.7 and η_r/η_0 vs r for various values of τ as in Figure 3.8. For small r, η_r % Error is initially 0 but increases as r increases and as τ decreases. 0.09999546 For example, for $\tau = 0.886$, and $r = 1$, $\eta_0-\eta_r$ is 0.0786, *i.e.* a drop of 13 % from the ideal HCE as shown in Figure 3.9 (a). From (3.1) we can show that:

$$\frac{\delta\tau}{\tau} = \frac{\delta\eta_0}{\eta_0}\left[\frac{1}{\tau} - \frac{1}{\eta_0} + 1\right]^{-1} \tag{3.11}$$

Consider, as an example, $\tau = 0.886$ and $r = 0.5$. From Figure 3.8, $\eta_r - \eta_0 \approx -0.0274$ so that $\delta\eta_0/\eta_0 \approx 0.0456$ and from (3.11), the error in τ, $\delta\tau/\tau = 0.099$ or 9.9%. At r =1, this error is 28.5% for τ = 0.886, and 40.8% for τ = 10. Clearly, the errors involved in extracting the carrier range can be significant under large signals and increase with τ. Figure 3.9 (b) shows the error in τ determination as a function of τ and r.

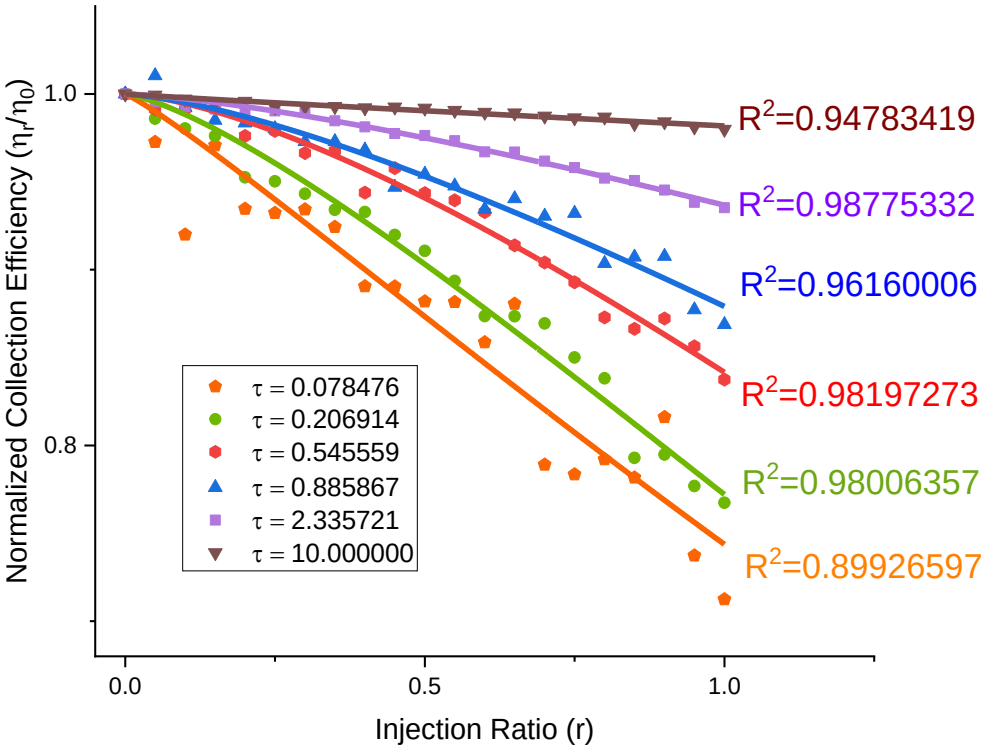

Figure 3.8: Normalized collection efficiency, NCE (η_r/η_0) vs. injection ratio r at various normalized trapping times

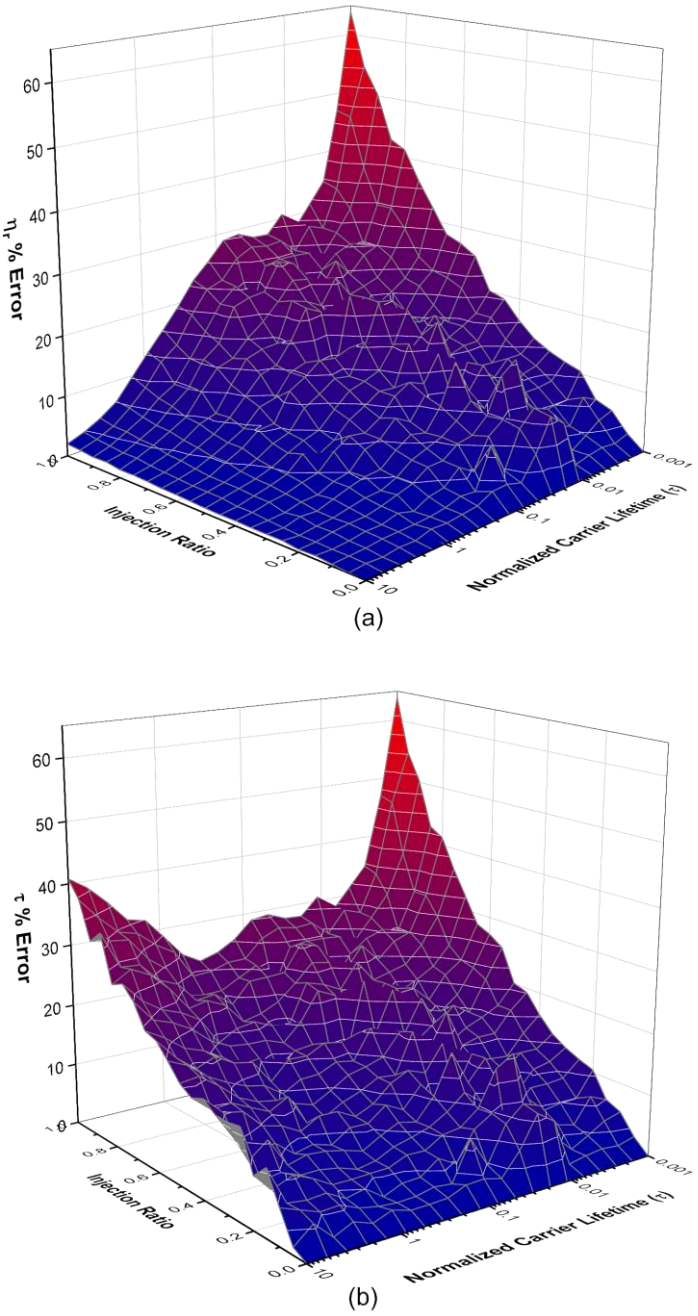

Figure 3.9: Percentage error of η_r (a) and τ (b) vs. r and τ

From Figure 3.8 (y-axis normalized) we can easily fit a scaled and compressed exponential function to the CCE results so that:

$$\eta_r = \eta_0 e^{-\alpha r^{\beta}} \tag{3.12}$$

where α and β are coefficients that depend only on τ, not on the injection ratio r.

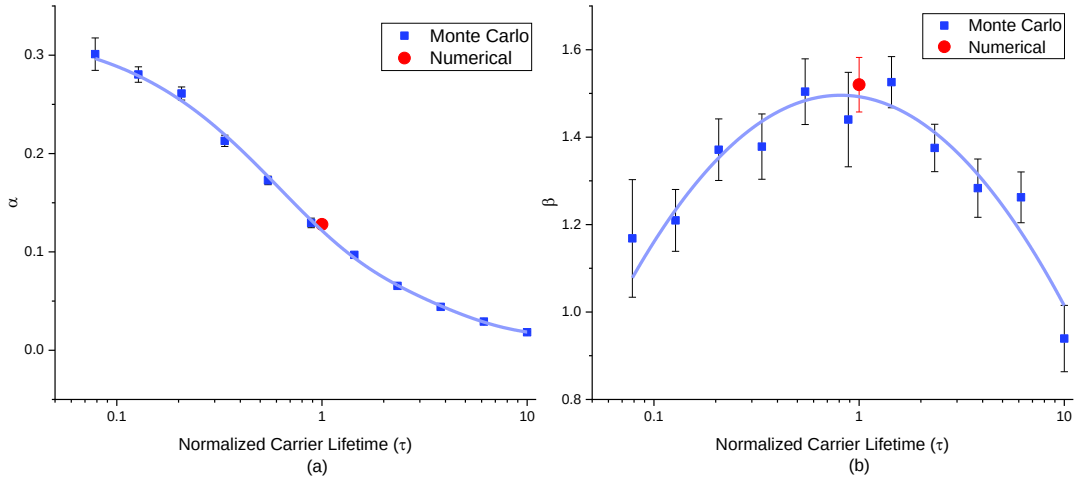

Figure 3.10: α and β coefficient vs. normalized trapping times τ

The τ dependences of the coefficients α and β with standard error bars are in Figure 3.10 (a) and (b), respectively. The data for these plots were generated with MC with a comparison point using a numerical solution method. These plots allow for corrections to be made or errors to be estimated when the small-signal HCE is used to extract carrier ranges when the injected charge perturbs the field. In the range of $\tau = 0.1$ to 10, fits of α and β have been made to:

$$\alpha(\tau) = A_0 + A_1 e^{-\frac{\tau}{T_1}} + A_2 e^{-\frac{\tau}{T_2}} \tag{3.13}$$

$$\beta(\tau) = B_0 + B_1 \log(\tau) + B_2 \log(\tau)^2 \tag{3.14}$$

where the A_0, A_1, A_2, B_0, B_1, B_2, T_1 and T_2 are constants determined by fitting as in Figure 3.10 and presented in Table 3.1. It should be noted that β has the largest magnitude around $\tau \sim 1$ and that error in α increased as τ approached Δt. The fit of α can be explained as τ decreases, the average particle has less free time to be affected by correlation. β shows the balance between τ and L, where the longer the particles are free the greater effect correlation will have on them, but if the particles are free past the transit time, they are more likely to be collected, no matter the injection ratio. These two properties lead to β have a maximum at $\tau \approx 1$, and most likely explain the inflection point of a, being also around $\tau \sim 1$. These two values suggest that if correlation effects are to be reduced in detector design that τ should be kept at least an order of magnitude away from $\tau \sim 1$.

Table 3.1: Coefficients of (3.13) and (3.14)

	Value	Standard Error
A_0	0.0145	0.0018
A_1	0.2084	0.0112
T_1	0.5287	0.0607
A_2	0.105	0.0105
T_2	3.0732	0.3638
B_0	1.4925	0.028
B_1	-0.0729	0.0297
B_2	-0.4051	0.0544

3.7 Conclusions

In summary, the collection efficiency in an integrating detector, or in a time-of-flight type transient photoconductivity experiment, under large signals deviates significantly from the well-known Hecht collection efficiency in (3.1). We have used Monte Carlo simulations and the numerical solution of the continuity, semiconductor rate and Poisson equations to calculate the collection efficiency (CCE). The deviation has been quantified in terms of the injection ratio r and normalized trapping time τ in Figure 3.6 - Figure 3.9. The CCE goes over into the HCE in (3.1) under small signals but drops significantly below HCE as r increases. The errors in extracting τ from the application of (3.1) can be very high (in some cases 40% or more) and may be estimated from Figure 3.9 and (3.11) or (3.12), the coefficients in Figure 3.10(a) and Figure 3.8(b) and the fits of the coefficients in (3.13) and (3.14).

3.8 Acknowledgements

The authors thank NSERC Discovery Grants Program and the University of Saskatchewan, Centennial Enhancement Chair funding for financial support. The MC simulations form part of the MSc thesis of Kieran Ramaswami.

3.9 References

[1] Hecht K 1932 For the mechanism of the photoelectric primary current in insulating crystals. *Z Phys* **77** 235-45

[2] Kasap S O 2000 X-ray sensitivity of photoconductors: application to stabilized a-Se *J Phys D Appl Phys* **33** 2853-65

[3] Kabir M Z and Kasap S O 2002 Charge collection and absorption-limited sensitivity of x-ray photoconductors: Applications to a-Se and HgI2 *Appl Phys Lett* **80** 1664-6

[4] Kabir M Z and Kasap S O 2002 DQE of photoconductive x-ray image detectors: application to a-Se *J Phys D Appl Phys* **35** 2735-43

[5] Street R A, Wong W S and Lujan R 2009 Low-temperature amorphous silicon p-i-n photodiodes *Phys Status Solidi B* **246** 1854-7

[6] Long Q, Dinca S A, Schiff E A, Yu M and Theil J 2014 Electron and hole drift mobility measurements on thin film CdTe solar cells *Appl Phys Lett* **105** 042106

[7] Guo R R, Jie W Q, Wang N, Zha G Q, Xu Y D, Wang T and Fu X 2015 Influence of deep level defects on carrier lifetime in CdZnTe:In *J Appl Phys* **117**

[8] Fang Y J, Dong Q F, Shao Y C, Yuan Y B and Huang J S 2015 Highly narrowband perovskite single-crystal photodetectors enabled by surface-charge recombination *Nat Photonics* **9** 679-89

[9] Wei H T, Fang Y J, Mulligan P, Chuirazzi W, Fang H H, Wang C C, Ecker B R, Gao Y L, Loi M A, Cao L and Huang J S 2016 Sensitive X-ray detectors made of methylammonium lead tribromide perovskite single crystals *Nat Photonics* **10** 333-9

[10] Dirin D N, Cherniukh I, Yakunin S, Shynkarenko Y and Kovalenko M V 2016 Solution-Grown CsPbBr3 Perovskite Single Crystals for Photon Detection *Chem Mater* **28** 8470-4

[11] Maynard B, Long Q, Schiff E A, Yang M J, Zhu K, Kottokkaran R, Abbas H and Dalal V L 2016 Electron and hole drift mobility measurements on methylammonium lead iodide perovskite solar cells *Appl Phys Lett* **108** 173505

[12] Kim Y C, Kim K H, Son D Y, Jeong D N, Seo J Y, Choi Y S, Han I T, Lee S Y and Park N G 2017 Printable organometallic perovskite enables large-area, low-dose X-ray imaging *Nature* **550** 87-91

[13] Semeniuk O, Grynko O, Decrescenzo G, Juska G, Wang K and Reznik A 2017 Characterization of polycrystalline lead oxide for application in direct conversion X-ray detectors *Sci Rep-Uk* **7**

[14] Kosyachenko L A, Aoki T, Lambropoulos C P, Gnatyuk V A, Melnychuk S V, Sklyarchuk V M, Grushko E V, Maslyanchuk O L and Sklyarchuk O V 2013 Optimal width of barrier region in X/gamma-ray Schottky diode detectors based on CdTe and CdZnTe *J Appl Phys* **113**

[15] Boothman V, Alruhaili A, Perumal V, Sellin P, Lohstroh A, Sawhney K and Kachanov S 2015 Charge transport optimization in CZT ring-drift detectors *J Phys D Appl Phys* **48**

[16] Semeniuk O, Grynko O, Decrescenzo G, Juska G, Wang K and Reznik A 2017 Characterization of polycrystalline lead oxide for application in direct conversion X-ray detectors *Sci Rep-Uk* **7** 8659
[17] Shrestha S, Fischer R, Matt G J, Feldner P, Michel T, Osvet A, Levchuk I, Merle B, Golkar S, Chen H W, Tedde S F, Schmidt O, Hock R, Ruhrig M, Goken M, Heiss W, Anton G and Brabec C J 2017 High-performance direct conversion X-ray detectors based on sintered hybrid lead triiodide perovskite wafers *Nat Photonics* **11** 436-40
[18] Kubicki T, Lubelsmeyer K, Ortmanns J, Pandoulas D, Syben O, Toporowsky M and Xiao W J 1994 Calculation of the Electric-Field in Gaas Particle Detectors *Nucl Instrum Meth A* **345** 468-73
[19] Yunus M, Kabir M Z and Kasap S O 2004 Sensitivity reduction mechanisms in amorphous selenium photoconductive x-ray image detectors *Appl Phys Lett* **85** 6430-2
[20] Kabir M Z, Emelianova E V, Arkhipov V I, Yunus M, Kasap S O and Adriaenssens G 2006 The effects of large signals on charge collection in radiation detectors: Application to amorphous selenium detectors *J Appl Phys* **99**
[21] Kabir M Z, Chowdhury L, DeCrescenzo G, Tousignant O, Kasap S O and Rowlands J A 2010 Effect of repeated x-ray exposure on the resolution of amorphous selenium based x-ray imagers *Med Phys* **37** 1339-49
[22] Uxa S, Grill R and Belas E 2013 Evaluation of the mobility-lifetime product in CdTe and CdZnTe detectors by the transient-current technique *J Appl Phys* **114**
[23] Zanichelli M, Santi A, Pavesi M and Zappettini A 2013 Charge collection in semi-insulator radiation detectors in the presence of a linear decreasing electric field *J Phys D Appl Phys* **46**
[24] Li H Y, Duan L, Li C, Wang L D and Qiu Y 2014 Transient space-charge-perturbed currents in organic materials: A Monte Carlo study (vol 15, pg 524, 2014) *Org Electron* **15** 524-30
[25] Williams M L and Donnelly I J 1996 An investigation of electric field behaviour in semi-insulating GaAs using current pulses *J Phys D Appl Phys* **29** 1997-2003
[26] Koughia K, Shakoor Z, Kasap S O and Marshall J M 2005 Density of localized electronic states in a-Se from electron time-of-flight photocurrent measurements *J Appl Phys* **97**
[27] Papadakis A C 1967 Theory of Transient Space-Charge Perturbed Currents in Insulators *J Phys Chem Solids* **28** 641-7
[28] Mirchina N R and Peled A 1996 Time of flight analysis of charge transport in insulators for a finite width charge packet with trapping *Solid State Electron* **39** 1205-11
[29] Many A and Rakavy G 1962 Theory of Transient Space-Charge-Limited Currents in Solids in Presence of Trapping *Phys Rev* **126** 1980-8

4 Charge Collection Efficiency in Photoconductive Detectors under Small to Large Signals

Published as: Kieran Ramaswami, Robert Johanson and Safa Kasap, "*Charge Collection Efficiency in Photoconductive Detectors under Small to Large Signals*", Journal of Applied Physics, 2019.

Author contributions: In this work, all programing, data generation, analysis and manuscript writing was done by Kieran Ramaswami. Safa Kasap and Robert Johanson contributed in the preparation of the manuscript.

4.1 Abstract

Hecht collection efficiency η_0 and its formulations for exponential absorption have been widely used in modeling charge collection efficiency in photoconductive detectors. The basic assumption of the Hecht formulation is that the electric field in the device is uniform i.e. the photoinjected carriers do not perturb the field. Here we have used Monte Carlo simulations to model the initial injection of electron and hole pairs and their subsequent transport and trapping in the presence of an electric field, which is calculated from the Poisson equation. Each injected carrier is tracked as it moves in the semiconductor until it is either trapped or reaches the collection electrode. Trapped carriers do not contribute to the photocurrent but continue to contribute to the field through the Poisson equation. The instantaneous photocurrent $i_{ph}(t)$ is calculated from the drift of the free carriers through the Shockley-Ramo theorem. $i_{ph}(t)$ is integrated over the duration of the photocurrent to calculate the total collected charge and hence the collection efficiency η_r. η_r has been calculated as a function of the charge injection ratio r, the electron and hole ranges (drift mobility and lifetime products, $\mu\tau$), mean photoinjection depth δ and drift mobility ratio b. The deviation of the collection efficiency η_r from the uniform field case η_0 can be as much as 30% smaller than the small signal model prediction. However, for a wide range of electron and hole schubwegs and photoinjection ratios, the typical error remained less than 10% at full injection, the worst case. The present study provides partial justification to the wide-spread use of the uniform field collection efficiency η_0 formula in various applications, even under high injection conditions.

4.2 Introduction and the Definition of the Problem

Photoconductive detectors are widely used in several commercial radiation detection and imaging applications. In many of the applications, the photocurrent generated by the incident radiation is integrated to measure the collected charge per incident amount of radiation, for example, per unit exposure to x-rays. The collected charge vs incident dose (in air) represents the responsivity of the detector. Whether the detector is a discrete device or one of the pixels in an imaging array, the collected charge Q_c is not necessarily identical to the total injected charge Q_i that is generated by the absorbed radiation within the detector volume of interest, due to carrier trapping and recombination effects in the semiconductor. Figure 4.1 illustrated the cross section of a semiconductor with electrodes A and B across which a voltage V_0 is applied and the field is E_0 =

V_0 / L and uniform. The detector in Figure 4.1 has noninjecting contacts (at *A* and *B*) so that the dark current is ideally zero. The situation depicted could easily represent the practical case of using a reverse biased *pin* photodetector. In the *pin* detector, the p^+ and n^+ regions are very narrow so that the absorption and charge transport occurs almost totally in the wide *i*-layer[1]. In the ideal case, the field in the *i*-layer is uniform or has a small gradient. Under a reverse bias, p^+ and n^+ layer do not injected carriers and essentially act as noninjecting contacts even though the metal to semiconductor contacts on the p^+ and n^+ layers are injecting or ohmic contacts. Thus, the ideal *pin* detector corresponds to the case shown in Figure 4.1. (In practical *pin* detectors, the i-region has a small amount of doping and the field is not entirely uniform.)

The absorption of photons in the semiconductor follows an exponential distribution of the form $\exp(-\alpha x)$ where α is the absorption coefficient for optical photons or the linear attenuation coefficient for x-rays and gamma rays. The absorption of an optical photon will generate an electron hole pair (EHP) with some internal quantum efficiency, specific to the semiconductor medium. The x-ray photogeneration is described in [2] and involves the x-ray photon knocking out a primary electron from an inner shell of the host atom. The energetic projectile primary electron then ionizes the medium and generates a Q_i amount of charge. The electron and hole concentration profiles are shown in Figure 4.1 at time $t = 0$, which corresponds to the photogeneration time, and then a bit later when the two distributions have drifted and some of the carriers have been collected. It is assumed that the photogeneration, whether by optical or x-ray photons, occurs over a negligibly short time compared with the drift time scale of the carriers, and we can assume that the carrier distributions are initially exponential. At time $t = 0$, right after photogeneration, there is no net space charge in the bulk, and electric field remains uniform at $E_0 = V_0 / L$. As soon as the charges start drifting, the separation of the electron and hole distributions results in a net space charge density across the detector, and the field is not uniform with a spatial dependence given by the Poisson law at each instant. It is assumed that there are no previously trapped charges before injection i.e., the field is uniform before photoinjection.

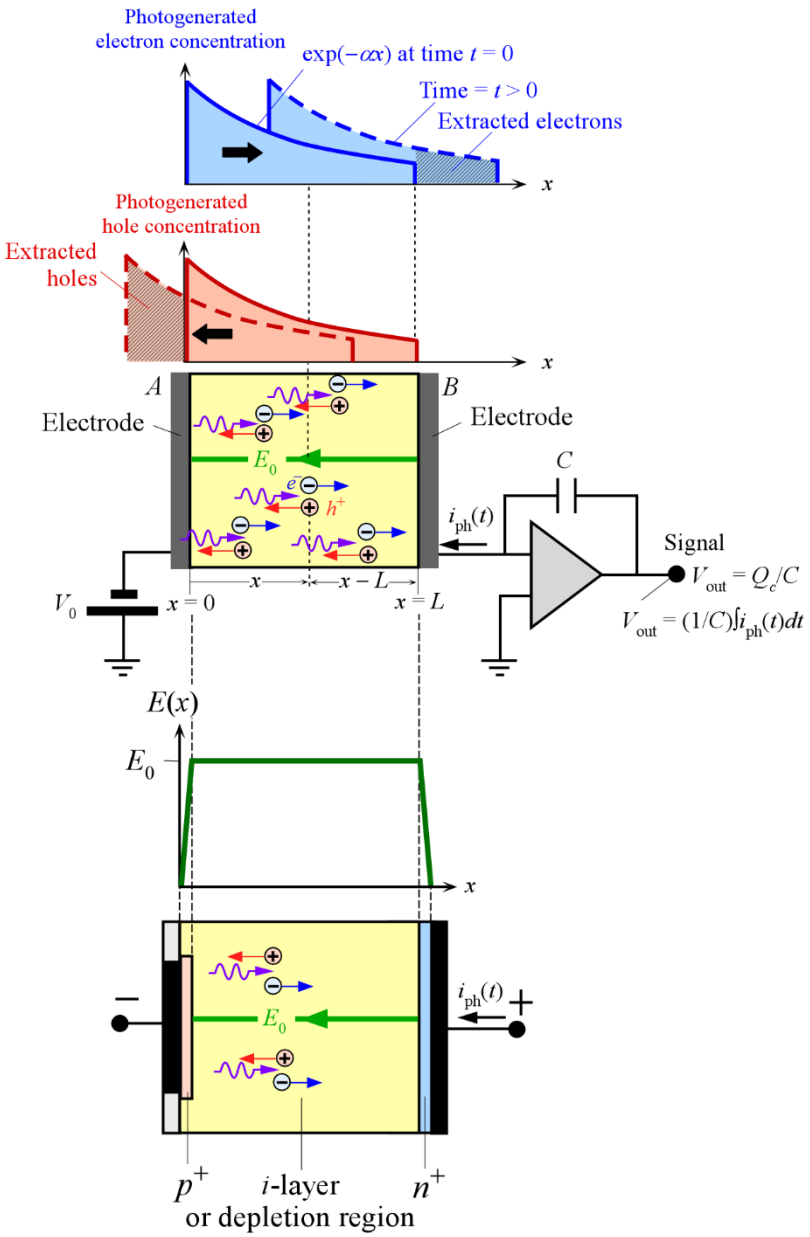

Figure 4.1: Electron and hole pair injection under an applied voltage. The EHPs are produced in a photoexcited semiconductor of length L. Both external and internal fields affect the drift of the EHPs.

As the electrons and holes drift toward their collection electrodes as shown in Figure 4.2, they induce an external photocurrent $i_{ph}(t)$, which can be calculated from the Shockley-Ramo theorem [3, 4]. Some of the carriers become trapped during their drift as illustrated in Figure 4.2. Thus, there is a decay in the external photocurrent $i_{ph}(t)$ due to trapping, and hence less charge is collected than injected: $Q_c < Q_i$. It should be apparent from Figure 4.2 that there are four contributions to the net space charge density $\rho_{net}(x,t)$ at any point x at any instant t: (a) trapped electrons, i.e., $n_t(x,t)$, (b) trapped holes, i.e., $p_t(x,t)$ (c) drifting electrons, i.e., $n(x,t)$, and (d) drifting, holes i.e., p (x,t).

Thus, the electric field is not uniform. The calculation of the photocurrent and the charge collection efficiency (CCE) becomes quite involved and one needs to seek numerical solutions to the continuity equation, trapping and recombination rate equations with trap filling as well as new trap generation, and Poisson's equation, as described, for example, in [5].

Most of the work on integrating detectors assume small signals and neglect the perturbation of the field by the above four factors. Assuming a uniform electric field, which is a good approximation under weak signals, the charge collection efficiency η_0 (subscript zero indicating small signals or uniform field), defined as Q_c/Q_i, can be written in terms of electron and hole collection efficiency as[2, 6-9]

$$\eta_0 = \eta_{0e} + \eta_{0h} \tag{4.1}$$

where the electron and hole CEs, η_{0e} and η_{0h} respectively, are given below. The electron CCE is

$$\eta_{0e} = \frac{Q_c^e}{Q_i^e} = \frac{s_e}{L}\left(1 - \frac{\left[\exp\left(-\frac{L}{s_e}\right) - \exp\left(-\frac{L}{\delta}\right)\right]}{\left[1-\exp\left(-\frac{L}{\delta}\right)\right]\left[\frac{\delta}{s_e} - 1\right]}\right) \tag{4.2}$$

in which the superscript e on Q refer to electrons, $s_e = \mu_e \tau_e E_0$ is the electron schubweg, μ_e is the electron drift mobility and τ_e is the electron trapping time or lifetime, and δ is the penetration depth ($1/\alpha$) of the photogeneration process (assumed to the same as photon attenuation depth) and L as the sample thickness. Schubwegs are defined for a uniform field, $E_0 = V_0/L$ which is a given operating condition.

The hole CCE is

$$\eta_{0h} = \frac{Q_c^h}{Q_i^h} = \frac{s_h}{L}\left(1 - \frac{\left[1-\exp\left(-\frac{L}{s_h} - \frac{L}{\delta}\right)\right]}{\left[1-\exp\left(-\frac{L}{\delta}\right)\right]\left[\frac{\delta}{s_h} + 1\right]}\right) \tag{4.3}$$

in which the superscript h on Q refer to holes where $s_h = \mu_h \tau_h E_0$ is the hole schubweg, μ_h is the hole drift mobility and τ_h is the hole lifetime. The reason we can write the CCE as in Equation (4.1) as the sum of electron and hole CEs is because the field is uniform, and we have ignored the recombination of oppositely charged drifting carriers and the recombination of drifting carriers with oppositely charged trapped carriers. Put differently, the continuity equation for holes is independent of the electron concentration, and similarly the continuity equation for electrons is independent of the holes[9]

The CCE in equations (4.1) to (4.3) have been widely used in formulating the sensitivity and the detective quantum efficiency of many detectors and is a key factor in the calculation of the sensitivity and detective quantum efficiency of direct conversion flat panel x-ray detectors [2, 8-17] . The distinct advantage in equations (4.1)–(4.3) is that the fact that η_0 does not depend on the

injected charge Q_i and hence one can use the linear system theory and apply the CCE above to any type of photogeneration process, whether it is a delta function or a pulse with a fixed duration. Secondly, the function η_0 is calculable and has a variance that is also calculable [7].

The scientific question we need to answer is this. What will be the errors when we calculate the CCE efficiency under large signals by using the small signal CCE (η_0)? How does the CCE depend on the amount of charge injected? Effectively, we are evaluating the usefulness of equations (4.1)–(4.3), and their limits. It will be shown that under large signals the CCE is less than the small signal case and the difference can be as much as 30% less. The work here is a follow-on from the work in which we considered only the injection of one type of carrier very near the radiation receiving electrode[18], for example electrons are suddenly injected at *A* in the detector in Figure 4.1. In this case the collection efficiency is simply the Hecht collection efficiency (HCE) [19] which is

$$\eta_0 = \frac{Q_c}{Q_i} = \frac{s_e}{L}\left[1 - \exp\left(-\frac{L}{s_e}\right)\right] \tag{4.4}$$

HCE is limited to near-surface EHP generation in which the carriers with the same polarity as the radiation receiving electrode drift to the collection electrode. It was shown that under large signals, the true CCE differs significantly from the HCE. An empirical expression was proposed to predict the CCE from the amount of injection (r). The CCE under EHP photogeneration with an exponential profile is referred to as the HCE with exponential distribution of carriers.

This work will examine the CCE under an initial exponential distribution for different amounts of charge injection into the semiconductor. We evaluate not only the errors involved in using equations (4.1)-(4.3) but also present the results in terms of the dependence of the CCE on charge transport parameters, absorption depth, and the relative amount of charge injection. Monte Carlo (MC) methods have been used as described previously [18] in which the Poisson equation is used with the four contributions to the net space charge density identified above. Thus, the model calculates the field at every small time interval as arising from the free charges on the electrodes (the applied field), concentrations of trapped electrons, $n_t(x,t)$ and holes $p_t(x,t)$, and the concentrations of drifting carriers, $n(x,t)$ and $p(x,t)$. The maximum amount of charge that can be injected is the charge residing on the electrodes, that is, $Q_0 = CV_0$ where C is the detector capacitance. The injection ratio $r = Q_i/Q_0$ and its maximum value is 1. The results are presented in terms of a parameter b that is commonly used for the drift mobility ratio i.e.

$$b = \frac{\mu_e}{\mu_h} \tag{4.5}$$

In addition, the definition of schubweg as $\mu\tau E_0$ for each carrier will be retained even though the field in the sample will not be uniform. It should be viewed as a charge transport property of the medium under a given field, had the field been uniform, V_0/L.

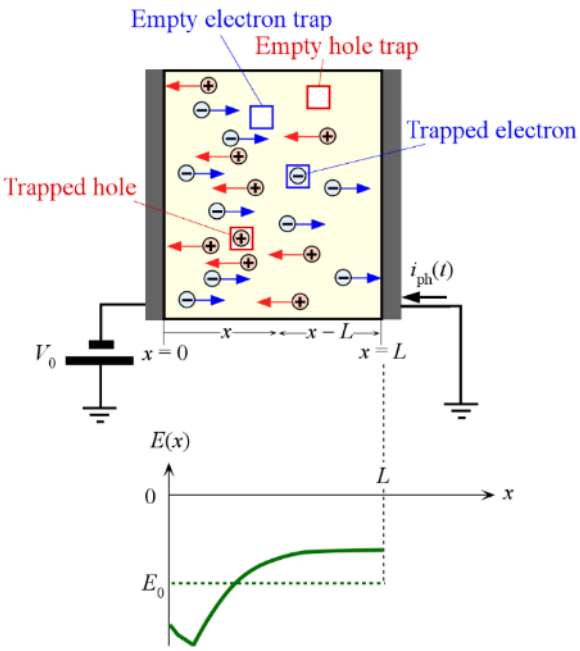

Figure 4.2: Electron hole pair injection with trapping and collection of charges under a voltage. The EHP are produced in a photoexcited semiconductor of length L, external and internal fields affect movement. This produces a current, i_{ph}, over time t that can be used to derive collection efficiency

4.3 Physical Model and the Monte Carlo Simulation

The Monte Carlo (MC) simulation technique in this work is an extension of the MC calculations described in reference[18] . The MC simulations were done with EHPs distributed exponentially. In this simulation, the initial absorption of photons and distribution of the photogenerated EHPs were not taken as a predefined truncated exponential function. Instead, the distribution was taken as a randomized truncated exponential to approximate exponential absorption $\exp(-\alpha x)$ while avoiding the loss of MC particles for large mean injection depths. Ideally, the number of EHPs to simulate would be $rQ_0/e = Q_i/e$ which is the number of charges on one of the electrodes, where e is the elementary charge and r is the ratio of the number of EHPs injected to Q_0. For the operation of a real detector, the actual number of injected EHPs involved would be too large to reasonably simulate. Therefore, an approximation is made using several scaled EHPs (N = 1000), with each scaled charge equal to $S = rQ_0/eN$ equivalent charges. Each photogenerated electron and hole, labeled by a unique n from 1 to N, is monitored as it drifts. The position and the state (whether free or trapped) of each electron and hole are monitored along the x-axis and in time. An index n is used as a particle identifier. A capture time τ_n from $\tau_n = -\tau \ln(X)$, where X is a random number from 0 to 1, is generated for each electron and hole separately. If at the time t, an electron or hole n has $\tau_n < t$, the electron or hole is trapped and no longer produces a current. These trapped charges are still considered in the Poisson equation as they contribute to the net space charge density in the bulk. During a time interval from t to $t + \Delta t$, the drift velocity of each free carrier at a position x is

calculated from the drift mobility and field product, $\mu_e E(x_e^n, t)$ for the electron at x_e^n and $\mu_h E(x_h^n, t)$ for the hole at x_h^n, where the superscript n is the particle identifier index defined above. The induced external photocurrent $i_{ph}(t)$ is then calculated from the Shockley-Ramo theorem,

$$i_{\text{ph}} = \frac{Se}{L}\sum_{n=1}^{N}\mu_e E(x_e^n, t) + \frac{Se}{L}\sum_{n=1}^{N}\mu_h E(x_h^n, t) \tag{4.6}$$

in which trapped carriers are excluded and both currents add in magnitude. The collected change Q_c and hence the collection efficiency CCE is

$$\text{CE} = \eta_r = \frac{Q_c}{Q_i} = \frac{1}{rQ_0}\int_0^T i_{\text{ph}}\, dt \tag{4.7}$$

where the upper time limit T corresponds to the time when all the carriers have been extracted.

Another quantity of interest is the uniform field transit time, which is represented by $t_0 = L/\mu_e E_0$.

The introduction of both holes and electrons into the semiconductor means that the Poisson equation at any point in time must include both electron and hole space charge densities whereas previously we only had one type of carrier[18]. The integration (summation) of the net space charge density gives the electric field, i.e.

$$\begin{aligned} E(x,t) = &\left(\frac{Se}{\varepsilon}\right)\sum_{n=1}^{N}\begin{Bmatrix} 1 & \text{if } (x_e^n \le x) \cap (x_e^n < L) \\ 0 & \text{else} \end{Bmatrix} \\ &- \left(\frac{Se}{\varepsilon}\right)\sum_{n=1}^{N}\begin{Bmatrix} 1 & \text{if } (x_h^n \le x) \cap (x_h^n > 0) \\ 0 & \text{else} \end{Bmatrix} + C(t) \end{aligned} \tag{4.8}$$

where x_e is the set of electron positions and x_h is the set of hole positions, $C(t)$ is the integration constant and ε is the permittivity of the medium. $C(t)$ is evaluated by the condition that the integration of the electric field over x up to L must be equal to V_0, which, for an infinitesimally small Δt, corresponds to

$$C(t) = E_0 - \overline{E(t-\Delta t)} + C(t-\Delta t) \tag{4.9}$$

where $\overline{E(t-\Delta t)}$ is the electric field averaged over the length of the semiconductor at time $t - \Delta t$, i.e.

$$\overline{E(t-\Delta t)} = (1/L)\int_0^L E(x, t-\Delta t)\, dx \tag{4.10}$$

The sampling of E is done at each electron and hole positions x_e^n, x_h^n Each particle n at the location x^n drifts with a velocity that produces a current given by the Shockley-Ramo theorem [3, 4]. The integral of the electron and hole photocurrent is the CE of the electrons and holes, respectively.

The accuracy of the Monte Carlo simulation increases with the number of scaled charges used and with decreasing Δt. In Figure 4.3, the results of Monte Carlo CCE with $r = 0$ (uniform field), $b = 0.1$, $\delta = 0.1$, $s_e = 0.1L$, $s_h = 100L$ are plotted against N and compared with the theoretical uniform-field CCE (η_0)[20]. Statistical error is found by running each point 100 times and finding the variance. The error decreases with increasing N and is considered to be negligible at $N = 1000$. The trapezoidal integration of photocurrent will typically underestimate the CE due to the characteristic knee of the photocurrent, so a sufficiently small Δt is required. In this work Δt was equal to $0.0002L/\mu_e E_0$ or $0.0002L/\mu_h E_0$ if smaller, with the simulation ending once all charges are either trapped or collected. It should be mentioned that the basic structure of the MC simulations used here was verified for photogeneration at the electrode followed by unipolar transport against numerical solutions of the continuity equations[18].

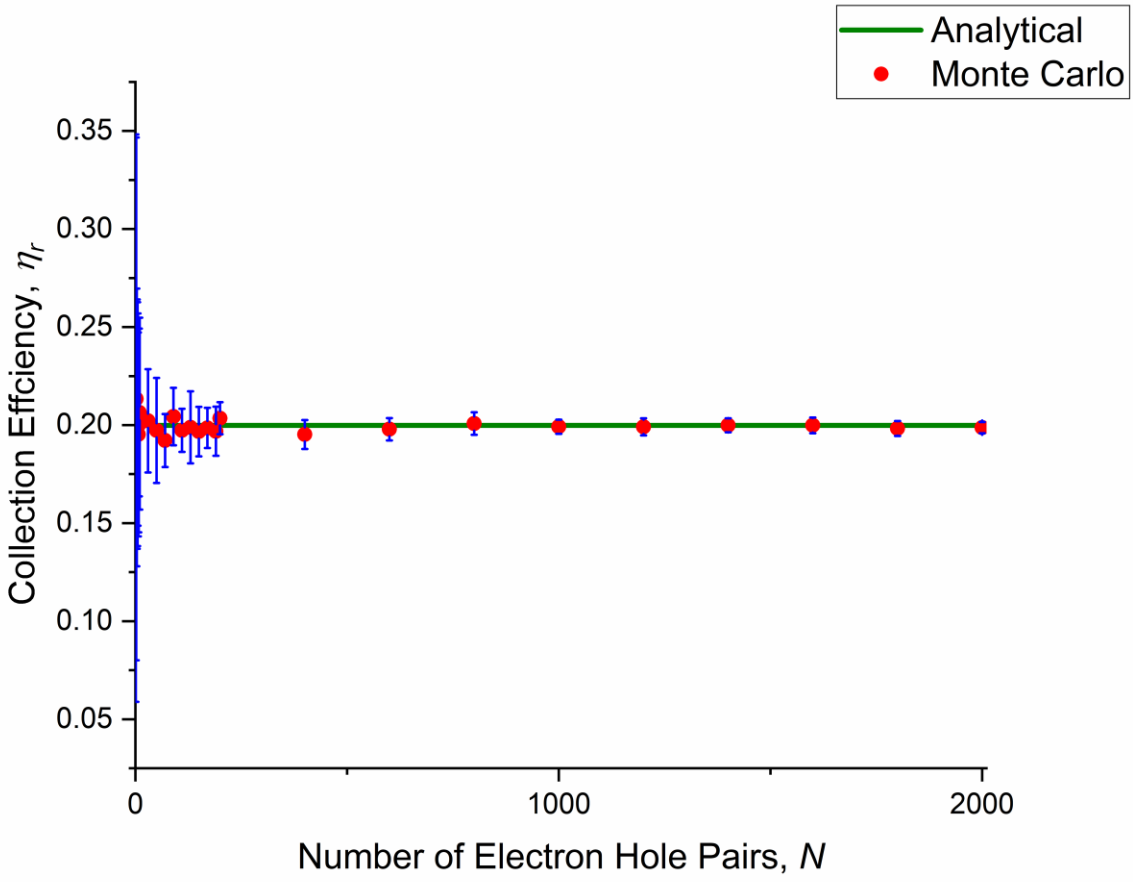

Figure 4.3: Monte Carlo collection efficiency results, at $r = 0$, vs number of EHPs used with associated statistical error compared to the analytical model where $\delta = 0.1L$, $b = 0.1$, $s_e = 0.1L$, and $s_h = 100L$.

4.4 Results and Discussion

All simulations were carried out with the radiation receiving electrode negatively biased as in Figure 4.2. Electrons drift toward the rear collection electrode, the "anode" and holes towards the radiation receiving electrode, the "cathode". The results of simulation were generated using the parameters listed in Table 4.1. CE depends on five quantities, r, s_e, s_h, b, and $\delta (= 1/\alpha)$. r and b are already unitless quantities representing the fraction of charge on the electrode that is photoinjected and the drift mobility ratio, respectively. Schubwegs s_e and s_h and attenuation depth (δ) are typically examined normalized to L, which is also the procedure adopted here, though we will not introduce new dimensionless variables. The minimum and maximum values were chosen based on the common ranges of these parameters used in experiments and detector modeling [2, 15, 16, 21-25].

Table 4.1: Parameters used in MC simulations of the collection efficiency

Parameter	**Minimum**	**Maximum**	**Intervals**	**Spacing**
r	0	1	5	linear
s_e/L	0.1	10	11	$\log_{10}$
s_h/L	$0.1/b$	$10/b$	11	$\log_{10}$
δ/L	0.01	100	5	$\log_{10}$
b	0.01	100	5	$\log_{10}$

Figure 4.4 shows the difference $\Delta\eta_r$, between the uniform-field CE (UFCE), η_0, and the simulated CE η_r at $r = 1$ (maximum injection), plotted against s_e and s_h at specific δ and b values($\Delta\eta_r = \eta_r - \eta_0$). Figure 4.5 is the percentage change ($\%\Delta\eta_r$) relative to the uniform-field CE. These figures are a representation of the dependence of CE on the five parameters listed in Table 4.1.

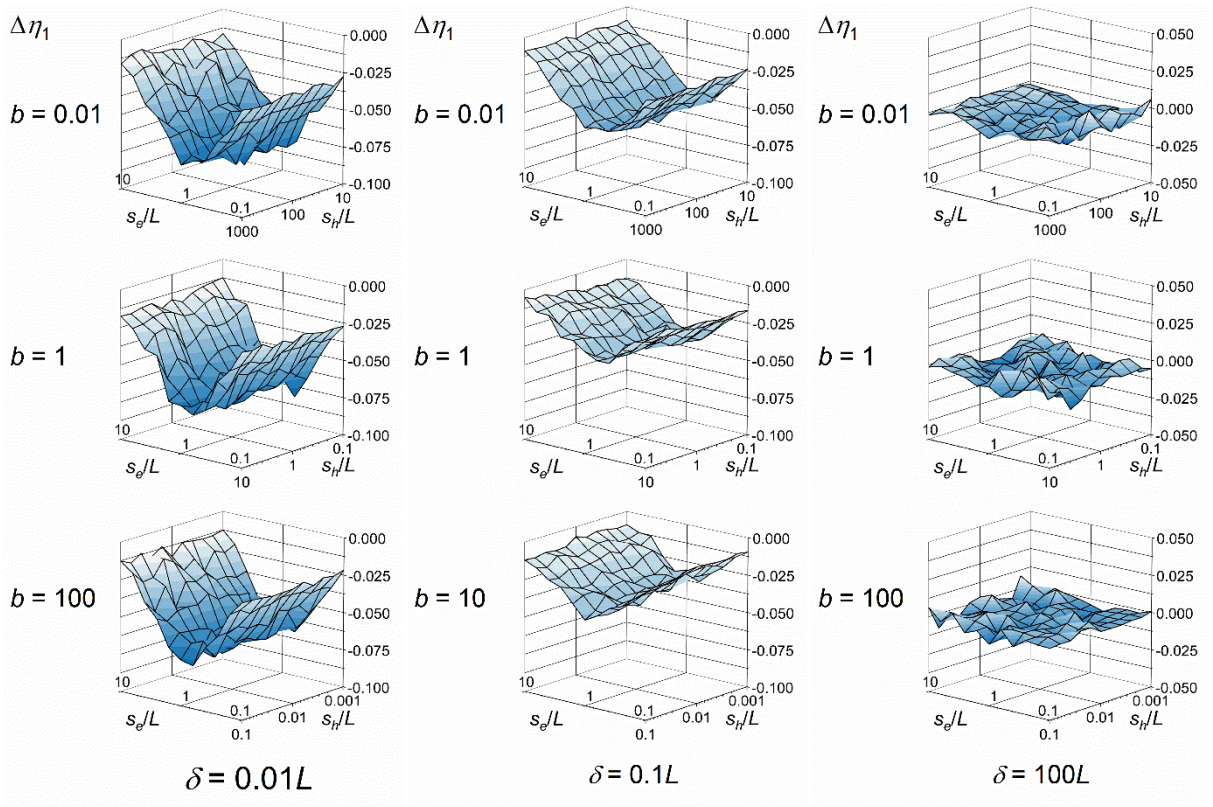

Figure 4.4: Plot showing the difference between CE and UFCE at $r = 1$, over b and δ values from 0.01 to 100, plotted vs s_e/L and s_h/L on a 3-dimensional plot.

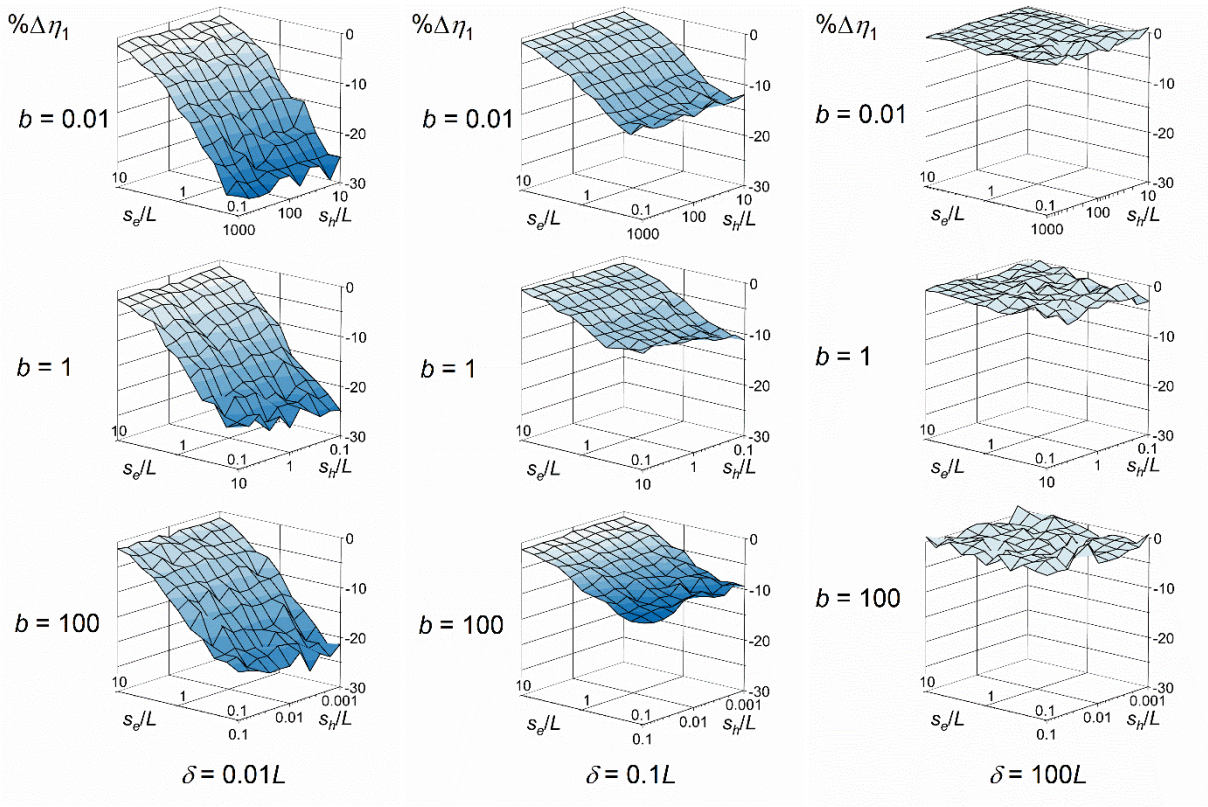

Figure 4.5: Plot showing the percentage difference between CE and UFCE at r = 1, over b and δ values from 0.01 to 100, plotted vs s_e/L and s_h/L on a 3-dimensional plot.

The plot of the difference between CE and UFCE and percentage difference $\%\Delta\eta_r$ shown in Figure 4.4 and Figure 4.5 presents how the mean injection depth δ and the mobility ratio affect the deviation of the high-injection CCE (η_r) from the UFCE (η_0).

The worst-case scenarios are those when the percentage difference magnitude $|\%\Delta\eta_r|$ is significant e.g. 10% or more. For absorption near the radiation receiving electrode (negative) where $\delta / L << 1$, all b (0.01 – 100) has differences up to 30% for schubwegs shorter than the sample thickness $\mu\tau E_0 < L$. When b is very small and δ is very small, the difference tends to only to depend only on s_e, which aligns to the case of near-surface generation with just drifting electrons. Although it appears as though the difference appears significant whenever the schubwegs are shorter than the sample thickness $\mu\tau E_0 < L$, this is not always true. One of the most interesting results is when there is a uniform distribution of initial charge carriers. In this instance, the difference between the CE and the UFCE model is close to zero even though the field inside the semiconductor is not uniform during the drift of the carriers as shown in Figure 4.6. The field near the electrodes is larger than

E_0 and less than E_0 in the center region, and these two opposite changes in the field seem to result in a CE that is similar to the UFCE.

Figure 4.6 and Figure 4.7 show the electric field is clearly symmetric in the *x*-axis at different times. Figure 4.6 to Figure 4.10 show the normalized electric field profile across the device under different trapping conditions as represented by the schubweg to thickness ratios s_e/L and s_h/L. The time axis has been normalized with respect to free electron transit time $t_0 = \mu_e E_0/L$. However, the equivalence of the UFCE and simulated CE does not mean the photocurrents are identical, only that their integrals are. When there is a deviation from these conditions, there is deviation in CCE from the UFCE.

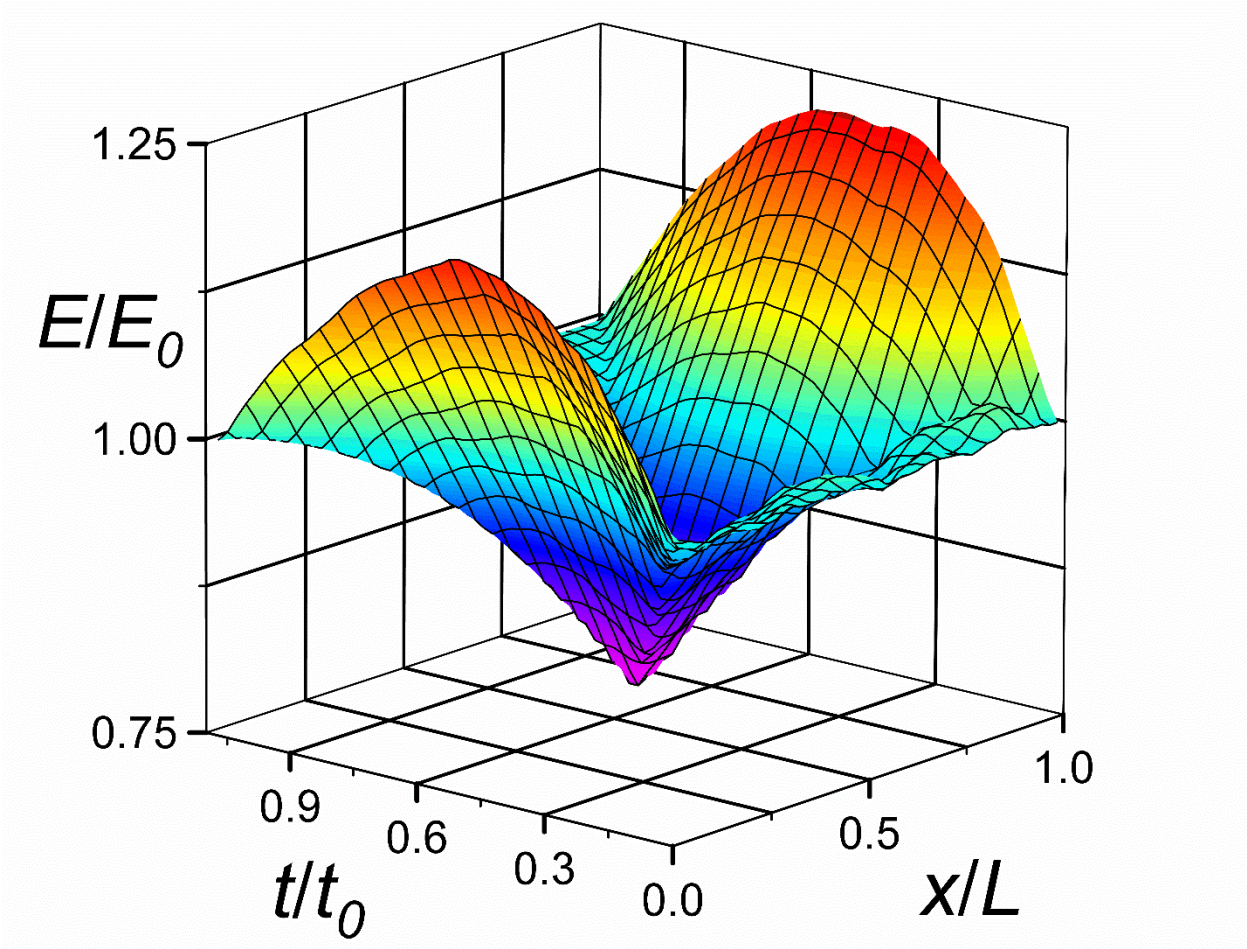

Figure 4.6: The symmetry of electrical field without any charge trapping and $r = 1$, $b = 1$ and δ is very large (>100*L*), represents nearly uniform photogeneration in the sample plotted as E/E_0 vs x/L and t/t_0 on a 3-dimensional plot. (The transit time t_0 is the same for both carriers for this case.)

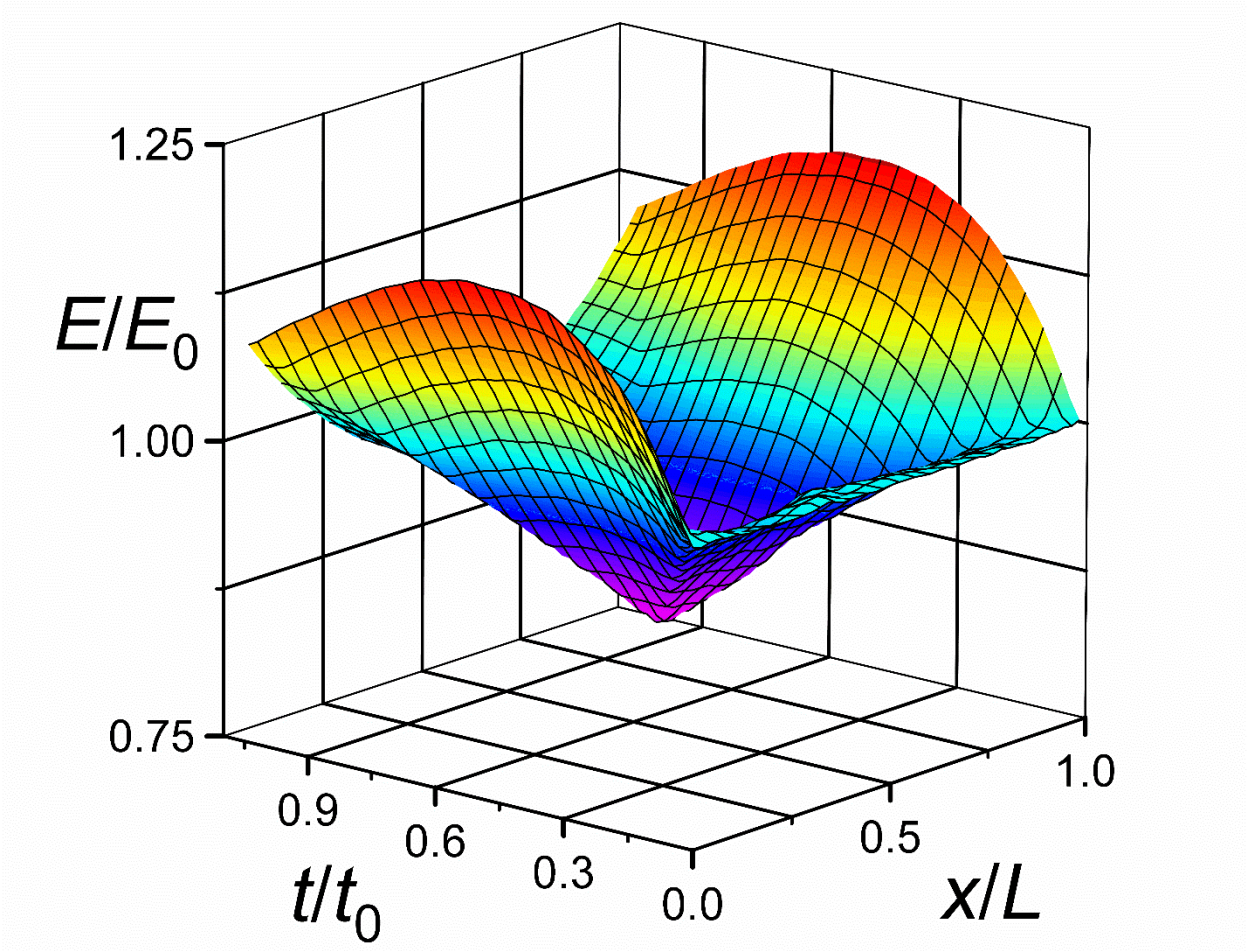

Figure 4.7: The symmetry of the electrical field with equal schubwegs, $s_e = s_h = L$, where $r = 1$, $b = 1$ and δ is very large ($>100L$), plotted as E/E_0 vs x/L and t/t_0 on a 3-dimensional plot.

When the injection depth is shallow (i.e. $\delta = 0.01L$) as in Figure 4.4 and Figure 4.5, the electrons appear to cause the greatest deviation in CE from the UFCE. This is because the electrons travel the largest distance relative to the holes over the longest time period (see Figure 4.1 and Figure 4.2) and so draw more charges from the battery. The electric field profile plots, as in Figure 4.8, show that the largest changes in electric field from E_0 occur near the positive electrode ($x/L = 1$). Since the electrons are moving toward the positive electrode to be collected, a larger change in the electric field in the region acting on those carriers would produce a larger change to the photocurrent and CE of the electrons. When the photogeneration has an absorption depth $\delta = 10L$, as in Figure 4.9 and Figure 4.10, the change in CE exhibits a significant dependence on the mobility ratio b and normalized schubwegs s_e/L and s_h/L, This dependence is due to the electrons and holes being evenly distributed across the semiconductor making the initial placement of charges relatively irrelevant to photocurrent or CE calculation. The effect of b can be seen in Figure 4.9 and Figure 4.10. When b is large ($b = 10$), as in Figure 4.10, the largest change in the electric field occurs near the negative electrode ($x/L = 0$), the collection point of holes, when $s_h << s_e$ and at the

positive electrode (x/L = 1) when s_e << s_h. The holes move much more slowly than the electrons under the same electric field so their trapping has a significant effect on the field near the negative electrode. This relative difference in speed and the significant change in the electric field cause a larger deviation of hole CE with respect to the UFCE. The opposite can be seen for small b (b = 0.1) in Figure 4.9, where electrons cause the greatest perturbation near the positive electrode.

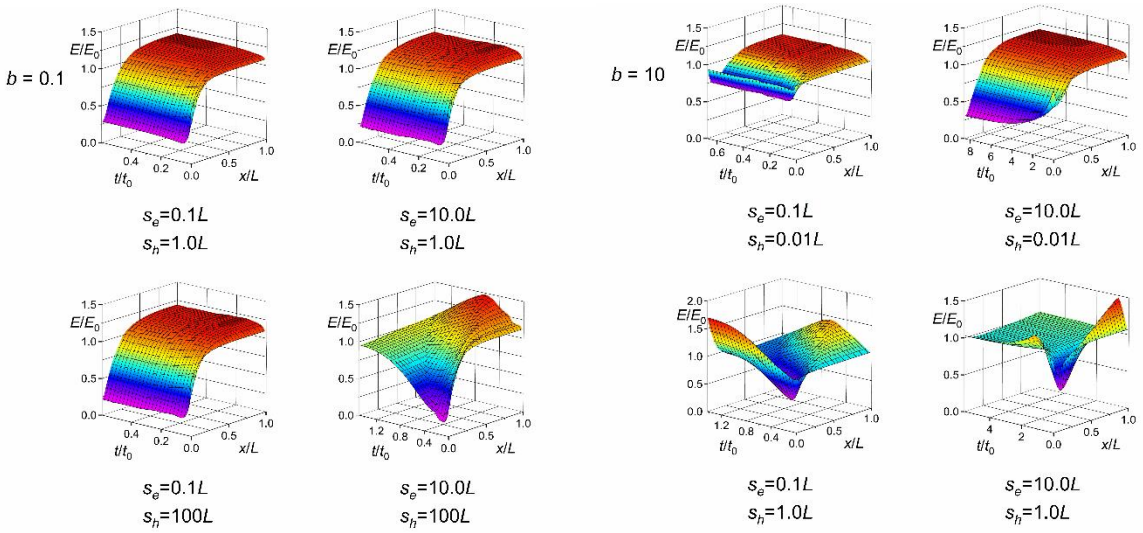

Figure 4.8: Normalized electric field profiles for small δ ($\delta = 0.1L$) as a function of b, s_e and s_h, plotted as E/E_0 vs x/L and t/t_0 on a 3-dimensional plot.

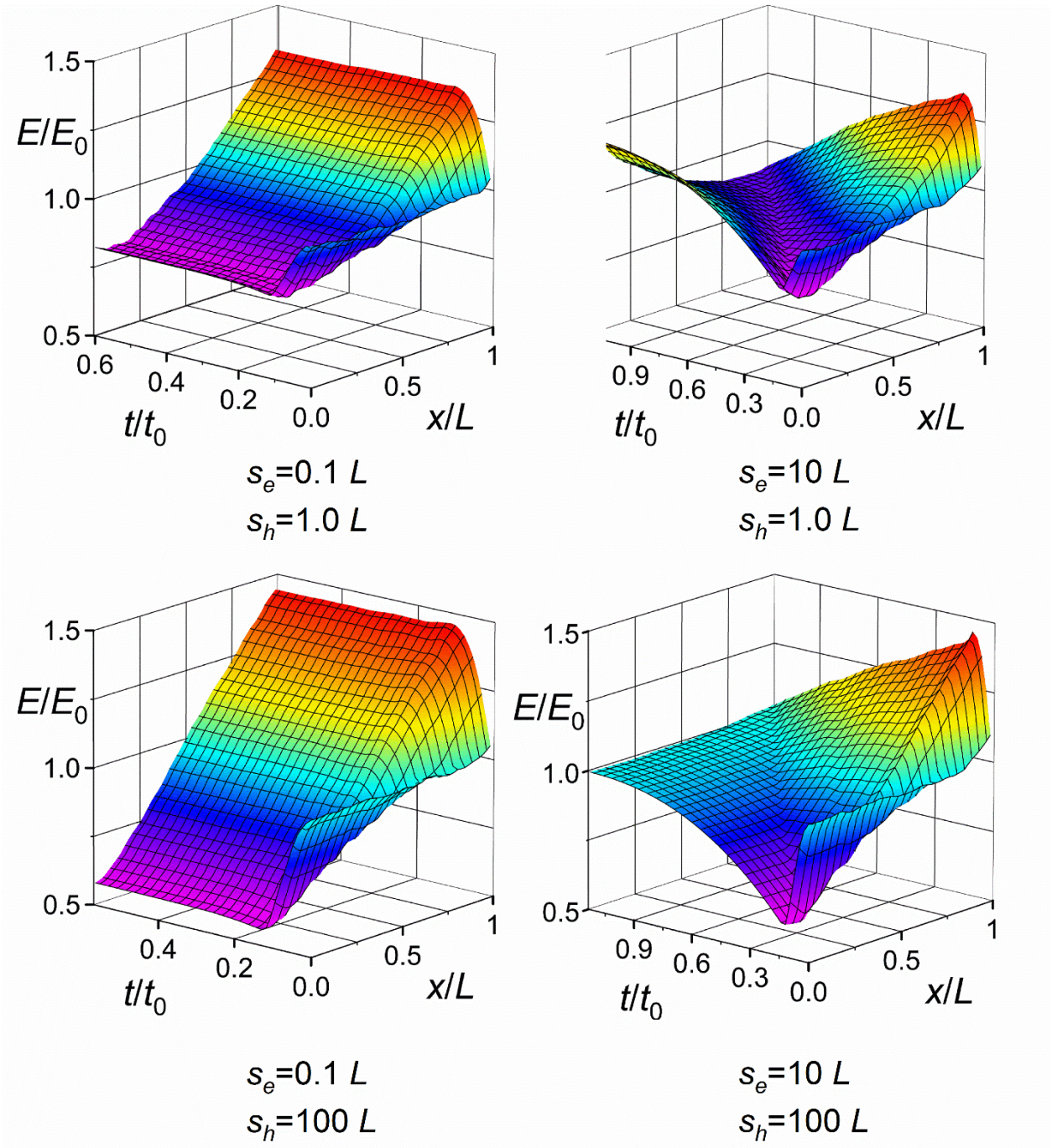

Figure 4.9: Normalized electric field profiles for δ = 10L and b = 0.1 as a function of s_e and s_h plotted as E/E_0 vs x/L and t/t_0 on a 3-dimensional plot.

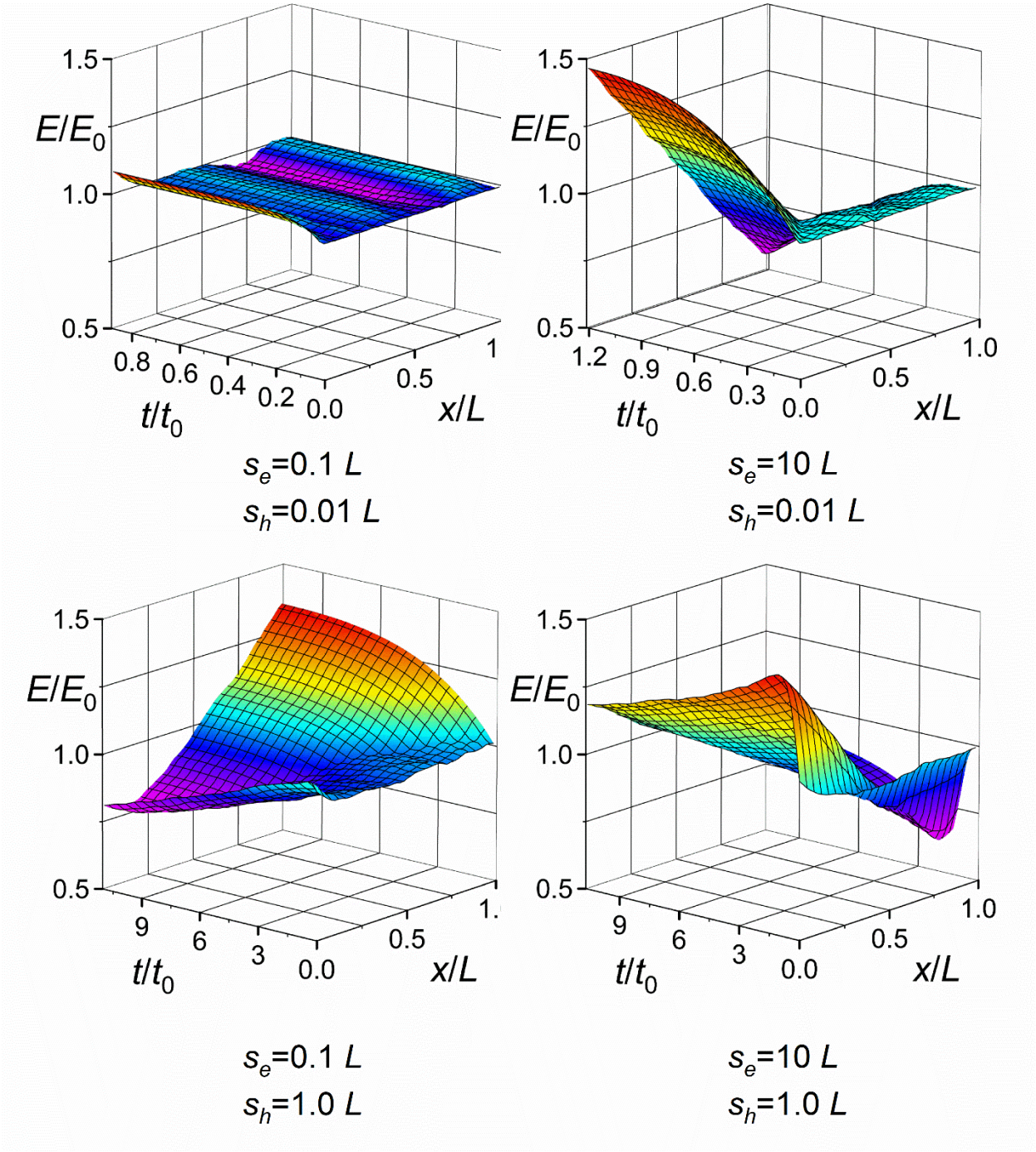

Figure 4.10: Normalized electric field profiles for $\delta = 10L$ (uniformlike photogeneration) and $b = 10$ as a function of se and sh, plotted as E/E_0 vs x/L and t/t_0 on a 3-dimensional plot.

The results in Figure 4.4 to 4.10, have been calculated for full injection to highlight the importance of bulk space charge. Under normal detector operation, this is unlikely to be the case, so under practical operating conditions, the deviation of the CE from the UFCE would be much smaller than the values calculated above. As an indication of the effect of r on the difference $\Delta\eta_r$, we have

taken selected examples and plotted $\%\Delta\eta$ vs. r for different scenarios in which $\delta = 0.1L$ and $1L$ for different schubwegs and b. The small absorption depth ($\delta << L$) case was excluded because this study would be very similar to the HCE case analyzed in reference [18]. The results are put into two classes: (i) $s_e/L = 10$ as shown in Figure 4.11***:*** and (ii) $s_e/L = 1$ as shown in Figure 4.12. In both Figure 4.11***:*** and Figure 4.12, the MC points have "error" (i.e. uncertainty) bars that correspond to one standard deviation error (full length of error-bar is 2σ). Consider Figure 4.11***:*** representing the case in which the electrons (moving away from the radiation receiving electrode) do not experience trapping. As expected, when both carriers have good transport properties ($s/L > 1$ for both), the errors in using the UFCE are under 2% for all injection levels. Notice also that when $s_h/L < 1$, the $|\%\Delta\eta_r|$ error increases with r and reaches 2% for full injection. Furthermore, if the injection depth is "large" e.g. greater than L, and the hole trapping is small, the UFCE formulas in Equations (4.1)-(4.3) work quite well with errors less than 2%.

In the presence of electron trapping ($s_e/L = 1$), as represented in Figure 4.12, $\%\Delta\eta_r$ error has more dependence on r and can be as large as 10% when the hole trapping is significant i.e. $s_h/L = 0.1$. Indeed, even small injection ratios can have $\%\Delta\eta_r$ errors over 2%.

It can be see from all 12 figures in Figure 4.11***:*** and Figure 4.12, that the errors in using UFCE formula are typically less than 10%, which is a partial vindication of the use of the UFCE formula in a wide range of applications where the signal is not necessarily a small signal.

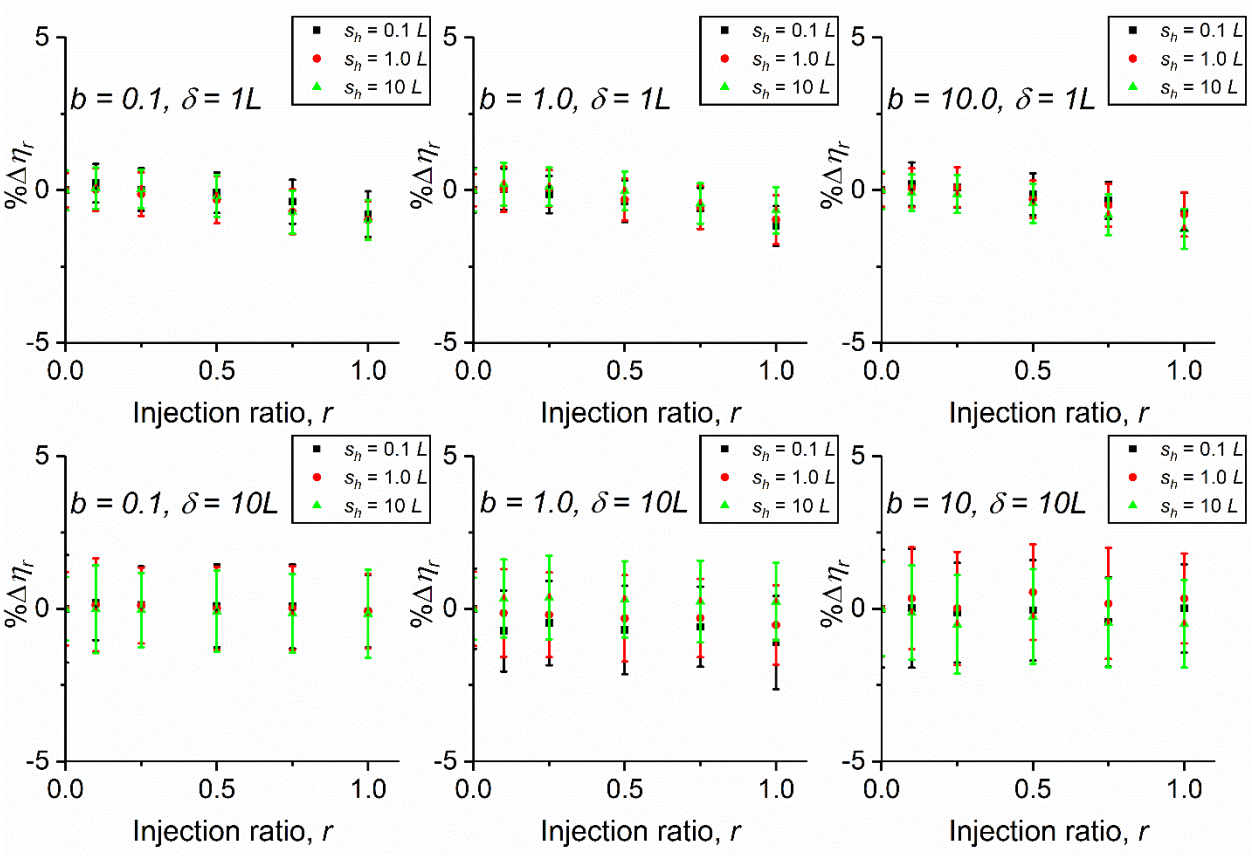

Figure 4.11: Selected examples of the difference between the CCE and the UFCE as a function of the injection ratio at s_e=10L. As r becomes very small, the difference approaches zero.

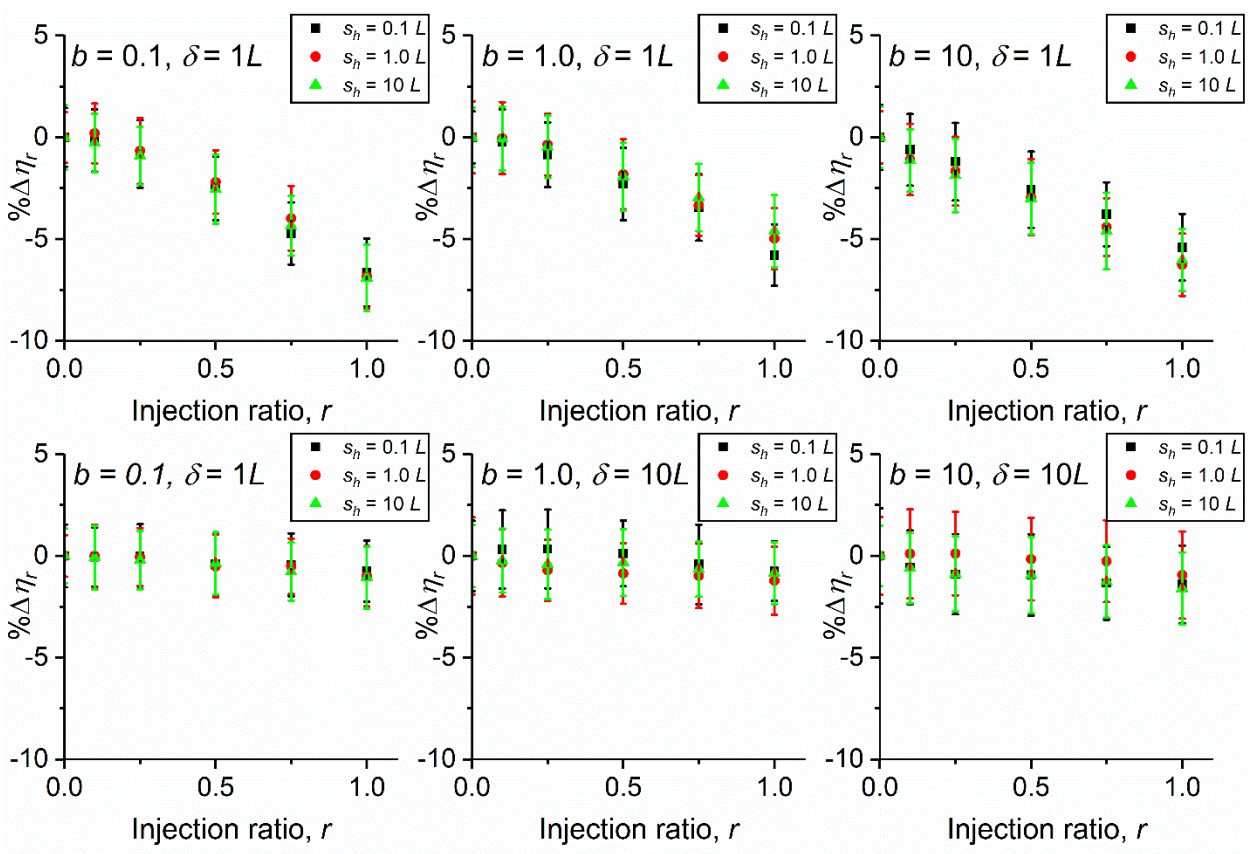

Figure 4.12: Selected examples of the difference between the CCE and the UFCE as a function of the injection ratio at s_e=1L. As r becomes very small, the difference approaches zero.

4.5 Conclusions

The collection efficiency (η_r) of photogenerated electrons and holes in a semiconductor detector deviates significantly from the uniform-field collection efficiency (UFCE) (η_0) as the photoinjection ratio (r) of injected charge to charge on the electrodes increases. Monte Carlo simulation of exponentially distributed photogenerated electrons and holes under well-defined electron and hole lifetimes, along with an accurate evaluation of the internal field (due to the space charge of trapped and drifting carriers and charges on the electrodes), has provided an assessment of the extent of validity of the standard UFCE equation (as stated in equations (4.1) to (4.3)) and its shortcomings. The deviations of η_r from the UFCE, η_0, have been quantified in terms of the injection ratio r, drift mobility ratio b, mean absorption depth δ and charge carrier schubwegs s_e and s_h for electrons and holes respectively, as presented in Figure 4.4 and Figure 4.5. These results have also been presented as $\%\Delta\eta_r$ vs injection ratio r for selected electron and hole schubwegs and absorption depths that are typical as in Figure 4.11***:*** and Figure 4.12. The latter figures represent the extent of errors involved in using the UFCE equation under a nonuniform field in the detector. Of particular interest was the uniform absorption case, $\delta >> L$, which showed that CCE is very close to the UFCE; $\eta_r \approx \eta_0$. In most cases, for a wide range of electron and hole schubwegs and

photoinjection ratios, the total errors remained less than 10% as quantified in Figure 4.11*:* and Figure 4.12. The present study provides partial justification to the wide-spread use of the UFCE in various applications, even under high injection conditions.

Acknowledgements

The authors acknowledge NSERC Discovery Grants Program and the University of Saskatchewan, Centennial Enhancement Chair funding for financial support.

4.6 References

[1] Kasap S 2012 *Optoelectronics and photonics : principles and practices* (Upper Saddle River, N.J.: Upper Saddle River, N.J. : Pearson)

[2] Kasap S, Frey J B, Belev G, Tousignant O, Mani H, Greenspan J, Laperriere L, Bubon O, Reznik A, DeCrescenzo G, Karim K S and Rowlands J A 2011 Amorphous and Polycrystalline Photoconductors for Direct Conversion Flat Panel X-Ray Image Sensors *Sensors-Basel* **11** 5112-57

[3] Shockley W 1938 Currents to conductors induced by a moving point charge *J Appl Phys* **9** 635-6

[4] Ramo S 1939 Currents Induced by Electron Motion *Proceedings of the IRE* **27** 584-5

[5] Kabir M Z, Emelianova E V, Arkhipov V I, Yunus M, Kasap S O and Adriaenssens G 2006 The effects of large signals on charge collection in radiation detectors: Application to amorphous selenium detectors *J Appl Phys* **99** 124501

[6] Vanheyningen R S and Brown F C 1958 Transient Photoconductivity in Silver Chloride at Low Temperatures *Phys Rev* **111** 462-71

[7] Ruzin A and Nemirovsky Y 1997 Statistical models for charge collection efficiency and variance in semiconductor spectrometers *J Appl Phys* **82** 2754-8

[8] Kasap S O 2000 X-ray sensitivity of photoconductors: application to stabilized a-Se *J Phys D Appl Phys* **33** 2853-65

[9] Kabir M Z and Kasap S O 2002 Charge collection and absorption-limited sensitivity of x-ray photoconductors: Applications to a-Se and HgI2 *Appl Phys Lett* **80** 1664-6

[10] Kabir M Z 2008 Effects of charge carrier trapping on polycrystalline PbO x-ray imaging detectors *J Appl Phys* **104** 074506

[11] Mainprize J G, Hunt D C and Yaffe M J 2002 Direct conversion detectors: The effect of incomplete charge collection on detective quantum efficiency *Med Phys* **29** 976-90

[12] Street R A, Ready S E, Van Schuylenbergh K, Ho J, Boyce J B, Nylen P, Shah K, Melekhov L and Hermon H 2002 Comparison of PbI2 and HgI2 for direct detection active matrix x-ray image sensors *J Appl Phys* **91** 3345-55

[13] Auden E C, Vizkelethy G, Serkland D K, Bossert D J and Doyle B L 2017 Modeling charge collection efficiency degradation in partially depleted GaAs photodiodes using the 1-and 2-carrier Hecht equations *Nucl Instrum Meth B* **399** 12-9

[14] Semeniuk O, Grynko O, Decrescenzo G, Juska G, Wang K and Reznik A 2017 Characterization of polycrystalline lead oxide for application in direct conversion X-ray detectors *Sci Rep-Uk* **7** 8659

[15] Kim H K 2006 Analytical model for incomplete signal generation in semiconductor detectors *Appl Phys Lett* **88** 132112

[16] Hossain A, Cui Y, Bolotnikov A E, Camarda G S, Yang G, Kochanowska D, Witkowska-Baran M, Mycielski A and James R B 2009 Vanadium-Doped Cadmium Manganese Telluride (Cd1-x Mn (x) Te) Crystals as X- and Gamma-Ray Detectors *J Electron Mater* **38** 1593-9

[17] Semeniuk O, Juska G, Oelerich J O, Jandieri K, Baranovskii S D and Reznik A 2017 Transport of electrons in lead oxide studied by CELIV technique *J Phys D Appl Phys* **50** 035103
[18] Kasap S, Ramaswami K O, Kabir M Z and Johanson R 2019 Corrections to the Hecht collection efficiency in photoconductive detectors under large signals: non-uniform electric field due to drifting and trapped unipolar carriers *Journal of Physics D: Applied Physics* **52** 135104
[19] Hecht K 1932 For the mechanism of the photoelectric primary current in insulating crystals. *Z Phys* **77** 235-45
[20] Nemirovsky Y 1999 Statistical modeling of charge collection in semiconductor gamma-ray spectrometers *J Appl Phys* **85** 8-15
[21] Qureshi S, Perezmendez V, Kaplan S N, Fujieda I, Cho G and Street R A 1989 Material Parameters in a Thick Hydrogenated Amorphous-Silicon Detector and Their Effect on Signal Collection *Mat Res S C* **149** 649-54
[22] Maynard B, Long Q, Schiff E A, Yang M J, Zhu K, Kottokkaran R, Abbas H and Dalal V L 2016 Electron and hole drift mobility measurements on methylammonium lead iodide perovskite solar cells *Appl Phys Lett* **108** 173505
[23] Long Q, Dinca S A, Schiff E A, Yu M and Theil J 2014 Electron and hole drift mobility measurements on thin film CdTe solar cells *Appl Phys Lett* **105** 042106
[24] Arnab S M and Kabir M Z 2014 An analytical model for analyzing the current-voltage characteristics of bulk heterojunction organic solar cells *J Appl Phys* **115** 034504
[25] Tyagi A, Ghosh K, Kottantharayil A and Lodha S 2018 Performance Evaluation of Passivated Silicon Carrier-Selective Contact Solar Cell *Ieee T Electron Dev* **65** 176-83

5 Conclusions

In this thesis, a simulation of electron and hole transport in semiconductors was carried out using Monte Carlo methods along with a numerical approximation of the Poisson equation. The results of the simulation of photocurrent and charge collection efficiency matched published numerical and analytical results using the same parameters. This simulation can also generate results outside of the bounds of previously used models. The strongest relationships shown in this thesis are in the photocurrent and charge collection efficiency where there is both inter-coulombic forces between charges and deep charge trapping. Other effects that have been implemented are exponential EHP generation, independent mobilities, electron and hole trapping.

5.1 Charge Collection Efficiency

In the paper, *Corrections to the Hecht Collection Efficiency in Photoconductive Detectors under Large Signals: Non-Uniform Electric Field due to Drifting and Trapped Unipolar Carriers*, the collection efficiency of electrons or holes in a semiconductor under large signals, are shown to deviate significantly from the well-known Hecht collection efficiency. Monte Carlo simulations and the numerical solutions of the continuity, semiconductor rate and Poisson equations were used to calculate the charge collection efficiency (CCE). The deviation has been quantified in terms of the injection ratio r and normalized trapping time τ, where the normalization is with respect to the carrier transit time across the semiconductor The CCE goes over into HCE under small signals but drops significantly below HCE as r increases. An analysis of the change in CCE resulted in Equations (3.13) and (3.14), which allows for the calculation of CCE if large signals are considered.

In the paper entitled *Charge Collection Efficiency in Photoconductive Detectors under Small to Large Signals*, the collection efficiency (η_r) of photogenerated electrons and holes in a semiconductor detector was shown to deviate significantly from the uniform-field collection efficiency (η_0) as the photoinjection ratio (r) of injected charge to charge on the electrodes increases. The deviations of η_r from the well-known unified field charge collection efficiency, η_0, has been quantified in terms of the injection ratio r, mobility ratio b, mean absorption depth δ and charge carrier schubwegs, s_e and s_h, as presented in Figure 4.4 and Figure 4.5. The latter figures represent the extent of errors involved in using the CCE equation under a nonuniform field in the detector, which can reach 20%. Of interest was the uniform absorption case, $\delta >> L$, and b was unity. which showed that CCE is very close to the UFCCE; $\eta_r \approx \eta_0$. Monte Carlo simulation of photogenerated electrons and holes under well-defined electron and hole lifetimes, along with an accurate evaluation of the internal field (due to the space charge of trapped and drifting carriers and charges on the electrodes), has provided an assessment of the extent of validity of the standard CCE equation and its shortcomings.

5.2 Future Work

This thesis in Monte Carlo simulation methods of semiconductors has only scratched the surface in analyzing the results this program can generate. There are methods developed that need to be analyzed yet, such as, shallow trapping, pulsed light sources, recombination and variance.

Shallow trapping is of particular interest in photocurrent analysis. As stated in chapter 2, we have implanted a solid method to simulate shallow trapping that improves on all other methods. In the future, analysis is to be done of the photocurrent, with shallow trapping, to evaluate their time features.

Code for multiple pulses has been developed. Using this code in conjunction with all other simulated effects, the modulation transfer function of a semiconductor detector can be estimated. Currently no data has been simulated in this regard. If simulations are to be done, their parameters, such as pulse width and pulse separation, will be chosen based on currently manufactured sources used in detectors.

Recombination is when an electron and electron hole recombine and are removed from their respective transport bands. In this thesis, the Onsager recombination model is used. With Onsager recombination, a free electron recombines with a trapped hole, or vice versa. This recombination occurs, when the thermal energy of the free charge is sufficiently small relative to the attractive columbic energy between them.[1, 2]. The critical point of recombination is defined as the thermal capture radius. Onsager recombination occurs when the charge carrier passes within the thermal capture radius of each other defined as [3]. Future work involving recombination would involve simulating the effect of recombination on photocurrent collection efficiency and initial photogeneration efficiency.

Variance is an inherent property of any system with probability or statistical distribution. Since phenomena such as trapping and EHP generation use probability, they must have an associated variance. This means that photocurrent and collection efficiency must also have variance. To calculate variance, the Monte Carlo simulation is run multiple times. The values of C.E. can then be used to generate a variance about their mean. The variance of the set of CE values multiplied by the number of charge carriers used, is the normalised variance. An analytical normalised variance equation is based on exponential EHP generation and deep trapping of electrons and holes under small signals [4, 5]. By calculating the variance of multiple simulation runs, the variance may be found under large signal conditions

5.3 References

[1] Onsager L 1938 Initial recombination of ions *Phys Rev* **54** 554-7

[2] Sharma D, Fang Y, Zafar F, Karim K S and Badano A 2011 Recombination models for spatio-temporal Monte Carlo transport of interacting carriers in semiconductors *Appl Phys Lett* **98**

[3] Groves C, Marsh R A and Greenham N C 2008 Monte Carlo modeling of geminate recombination in polymer-polymer photovoltaic devices *The Journal of Chemical Physics* **129** 114903

[4] Nemirovsky Y 1999 Statistical modeling of charge collection in semiconductor gamma-ray spectrometers *J Appl Phys* **85** 8-15

[5] Ruzin A and Nemirovsky Y 1997 Statistical models for charge collection efficiency and variance in semiconductor spectrometers *J Appl Phys* **82** 2754-8

Appendix A: Code

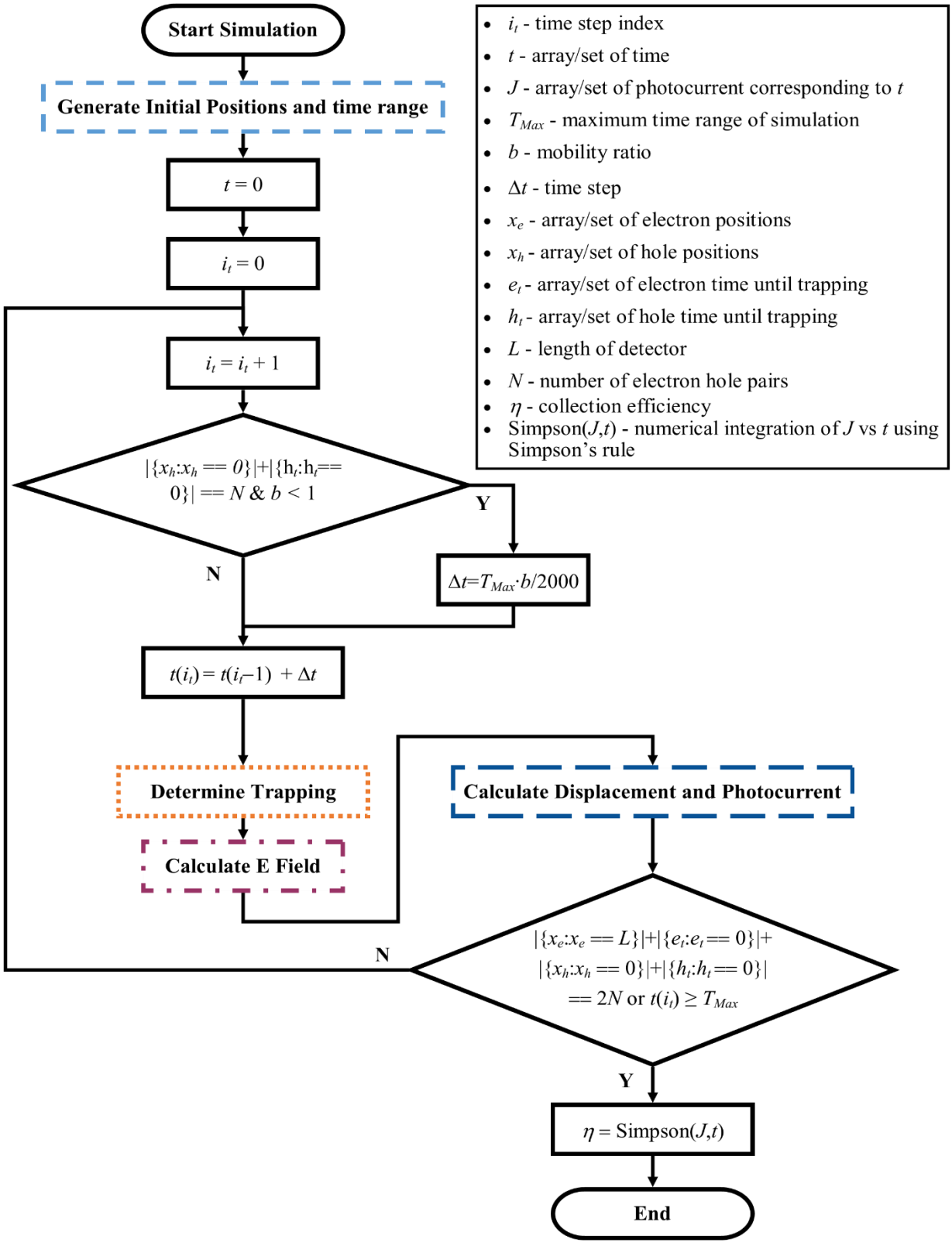

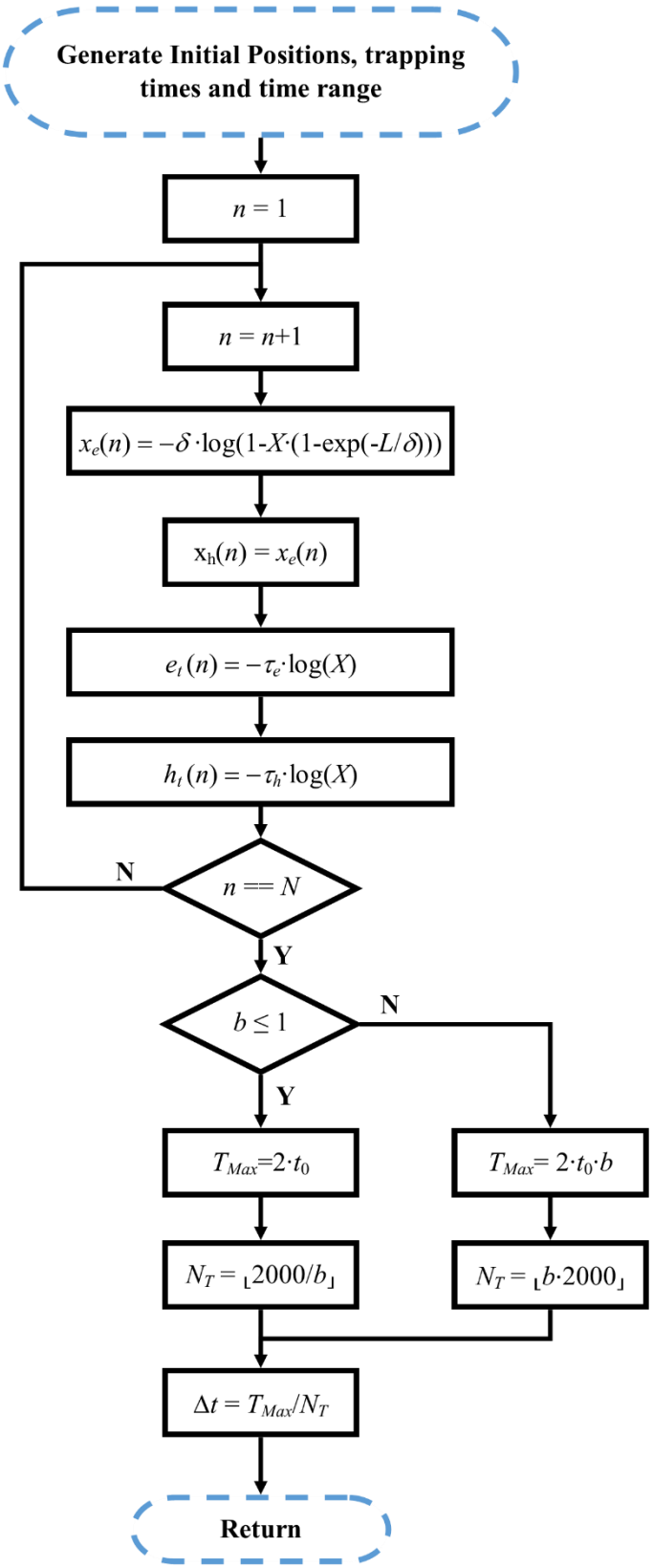

- t_0 - electron free transit time
- T_{Max} - maximum time range of simulation
- b - mobility ratio
- Δt - time step
- x_e - array/set of electron positions
- x_h - array/set of hole positions
- e_t - array/set of electron time until trapping
- h_t - array/set of hole time until trapping
- τ_e - mean electron tapping time
- τ_h - mean hole trapping time
- L - length of detector
- n - EHP index
- N - number of electron hole pairs
- δ - mean injection depth
- X - random number from 0 to 1

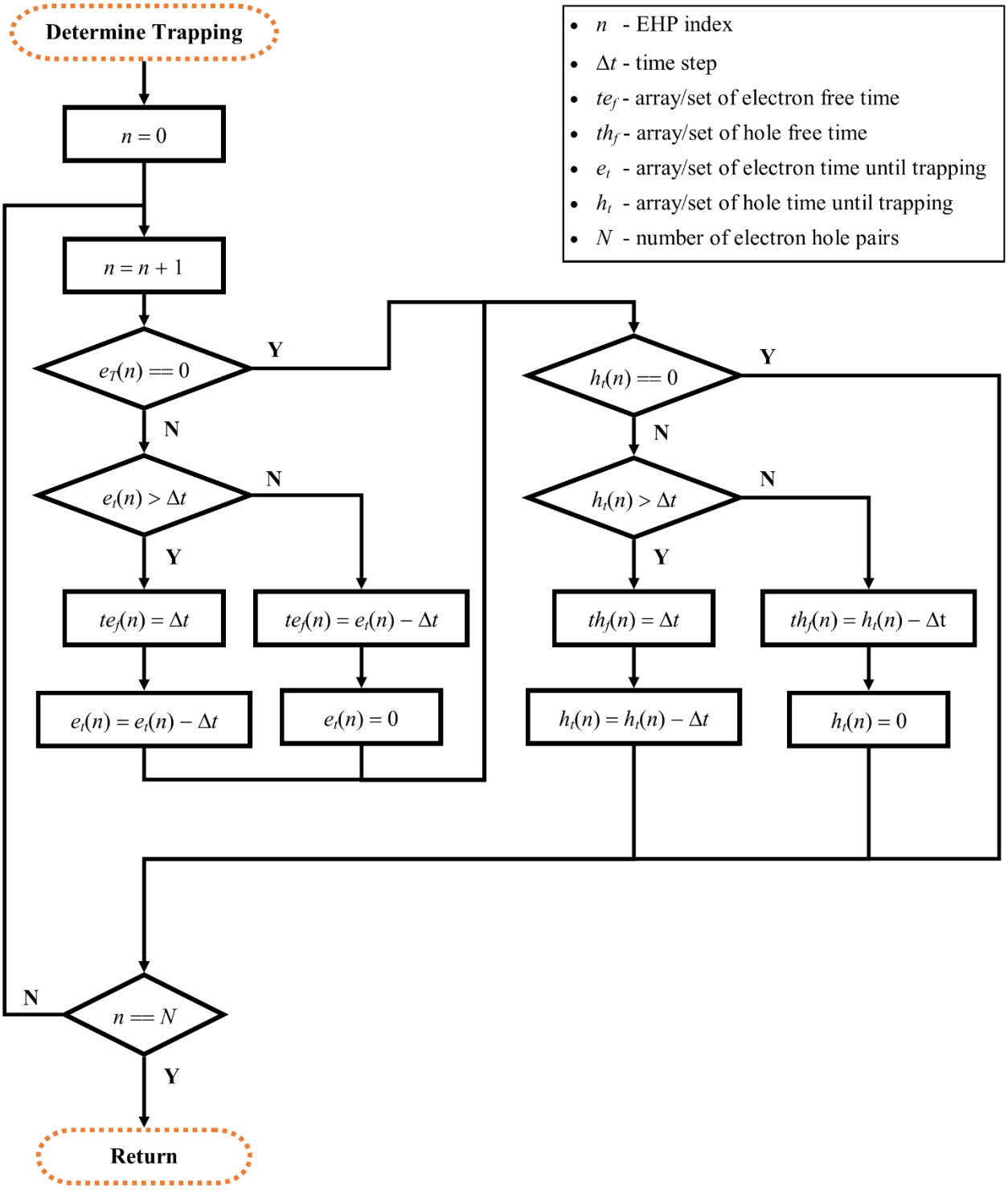
Determine Trapping
$n = 0$
$n = n + 1$
$e_T(n) == 0$
Y
N
$e_t(n) > \Delta t$
N
Y
$te_f(n) = \Delta t$
$te_f(n) = e_t(n) - \Delta t$
$e_t(n) = e_t(n) - \Delta t$
$e_t(n) = 0$
$h_t(n) == 0$
Y
N
$h_t(n) > \Delta t$
N
Y
$th_f(n) = \Delta t$
$th_f(n) = h_t(n) - \Delta t$
$h_t(n) = h_t(n) - \Delta t$
$h_t(n) = 0$
N
$n == N$
Y
Return
n - EHP index
Δt - time step
te_f - array/set of electron free time
th_f - array/set of hole free time
e_t - array/set of electron time until trapping
h_t - array/set of hole time until trapping
N - number of electron hole pairs

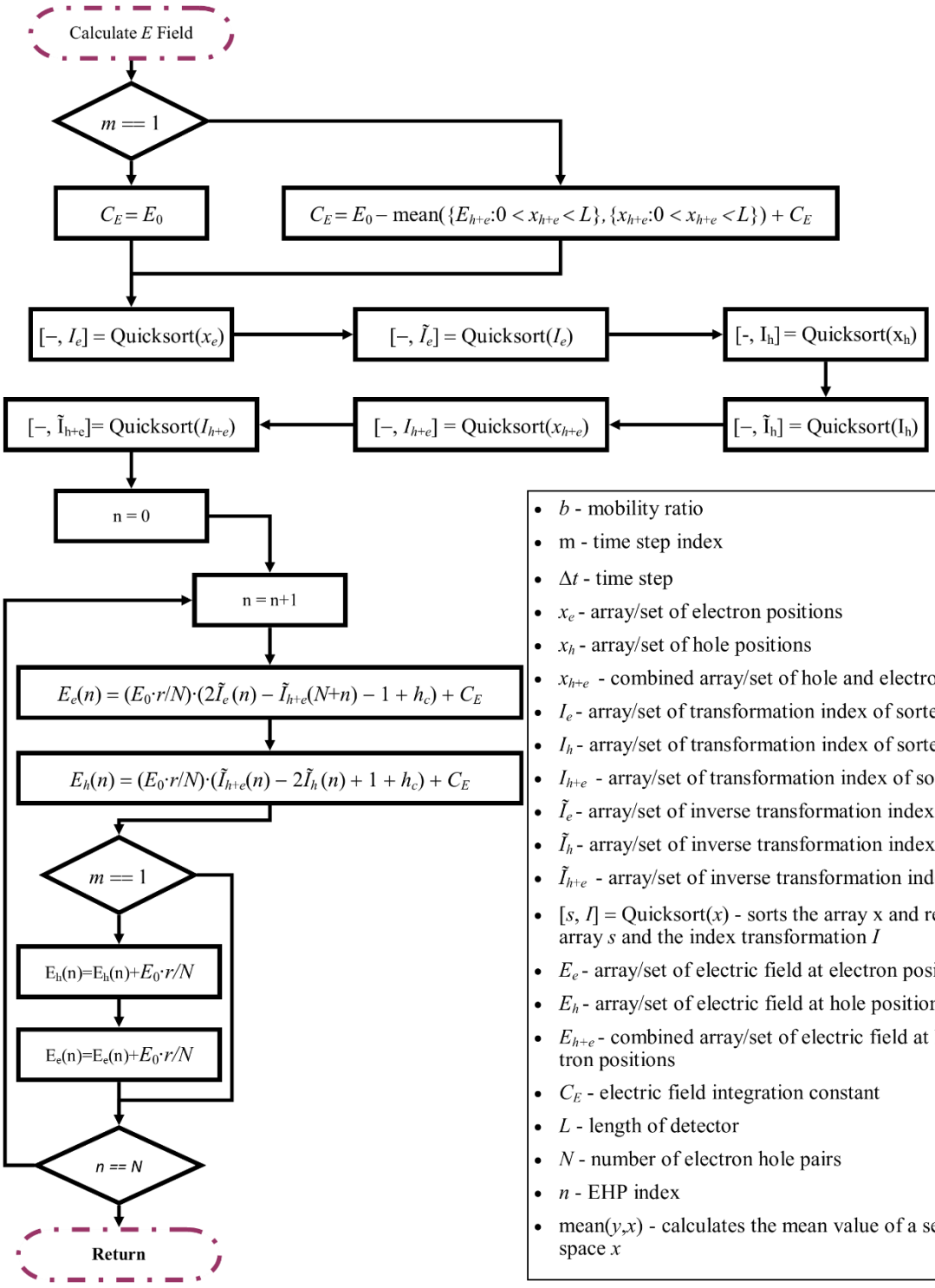

- b - mobility ratio
- m - time step index
- Δt - time step
- x_e - array/set of electron positions
- x_h - array/set of hole positions
- x_{h+e} - combined array/set of hole and electron positions
- I_e - array/set of transformation index of sorted x_e
- I_h - array/set of transformation index of sorted x_h
- I_{h+e} - array/set of transformation index of sorted x_{h+e}
- $\tilde{I}_e$ - array/set of inverse transformation index of sorted x_e
- $\tilde{I}_h$ - array/set of inverse transformation index of sorted x_h
- $\tilde{I}_{h+e}$ - array/set of inverse transformation index of sorted x_{h+e}
- $[s, I] = \text{Quicksort}(x)$ - sorts the array x and returns the sorted array s and the index transformation I
- E_e - array/set of electric field at electron positions
- E_h - array/set of electric field at hole positions
- E_{h+e} - combined array/set of electric field at hole and electron positions
- C_E - electric field integration constant
- L - length of detector
- N - number of electron hole pairs
- n - EHP index
- $\text{mean}(y,x)$ - calculates the mean value of a set $y(x)$ over a set space x

Appendix B: Comparison of Trapping Models

The trapping of electrons and holes can be simulated many ways. In this section, the method for Monte Carlo description of trapping in this work is shown to be one of the most efficient techniques. The methods in current use are: the $P(\Delta t)$ methods, which determines where a charge is trapped at each time step; the $m\Delta t$ method, which approximates a generated trapping time with an integer multiple of Δt and the $m\Delta t + \tau_f$, which is the free time method.

The ideal number of time steps, per transit time, for the $P(\Delta t)$ method is achieved when the probability of trapping in each time step is 50%:

$$P(\Delta t) = 0.5 = 1 - e^{-\tau/\Delta t} \tag{B.1}$$

The ideal time step Δt is then:

$$\Delta t = -\tau \ln(0.5) \tag{B.2}$$

Unfortunately, the value for Δt will always be an irrational number, so it must be approximated as a ratio of two integers. This ratio has been translated to the number of time steps taken within the time domain 2 times t_0.

$$N_{2t_0} = \left[\frac{2t_0}{-\ln(0.5)\tau} \right] \tag{B.3}$$

where the square brackets [], indicate rounding to the nearest integer. The approximate Δt determined from N_{2t_0} value is given as:

$$\Delta t = \frac{2t_0}{N_{2t_0}} \tag{B.4}$$

To compare the trapping simulation methods a mean trapping of 0.1 t_0 was chosen. The Δt, the time steps chosen, are based on 0.5, 1, 10 and 100 times the approximate ideal $P(\Delta t)$ time step size, 2/29 t_0.

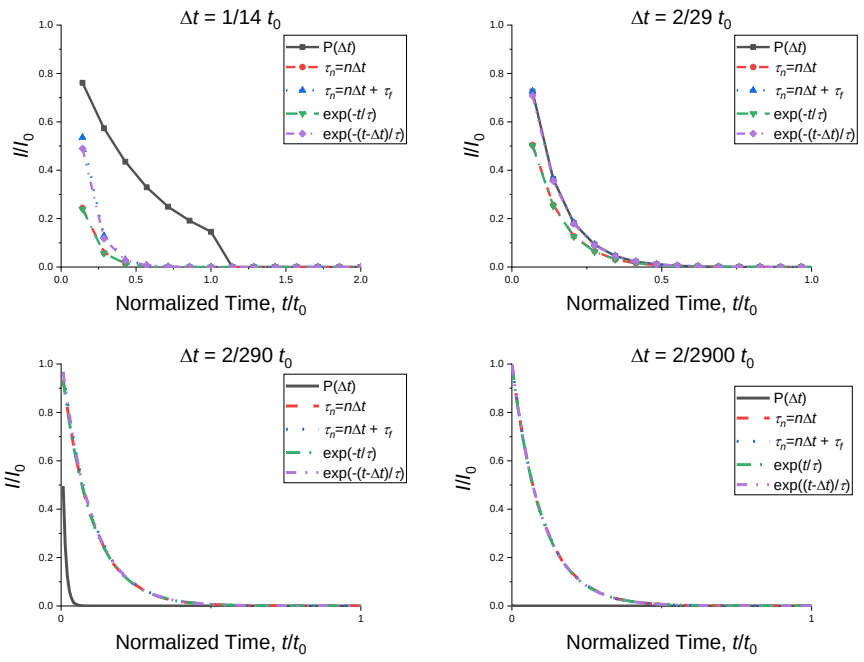

Figure B.1: Plots of photocurrents vs time predicted using different simulation methods and analytical definitions, with near-surface generation of electrons where $\tau = 0.1\ t_0$ and $r = 0$.

It can be seen from Figure B.1 that the $P(\Delta t)$ is only close to a correct photocurrent simulation when

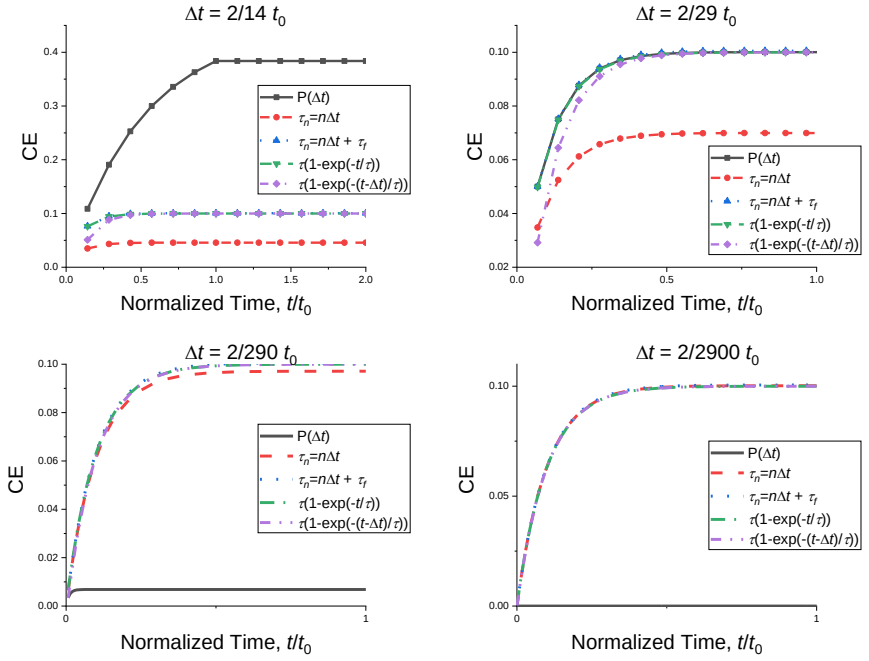

Figure B.2: Plots of CE vs time predicted using different simulation methods and analytical definitions with near-surface generation of electrons where $\tau = 0.1\ t_0$ and $r = 0$.

Table B.1: Total CE calculated from numerical integrals of photocurrents simulated with trapping methods when all charge carriers are trapped or collected with near-surface generation of electrons where $\tau = 0.1\ t_0$ and $r = 0$.

Trapping method	**Time step sizes**			
	$\Delta t = 2/14\ t_0$	$\Delta t = 2/29\ t_0$	$\Delta t = 2/290\ t_0$	$\Delta t = 2/2900\ t_0$
$P(\Delta t)$	0.383785714286	0.100050297972	0.006854482759	0.000005172414
$\tau_n = m\Delta t$	0.045757142857	0.069944827586	0.097101379310	0.100212482759
$\tau_n = m\Delta t + \tau_f$	0.100556548181	0.100556548181	0.100556548181	0.100556548181

The expected CE from the HCE model is 0.099995456001, which is overshot by the numerical integrals of the simulated photocurrents. This overshooting is because a scaled cumulative sum of the photocurrent was used to numerically integrate. This integral method will always overestimate an integral of a decreasing function. In final assessment of CE, a more accurate numerical integral method, such as Simpson's rule, should be used. For illustrative purposes of Δt dependence, this basic integral method is used the comparisons of trapping simulation methods.

It can be clearly seen from Figure B.2 and Table B.1 that the free time method is independent of the Δt value used, however all other methods do vary. The $P(\Delta t)$ is clearly only accurate at the approximated Δt step from equation (B.4). The integer Δt methods only approaches the same CE value when the size of Δt deceases, confirming the truncation issue. These results confirm that the free time method is the methods to use to simulate photocurrent and CE in MC.